# Bond Mean Field Theory for Electron Spin Resonance Frequency Shift Analysis

by

Clifford John Rodger

A thesis submitted in partial fulfillment
of the requirements for the degree of
Master of Science (MSc) in Physics

The Faculty of Graduate Studies
Laurentian University
Sudbury, Ontario, Canada

**THESIS DEFENCE COMMITTEE/COMITÉ DE SOUTENANCE DE THÈSE**
**Laurentian Université/Université Laurentienne**
Faculty of Graduate Studies/Faculté des études supérieures

| | |
|---|---|
| Title of Thesis<br>Titre de la thèse | Bond Mean Field Theory for Electron Spin Resonance Analysis |
| Name of Candidate<br>Nom du candidat | Rodger, Clifford John |
| Degree<br>Diplôme | Master of Science |
| Department/Program<br>Département/Programme | Physics |
| Date of Defence<br>Date de la soutenance | January 08, 2015 |

**APPROVED/APPROUVÉ**

Thesis Examiners/Examinateurs de thèse:

Dr. Mohamed Azzouz
(Co-supervisor/Co-directeur de thèse)

Dr. Ubi Wichoski
(Co-supervisor/Co-directeur de thèse)

Dr. Rizwan Haq
(Committee member/Membre du comité)

Dr. Hae-Young Kee
(External Examiner/Examinateur externe)

Approved for the Faculty of Graduate Studies
Approuvé pour la Faculté des études supérieures
Dr. David Lesbarrères
M. David Lesbarrères
Acting Dean, Faculty of Graduate Studies
Doyen intérimaire, Faculté des études supérieures

**ACCESSIBILITY CLAUSE AND PERMISSION TO USE**

## Abstract

Electron spin resonance (ESR) is an important experimental technique. A comprehensive theory of ESR has been difficult to establish, and as such several different approximations are used to predict and explain experimental results. This thesis applies the bond-mean-field theory to the problem of ESR frequency shift for the one-dimensional antiferromagnetic Heisenberg spin chain with uniaxial exchange anisotropy. We use this theory to calculate the ESR resonance frequency shift as a function of temperature and magnetic field. We perform numerical calculations using the expression obtained. These results are compared to existing results in the literature; they are in broad agreement with theoretical results such as those of Oshikawa and Affleck obtained via bosonisation, but they show discrepancies with experimental results. We agree with the theoretical authors that the discrepancy is due to our use of the simplest-case interaction model.



**Keywords**

ESR, spin lattices, bond-mean-field theory, solid state, magnetism, resonance, susceptibility

# Acknowledgements

I would like to thank my supervisor Dr. Mohamed Azzouz for much support and patience, as well as the other members of my committee, Drs. Rizwan Haq and Ubi Wichoski, for their feedback and assistance. I would additionally like to thank Dr. Hae-Young Kee for her commentary as external review member.

I would also like to thank all of my past teachers and professors for their instruction and guidance along the way.

# Dedication

To the memory of John Edward Buell and Ruth Cotter Rodger.

# Table of Contents

# List of Figures

# Chapter 1

## Introduction, Background, and Motivation

This section will introduce the topic of electron spin resonance (ESR). It begins with a definition of ESR and an explanation of the basic ESR theory (section 1.1), including the nature of the resonance frequency shift. This is followed by a review of the history of ESR (section 1.2), containing a history of theoretical models for calculating the resonance shift and a history of past and present experimental methods and materials. We then engage in a brief digression into applications of ESR analysis. Finally in light of the preceding we define our problem and present the motivation for our calculations.

## 1.1 Electron Spin Resonance

ESR is a spectroscopic technique that uses an applied magnetic field to break spin degeneracy, and using absorption to detect this energy level splitting. The topic of ESR is covered in

two areas. First is a definition and overview of the principles of ESR, with specific mention of the role of anisotropy in complicating analysis. Second is a derivation of the basic ESR frequency shift equations for the case of the antiferromagnetic Heisenberg spin chain.

### 1.1.1 Definition

ESR, also referred to as electron paramagnetic resonance (EPR), is an experimental technique used to study magnetic properties. It uses the interaction of magnetic moments in external magnetic fields to induce a split in the energy levels of a sample, and then measures that split by resonance absorption. ESR is very similar to Nuclear Magnetic Resonance (NMR), as the names suggest. Where NMR targets nuclei, ESR instead targets electrons (hence *electron* resonance rather than *nuclear* resonance) [1]. ESR is thus concerned with the interactions of an electron's spin. Spin angular momentum is a quantum property; electrons possess a spin value of one half – $S = 1/2$. They are therefore fermions, subject to the exclusion principle. For a spin of $S$, spin states along the axis of quantisation may exist in increments from $-S$ to $+S$. A free electron's spin state is therefore either $S = +1/2$ or $S = -1/2$.

Resonance techniques (such as ESR) use an applied energy input to probe the energy levels of a material. If this energy input matches the energy level separation in a substance, the input is absorbed and causes a transition in the material between energy states. Such

techniques therefore rely on the existence of an energy level differential within a substance. In an isolated (i.e., lone, non-interacting) system, electron spin does not affect energy - the two spin states of a single $S = 1/2$ electron are energetically degenerate. Microscopically, spin leads to magnetism. Due to its intrinsic spin, an electron also possesses a magnetic moment. This magnetic moment is given by

$$\mathbf{m}_S = \frac{g_S \mu_B \mathbf{S}}{\hbar} \ , \tag{1.1.1}$$

and the magnetic moment $\mathbf{m}_S$ is a function of the spin $\mathbf{S}$, proportional to the constant g-factor ($g_S$ for spin) and the Bohr magneton ratio ($\mu_B$). Because the electron spin may exist in either the spin up or spin down states ($S = \pm\hbar/2$), the magnetic moment is then

$$\mathbf{m}_S = \pm \frac{g_S \mu_B}{\hbar} \frac{1}{2} \ . \tag{1.1.2}$$

This magnetic moment will interact with an applied magnetic field. If a field $\mathbf{H}$ is applied (where $\mathbf{H} = H_z \hat{z}$, and we call the direction of the applied field the $z$ axis) then the energy

of the electron (due to this interaction) becomes

$$\begin{aligned} E &= \mathbf{m}_S \cdot \mathbf{h} \\ &= \frac{g_S \mu_B \mathbf{S}}{\hbar} \cdot \mathbf{h} \\ &= \frac{g_S \mu_B S_z}{\hbar} h_z \\ &= \pm \frac{g_S \mu_B h_z}{2} \ , \end{aligned} \tag{1.1.3}$$

with the lower energy, $E_- = -g_S \mu_B H_z/2$, as the unexcited level, and the higher energy, $E_+ = +g_S \mu_B H_z/2$, as the excited level, within the presence of the applied magnetic field. This is known as the Zeeman interaction. Therefore, the energy level splitting created by applying the magnetic field is

$$\begin{aligned} \Delta E &= \mathbf{m}_S \cdot \mathbf{h} \\ &= g_S \mu_B h_z \ . \end{aligned} \tag{1.1.4}$$

We illustrate this phenomenon in figure 1.1.

Within an atom, an electron's spin angular momentum may further couple to its orbital angular momentum. This total angular momentum $\mathbf{J}$ – equal to the summation, $\mathbf{J} = \mathbf{L} + \mathbf{S}$ – leads instead to a total magnetic moment of

$$\mathbf{m}_J = \frac{g_L \mu_B \mathbf{J}}{\hbar} \ . \tag{1.1.5}$$

If more than the spin is involved we use the Landé g-factor $g_L$ instead of the spin g-factor $g_S$.

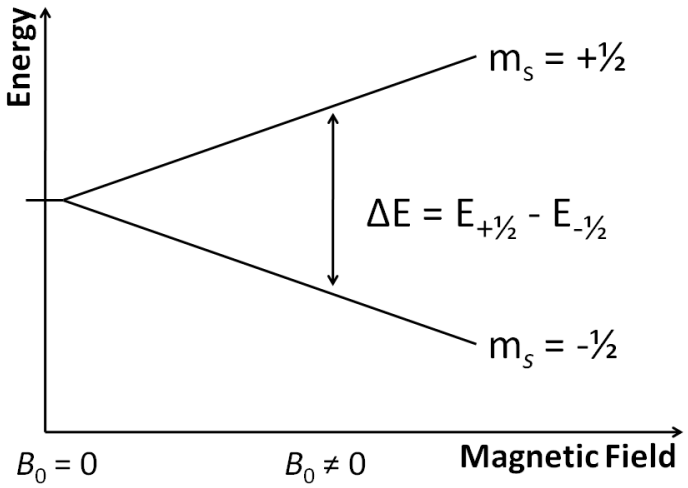


Figure 1.1: A demonstration of energy degeneracy breaking due to the Zeeman interaction. At zero applied field ($B_0 = 0$) there is only one energy level. Increasing $B_0 > 0$ separates the energies of the $S = +1/2$ and $S = -1/2$ states, in proportion to $B$ as in equation (1.1.4).

The number of states of the magnetic moment will therefore vary in accordance with the total angular momentum. This in turn will determine the number of, and separation between, energy levels within an applied magnetic field. In dealing with the Zeeman interaction for the purposes of ESR, there is no need to differentiate between the pure spin magnetic dipole moment, and the effective electron magnetic dipole moment due to total angular momentum, and in this work we therefore follow the literature in referring to the total angular momentum as the effective spin, unless the distinction must be made explicit – we state as shorthand that, e.g., the valence electron in a manganese(III) ion possesses effective spin $S = 5/2$. In all of our calculations in this work we only deal with $S = 1/2$ electrons, with no coupling of orbital angular momentum, but the effective spin is important in discussing the history of spin chain model compounds, as reviewed in section 1.2.2.

It is the energy difference – due to the Zeeman interaction – which is probed by the second incident field. The incoming field has energy $E = \hbar\omega$, and therefore, when this energy is equal to the energy gap, as

$$\hbar\omega = \Delta E \ , \tag{1.1.6}$$

it may be absorbed, producing resonance. The absorption is measured by the field intensity before and after passing through the sample. This electromagnetic field is usually a beam in the microwave range [1, 2]. For experimental purposes it is possible to vary either side of equation (1.1.6) – either the frequency or the size of the energy gap (proportional to the field strength). In the early history of ESR experiments, it was more common to fix the field strength (with a static magnet or electromagnet) and vary the frequency. Modern implementations use fixed frequency sources such as lasers and vary the field strengths with pulsed electromagnets.

ESR is only applicable to substances with unpaired or free electrons. This is because absorption occurs due to the transitions between split energy levels. Electrons are Fermions, and thus obey the Pauli exclusion principle: two electrons cannot exist in the same quantum state. Therefore if two electrons are present, an applied magnetic field will break the energy degeneracy between spin states, but both levels will be occupied, and no transition between them – and thus no absorption – can occur.

### 1.1.2 The Importance of Anisotropy

Under ideal, theoretical conditions, a single electron, or a system of non-interacting electrons, will exhibit the same energy levels and associated splitting, and the system's absorption will be a delta function at the exact resonance frequency. In real materials, the situation is more complicated. In addition to the Zeeman effect described above, other higher-order effects may contribute to the total energy separation, causing both a shift in and a broadening of the resonance frequency. This includes hyperfine coupling (interaction of the electron magnetic moment with the nuclear magnetic moment) and exchange interaction between electrons. Those interactions may be isotropic (rotationally or directionally invariant – symmetrical, or more rigorously, conforming to SU(2) symmetry) or anisotropic (dependent on orientation) [1].

The presence of isotropic interaction does not shift the resonance frequency. This is physically intuitive, as the energy gap – and thus the peak resonance frequency – is created by the symmetry-breaking spin-magnetic field coupling. The presence of anisotropy similarly breaks the symmetry of the isotropic system, and thus affects the size of the energy gap, and in turn, the corresponding resonance frequency. What isotropic interaction may do is split the absorption – higher order interactions causes further splitting of energy levels, beyond the primary split due to the Zeeman effect. This causes the energy differences to vary slightly

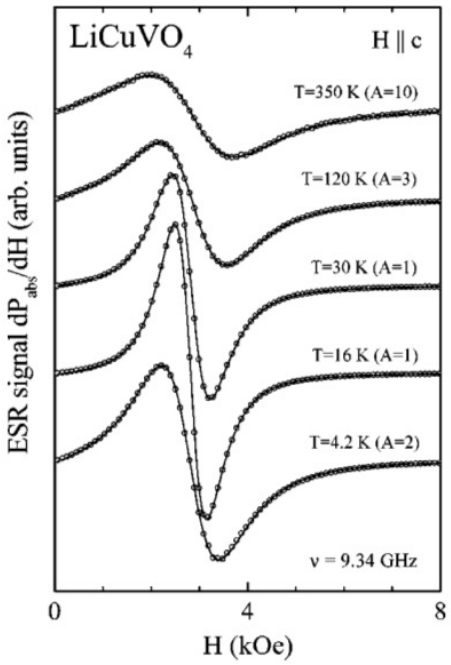


Figure 1.2: An example of an ESR spectrum, in this case for Lithium Copper(II) Vanadate [3]. Displayed is the first derivative of absorption, for several temperatures. Peak resonance is represented by the point at which the derivative curve crosses zero.

from the pure case above. Due to the selection rules for transitions, the usual effect is that the single resonance peak is split into two (or more) smaller peaks, symmetrically located about the single peak [1].

Systems also exhibit thermodynamic effects above the zero temperature limit. That is, values will begin to exhibit statistical variation. This causes broadening, and the resonance behaves as a generally Lorentzian curve rather than a pure delta function.

The presence of anisotropy results in a shift of frequency and a broadening of absorption

compared to isotropic models. All real systems exhibit some degree of anisotropy, due to a combination of intrinsic factors, such as dipole effects, and extrinsic factors, such as structural imperfections and inter-system coupling – it is not possible to construct real systems that are purely isotropic. A sample plot of absorption is displayed in figure 1.2, illustrating the resonance peak. The presence of anisotropy causes a shift in the peak resonance frequency from the idealised, isotropic case. The anisotropic case is therefore of experimental and theoretical interest.

### 1.1.3 The Antiferromagnetic Spin=1/2 Chain

A spin chain is a one-dimensional (1D) structure composed of interacting spins. In practice this arises from structures where there is much stronger interaction between electrons at sites along one axis of a substance than the others; some examples are given in section 1.2.2. In the ideal case each chain is sufficiently isolated from others that the interchain interactions are entirely negligible, and although this is unattainable, many substances have been found or synthesised which come close, with intrachain interaction orders of magnitude stronger than interchain interaction.

In this section we begin with the antiferromagnetic, anisotropic $S = ½$ chain, define its Hamiltonian, and derive the basic equations for the ESR resonance frequency shift. Much of the material in the following derivation is drawn from reference [4]. This derivation is

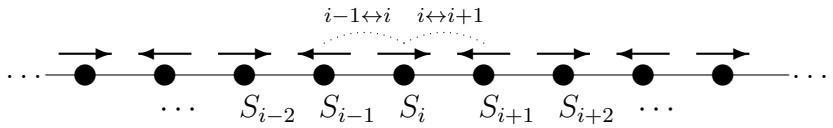


Figure 1.3: A spin chain in its ground state. Circles represent sites along the chain, and arrows the spins at those sites. This chain is antiferromagnetic, with alternating spins, and uniaxial, with spin quantised along the chain axis (defined as $z$). Spin $S_i$ interacts only with its nearest neighbours, $S_{i-1}$ and $S_{i+1}$.

accurate only to first order [5–7]. This level of accuracy, however, is sufficient for many cases of interest [8], including our calculations in this work.

We first consider the antiferromagnetic $S = 1/2$ Heisenberg chain, with an applied magnetic field $\mathbf{h}$ oriented along the chain (with the axis of the spin chain denoted as the $z$ axis). The Hamiltonian is defined as:

$$\mathcal{H} = -J \sum_{j=1}^{N} \left[ \left( S_j^x S_{j-1}^x + S_j^y S_{j-1}^y + S_j^z S_{j-1}^z \right) + \delta S_j^z S_{j-1}^z \right] - \sum_{j=0}^{N-1} \mathbf{S}_j \cdot \mathbf{h} \ . \tag{1.1.7}$$

In this case only nearest-neighbour interaction is considered. Often the Hamiltonian of a spin system is expressed as $\mathcal{H} = \mathcal{H}_0 + \mathcal{H}' + \mathcal{H}_Z$ [9]; that is, the total $\mathcal{H}$ in the presence of an external field is expressed as a combination of an isotropic term $\mathcal{H}_0$, an anisotropic term $\mathcal{H}'$, and the Zeeman term $\mathcal{H}_Z$. For the above Hamiltonian, this (after gathering isotropic and

anisotropic terms) breaks down into

$$\begin{aligned}\mathcal{H}_0 &= -J\sum_{j=1}^{N}\mathbf{S}_j\cdot\mathbf{S}_{j-1}\ .\\ \mathcal{H}' &= -J'\sum_{j=1}^{N}S_j^zS_{j-1}^z\ .\\ \mathcal{H}_Z &= -g\mu_Bh_z\sum_{j=0}^{N-1}S_j^z\ .\end{aligned}\tag{1.1.8}$$

Hereafter in this work we denote the anisotropic exchange constant as $J' \equiv \delta J$.

The simplest derivation for the resonance frequency, and its anisotropy-dependent shift, originates with reference [4], and proceeds directly from the above Hamiltonian, beginning with the Heisenberg equation of motion for $S^+$,

$$\imath\hbar\dot{S}^+ = [S^+, \mathcal{H}]\ . \tag{1.1.9}$$

It is assumed that $\dot{S}^+$ has a constant rate of change; that is, $\dot{S}^+ = \imath\omega S^+$ [4]. For the isotropic case, under the applied $h_z$ field, $S^+$ would oscillate at the Larmor frequency, which would then also be the resonant frequency; this is a consequence of the fact that $[S^+, \mathcal{H}] = [S^+, \mathcal{H}_Z]$ in the absence of any $\mathcal{H}'$ term. Following reference [4], we assume that for sufficiently small anisotropy $\mathcal{H}' \ll \mathcal{H}$, the contribution of $\mathcal{H}'$ is minimal: $[S^+, \mathcal{H}_Z] \gg [S^+, \mathcal{H}']$. Tnat is, we assume that the anisotropy may be treated as a perturbation, and that the first-order result is sufficiently accurate to proceed with [10]. With that assumption, the equation of motion

(1.1.9) is equivalent to

$$-\hbar\omega S^+ = [S^+, \mathcal{H}] \ . \tag{1.1.10}$$

So, taking the commutator with respect to $S^-$ of both sides,

$$-\hbar\omega[S^-, S^+] = [S^-, [S^+, \mathcal{H}]] \ ; \tag{1.1.11}$$

then, taking the thermal average,

$$\hbar\omega = \frac{\langle [S^-, [S^+, \mathcal{H}]] \rangle}{\langle 2S^z \rangle} \ , \tag{1.1.12}$$

since $[S^-, S^+] = -2S^z$. The above derivation represents a very simplistic treatment, but the general result is used throughout the literature [1, 4–6, 8–10].

## 1.2 History of ESR Analysis

We now proceed to review the historical development of ESR, first by examining analytical and theoretical approaches then by considering some of the experimental methods and materials used.

### 1.2.1 Theoretical Analysis

Electron Spin Resonance investigation has a long history. Early work was performed by Mori and Kawasaki [11, 12]. They noted the existence of the resonance frequency shift due to anisotropy as well as its effect on lineshape – anisotropy also leads to a broadening of the absorption spectrum. Similar work was also done by Kanamori and Tachiki at the same time [13]. Several years later Nagata and Tazuke [4] revised these methods to produce the familiar form for the ESR frequency,

$$\hbar\omega = \frac{\langle [S^-, [S^+, \mathcal{H}]] \rangle}{2\langle S^z \rangle} \ . \tag{1.2.1}$$

In this and other analyses $\mathcal{H}$ is assumed to be a modified Heisenberg hamiltonian as in equation (1.1.8). The authors note that only anisotropy $\mathcal{H}'$ in $\mathcal{H}$ contributes to the frequency shift - thus, the frequency appears as $\hbar\omega = \hbar\omega_0 + \Delta\hbar\omega$, and the frequency shift $\Delta\hbar\omega$ is given by

$$\Delta\hbar\omega = \frac{\langle [S^-, [S^+, \mathcal{H}']] \rangle}{2\langle S^z \rangle} \ . \tag{1.2.2}$$

The procedure used by each of the preceeding authors was to consider the anisotropy as a perturbation on the behaviour of the unperturbed isotropic spin chain Hamiltonian; these calculations were performed only to the first order. Nagata and Tazuke derived their result

from the dynamic magnetic susceptibility, given by

$$\chi_{+-}(\omega) = \left[\imath(g\mu_B)^2/\hbar\right] \int_{-\infty}^{\infty} dt\theta(t)\langle[S^-, S^+(t)]\rangle e^{\imath\omega t} \ . \tag{1.2.3}$$

Representing $\chi_{+-}$ with a Fourier series, they found the moments of resonance as

$$\mu_n = \int_{-\infty}^{\infty} \omega^n \mathrm{Im}\{\chi_{+-}(\omega)\} d\omega \ , \tag{1.2.4}$$

and obtained the resonance frequency equation (1.2.1) as $\hbar\omega = \hbar\frac{\mu_1}{\mu_2}$, resulting in $\hbar\omega \equiv \langle[S^-, [S^+, \mathcal{H}]]\rangle/2\langle S^z\rangle$. To calculate the value of the expressions such as (1.2.2), the classical approximation of the spins and spin interaction was used. The classical approach involves treating the spins as classical objects able to exist at any angle and angular momentum. The expressions derived by Mori and Kawasaki and confirmed by Nagata and Tazuke - equations (1.2.1) and (1.2.2) - have formed the starting point for much subsequent analysis [5, 6, 14]. As experimental techniques improved and compounds exhibiting spin chains and other spin lattices were synthesized, the need arose for more accurate theories of ESR, including anisotropy-induced ESR shift [15].

One more recent method is a field-theory approach based on bosonisation [5, 16]. The latter method is a procedure for transforming fermion problems into problems involving bosons. It is used where the bosonic representation is easier to manipulate or solve than the equivalent

fermionic representation. The authors Oshikawa and Affleck re-derived the expressions for ESR frequency shift, which they found to be similar to equation (1.2.2) but with an additional term, as

$$\Delta\hbar\omega = -\frac{\langle[[\mathcal{H}', S^+], S^-]\rangle - \mathrm{Re}\{G^R_{AA^\dagger}(\omega = h)\}}{2\chi h} \ . \tag{1.2.5}$$

For the low-field regime – as $h/J \to 0$ – the expression $\chi h$ evaluates as $\chi h \approx M_z \equiv \langle S^z \rangle$, reflecting the form given in other results, since the antiferromagnet exhibits zero magnetisation in the zero-field limit. This additional correction in equation (1.2.5), as compared to equation (1.2.2), arises from a more rigorous evaluation of the equations of motion, as $\dot{S}^\pm = \mp\imath h S^\pm \pm \imath A^{(\dagger)}$, where $A = [\mathcal{H}', S^+]$. The full solution to these equations requires the introduction of the Green's function:

$$G^R_{AA^\dagger}(t) = -\imath\theta(t)\langle[A(t), A^\dagger(0)]\rangle_0 \ , \tag{1.2.6}$$

and its Fourier transform (for $G^R_{AA^\dagger}(t) \to G^R_{AA^\dagger}(\omega)$).

To evaluate such expressions requires calculating the correlation functions, and the bosonisation is employed to do so. An in-depth consideration of the method is beyond the scope of the current work, but we include a brief overview of [5] here. The initial treatment is of the isotropic Hamiltonian $\mathcal{H}_0 = J\sum \vec{S}_j \cdot \vec{S}_{j+1}$. For this case, the free boson Lagrangian is

stated to be:

$$\mathcal{L} = \frac{1}{2}\left[(\partial_0\phi)^2 - (\partial_1\phi)^2\right] \ , \tag{1.2.7}$$

where $\phi$ represents the bosonic wave function. The subscripts denote $x^0 = \nu t$ and $x^1 = x$; the differentials, therefore, represent $\partial_0 = {}^{\partial}/_{\partial t}$ and $\partial_1 = {}^{\partial}/_{\partial x}$. At this point the additional terms are considered, as in equation (1.1.8). The introduction of the Zeeman term $\mathcal{H}_Z$ has the effect of adding the term

$$\mathcal{L}_Z = \frac{H}{\sqrt{2\pi}}\frac{\partial\phi}{\partial x} \tag{1.2.8}$$

to the bosonic Lagrangian. These then lead to the $S^{\pm}$ correlation functions, which are calculated in terms of bosonic current operators $J^{\alpha}_{R,L}$ (for left- and right-moving components) and confirm the isotropic resonance (a delta-function peak in the zero-temperature limit). At this point anisotropies are considered. The definition of exchange anisotropy in [5] is

$$\mathcal{H}' = \delta \sum_j S^n_j S^n_{j+1}, \tag{1.2.9}$$

which, for the simplest case of $n \equiv z$, is the same anisotropy we have considered in equation (1.1.8). The authors state that including the anisotropy as a perturbation, the Langrangian under the applied magnetic field is

$$\mathcal{L}_a = -\lambda J^z_R J^z_L - \frac{\lambda H}{\sqrt{2}}(J^z_R + J^z_L) - \frac{\lambda H^2}{2} \ . \tag{1.2.10}$$

The term $\lambda$ arises from the anisotropy; in terms of the bosonic current operators the total Hamiltonian – including anisotropic terms – is

$$\mathcal{H} = \mathcal{H}_0 - (g^x(J_R^x J_L^x + J_R^y J_L^y) + g^z J_R^z J_L^z) \ , \tag{1.2.11}$$

and $\lambda = -g^z + g^x$. Therefore $\lambda$ is directly proportional to the anisotropy $J'$ in the spin operator formulation. Using these bases the authors analyse each term in equation (1.2.10). The first leads of a renormalisation of the compactification radius, which does not affect the peak resonance frequency; neither does the third term, which is constant and independent of the current operators $J_{R,L}^{\alpha}$. The second perturbative term in equation (1.2.11) is evaluated by renormalisation of the applied magnetic field. This gives a shift in resonance frequency equal to $-2\pi\lambda H$, which is in turn linearly proportional to both the applied field $H$ and the anisotropy $J'$. The authors conclude with the observation that, because their calculations assume an overall Lorentzian lineshape, their bosonisation approach is only valid at low temperatures, because the lineshape is only Lorentzian for $T \ll J$.

An alternative method is to perform the calculations through direct numerical simulation. This avoids the problem of potentially inaccurate simplifying assumptions, and is not limited to either high or low temperature regions. However, the number of spins which may be simulated is relatively small, with recent analyses using $N = 8$ [14] and $N = 16$ [17] (in 2002 and 2010 respectively). The latter authors suggest their method (valid at high temperatures)

complements the low-temperature field theory approach of reference [5].

The properties of the isotropic spin-1/2 chain (the Heisenberg model) may be calculated exactly by means of the Bethe ansatz method in the ground state ($T \to 0$). This result may also be used as a starting point for analysing the frequency shift due to anisotropic perturbations [6]. In the article by Maeda, Sakai, and Oshikawa [6], the expression (1.2.2) is once again derived from the dynamical magnetic susceptibility, $\chi$, as

$$\Delta\hbar\omega_{\sigma\sigma} = \frac{\int_0^\infty d\omega\omega\chi''_{\sigma\sigma}(\omega)}{\int_0^\infty d\omega\chi''_{\sigma\sigma}(\omega)} - h \ . \tag{1.2.12}$$

Here, $\chi''$ gives the imaginary part of the susceptibility $\chi = \chi' + \imath\chi''$, and $\sigma$ represents the polarisation. This may be compared to the earlier result of Nagata and Tazuke in equation (1.2.3): in general, $\chi = \chi_{zz} + \chi_{+-}$. For the magnetic field $\mathbf{h} = h_z\hat{z}$, it is assumed for simplicity that $\sigma \in \{x, y\}$. The integral in the numerator is equivalent to to $-\pi\langle[[\mathcal{H}, S^\sigma], S^\sigma]\rangle/2$, but the integral in the denominator cannot be calculated analytically. When calculated perturbatively, the result is

$$\Delta\hbar\omega_{\sigma\sigma} = -\frac{\langle[[\mathcal{H}', S^+], S^-]\rangle}{2\langle S^z\rangle} + O(\mathcal{H}'^2) \ , \tag{1.2.13}$$

where the first order result is equivalent to equation (1.2.2). Evaluating this expression for

the anisotropic chain results in the expression

$$\Delta\hbar\omega \propto Y(T,H) = \frac{\langle S_j^z S_{j+1}^z - S_j^x S_{j+1}^x \rangle}{\langle S_j^z \rangle} \ . \tag{1.2.14}$$

Because the averages $\langle \dots \rangle$ are evaluated with respect to the unperturbed (isotropic) Hamiltonian, this may be evaluated with the Bethe ansatz technique. Plots of these results are included in chapter 4.2.1, where they are compared to the calculations performed in this work.

The resonance frequency, and the resonance frequency shift, can also be determined from the absorbed power [7]. Absorbed power $Q$ is defined as

$$Q = \frac{1}{N}\frac{\partial \langle \mathcal{H} \rangle}{\partial t} \ , \tag{1.2.15}$$

where the brackets $\langle \dots \rangle$ denote the average against the system's density matrix. The absorption $Q$ is calculated from the quantum Boltzmann equations, giving consistency equations of the form $\imath\hbar\langle \dot{S}^{(z,\pm)} \rangle = f(\langle S^z \rangle, \langle S^+ \rangle, \langle S^- \rangle)$. In [7], this is first considered for the isotropic case, and then extended to the anisotropic case, with anisotropy defined as follows:

$$\mathcal{H}' = -\sum_{i,k} A_k S_i^z S_{i+k}^z \ . \tag{1.2.16}$$

This is equivalent to the anistropy introduced in equation (1.1.8), if only nearest-neighbour

$(k \equiv 1)$ interactions on the $n \equiv z$ axis are considered.

Spin chains are of particular interest in ESR analysis because they are the simplest structures, but also because some more complicated structures may be mapped onto effective spin chain Hamiltonians, particularly spin ladders [18]. A recent review of ESR behaviour [19] summarizes the current approaches, although the frequency shift is not directly addressed. Most prominent is numerical calculation via the method of the density matrix renormalisation group. The authors also utilise the Bethe ansatz method used in [6], as well as the bosonisation technique of [5].

The difficulty in these analyses lies in calculating the multi-term correlation functions between spin operators [5, 8, 20]. In the absense of exact analytical methods, a variety of approximations and numerical methods must be used. The goal of the present work is to determine how closely the results of the bond mean-field theory resemble the existing results and current data.

### 1.2.2 Experimental Analysis

The fundamental ESR relation is given by:

$$\hbar\omega \simeq g\mu_B h \ . \tag{1.2.17}$$

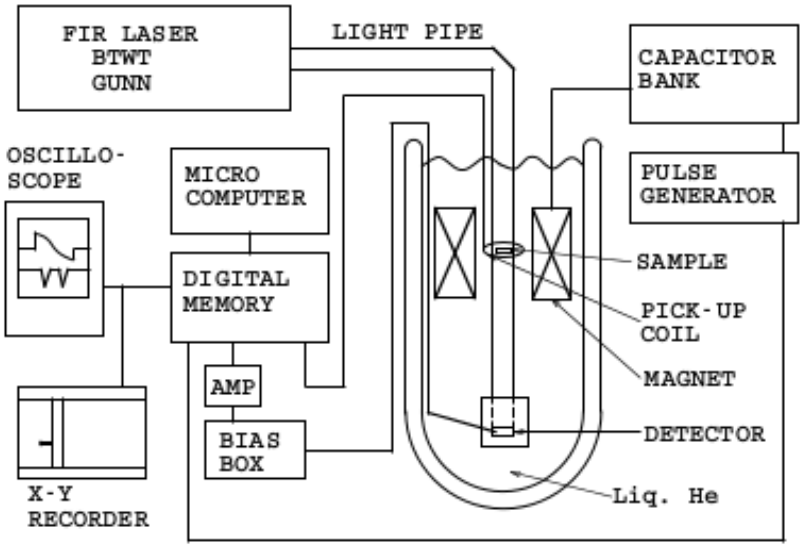


Figure 1.4: A block diagram of a generic ESR apparatus [2]. The magnetic field is provided by pulsed electromagnets, and the sample is probed with a fixed-frequency source – possible examples are lasers in the far infrared or microwave range, or a backward travelling wave tube.

Experimentally, ESR is a measure of absorption, and therefore any implementation will involve passing an electromagnetic signal (of frequency $\omega$) through a sample. If the energy of the signal ($\hbar\omega$) matches the induced energy gap ($\Delta E$), absorption will occur. By comparing the intensity of the signal before and after passing through the sample, the absorbed intensity can be determined. Figure 1.4 (from reference [2]) shows a generic experimental setup, illustrating the components of modern ESR implementations. ESR must be performed at low temperatures ($T < 100K$). The experiment may be set up in different ways – either $\omega$ or $h$ in equation (1.2.17) may be varied. Because it is easier to generate a fixed frequency, it is more common to vary the magnetic field strength. This is shown in Figure 1.5.

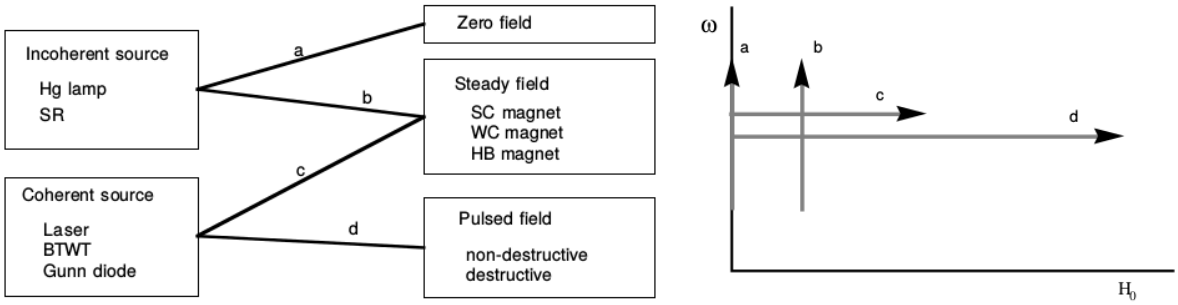


(a) (b)

Figure 1.5: A comparison of possible modes of ESR analysis [2]. Either the magnetic field strength is held and the frequency source swept (as in modes $a$ or $b$), or the frequency is fixed and magnetic field strength varied (as in modes $c$ or $d$).

There are a number of compounds that have been found to contain low-dimension spin systems. Some of the first such compounds discovered, known from the 1960s, incorporate manganese(II) ions ($Mn^{2+}$) with active spin $S = 5/2$ electrons [21]; an example is tetramethylammonium manganese(II) chloride (chemical formula: $N(CH_3)_4MnCl_3$, and usually denoted TMMC). Ions such as copper(II) ($Cu^{2+}$) or vanadium ($V^{4+}$) contain $S = 1/2$ valence electrons, which allows for $S = 1/2$ spin lattices exhibiting more purely quantum behaviour [3,22], compared to the $S = 3/2$ or the $S = 5/2$ compounds first studied. Two examples of copper-based compounds are copper benzoate (chemical formula: $Cu(C_6H_5COO)_2 3\,H_2O$) and lithium copper(II) vanadate (chemical formula: $LiCuVO_4$). These three compounds – TMMC, copper benzoate, and lithium copper(II) vanadate – are now described in some additional detail as exemplars.

In TMMC, linear chains are formed by manganese ions surrounded by chlorine, and these

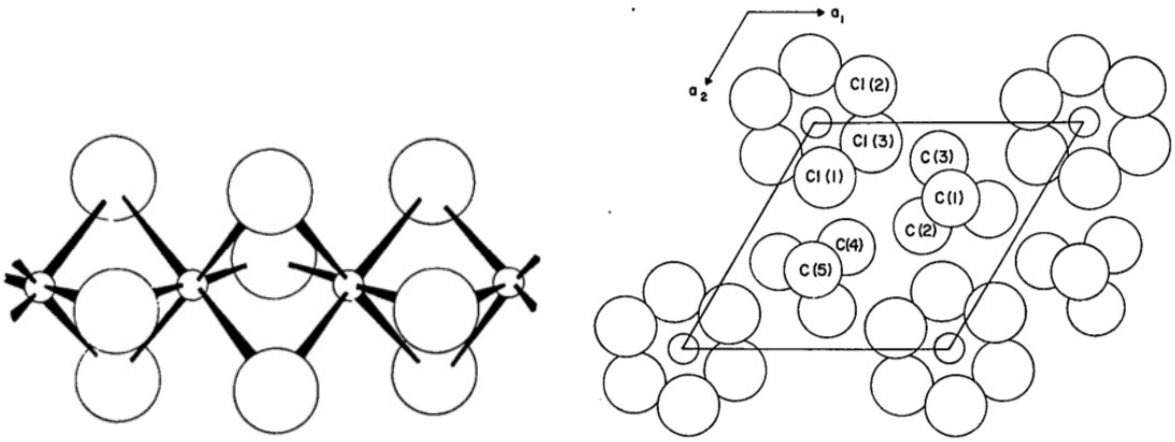


(a) (b)

Figure 1.6: Structure of TMMC. Figure 1.6(a) illustrates the manganese S=5/2 chains found in TMMC; small spheres represent manganese atoms and large spheres chlorine atoms. Figure 1.6(b) shows how these chains are arranged. The chains exist along crystal axis $c$, with ammonium ions occupying the space between them [23].

chains are interspersed with ammonium ions, as illustrated in Figure 1.6. TMMC exhibits a very pure one-dimensional spin chain (with low strength interchain coupling), but the interacting electrons provided by the manganese atoms possess $S = {}^5\!/_2$ [23]. As such the quantum effects are less dominant and the classical approximation is a very good model for its experimental results [4] (since $S = {}^n\!/_2 \rightarrow S = \infty$ is the classical limit).

Copper benzoate exhibits near-ideal $S = {}^1\!/_2$ antiferromagnetic linear spin chain behaviour [24]. It forms a base-centred monoclinic lattice, with copper ions ($Cu^{2+}$) providing the active electrons, as depicted in Figure 1.7. The strongest exchange interaction occurs between spins located at copper sites along the crystal axis c; interchain coupling is negligible due to the much greater separation along crystal axis b, and the much greater superexchange between copper sites along axis c than across axis a due to the asymmetry of the unit octahedra.

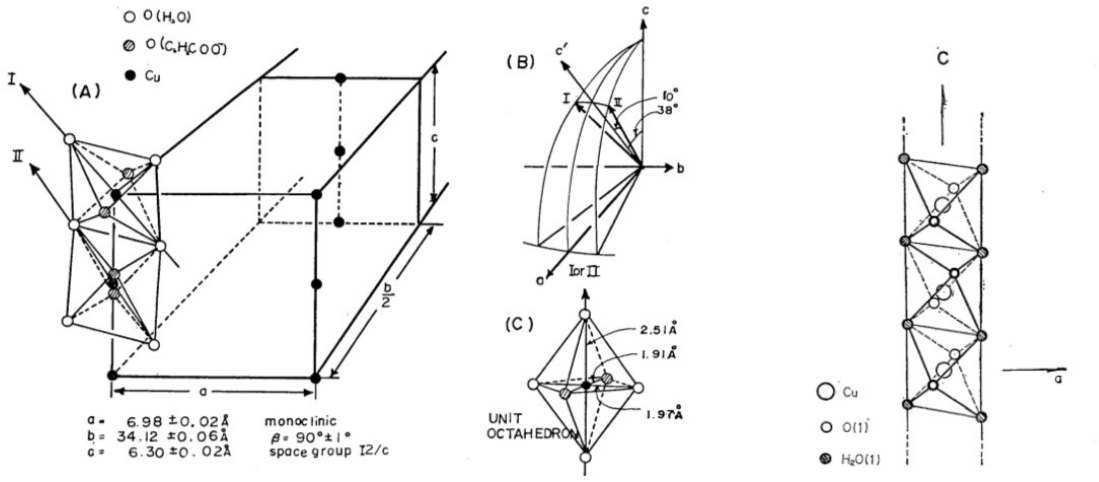


(a) (b)

Figure 1.7: Crystal structure of copper benzoate. Point representations are as indicated. Figure 1.7(a) shows the octahedral unit cell in subfigure (C) and the general structure in subfigure (A); the unit cell contains two benzoate vertices and four water vertices, leading to asymmetry as illustrated in subfigure (B). Figure 1.7(b) emphasises the chain structure arising from the arrangement of cells [25].

ESR analysis of copper benzoate behaviour was a long-standing difficulty [5,21], because the classical approximations [4,12,13] did not provide a very good fit for the data [24].

Another substance exhibiting a chain-like S=1/2 structure is lithium copper(II) vanadate ($LiCuVO_4$) [3,22]. As with copper benzoate, the active spin=1/2 electrons are provided by $Cu^{2+}$ ions. It possesses an inverse spinel structure of lithium ($Li^+$) and copper ($Cu^{2+}$) ions surrounded by oxygen in octahedra, with non-magnetic vanadium ($V^{5+}$) ions infilling surrounded by oxygen tetrahedra. The octahedra form chain structures which appear as alternating layers of rod-like arrangements. The crystal structure is illustrated in Figure 1.8. Oxygen-mediated superexchange between copper sites along crystal axis b is the dominant interaction, leading to the strongly chain-like behaviour.

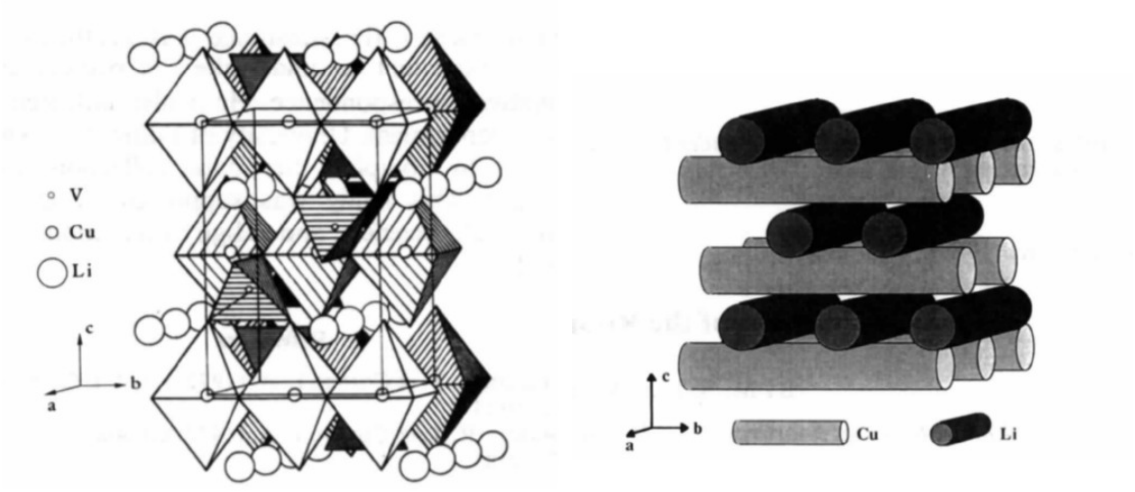


(a) (b)

Figure 1.8: Crystal structure of lithium copper(II) vanadate. The difficulty in describing a unit cell for figure 1.8(a) leads to the rod packing model depicted in figure 1.8(b). The tetrahedra around the vanadium ions and the octahedra around the copper and lithium ions share oxygen as vertices [26].

As mentioned in section 1.1.2, all real systems exhibit some degree of anisotropy; these anisotropies are due to a variety of effects. The largest portion of these effects are due to spin-orbit coupling; this coupling breaks the SU(2) symmetry of the isotropic case [17, 27]. Spin-orbit coupling may lead to both symmetric and antisymmetric spin exchange anisotropy; we treat only the symmetric case in this work. Other symmetry-breaking effects include dipole interaction with surrounding sites.

In experimental data, ESR shift is often expressed by a relative $g$ value [2, 6]. This arises from the fundamental relation given above, $\hbar\omega \simeq g\mu_B h$. In the presence of a frequency shift $\hbar\omega \to \hbar\omega_0 + \Delta\hbar\omega$, this can be expressed as $(g + \Delta g)\mu_B h$.

### 1.2.3 Applications of ESR

It is also important to note the broader applications of ESR. The natural comparison is to NMR (as alluded to in chapter 1.1.1). In principle electron resonance is more sensitive for imaging and detection than nuclear resonance, because the frequency range for ESR is much higher than for NMR - on the order of 10 to $10^2$ GHz for ESR, compared to 10-100 MHz for NMR [1]. There are, however, several difficulties in implementing ESR in similar biomedical roles, in applications beyond crystallography and more purely theoretical investigation [28]. ESR is more limited in application, as it relies on unpaired electrons, and such unpaired electrons are only found in certain materials, whereas all substances contain nuclei. Many of these materials fall into two broad categories. The first is metallic and crystalline structures, such as the spin chains that are the focus of this spin lattice. Such structures are composed of regular lattices, with a single electron at each lattice site in some geometric arrangement, such as chains, ladders, and other, more complex arrangements. The second class of material is radicals, which are highly reactive chemical species with one or more unpaired valence electrons or dangling covalent bonds [28]. These radicals are of great importance in many areas of chemistry, since they are generally found as reaction intermediates.

Most biochemical processes occur through redox (reduction and oxidation) reactions - i.e., the transfer of free electrons. Radicals disrupt the balance between these, and this imbal-

ance (termed oxidative stress) can lead to damage to biological components such as lipids, proteins, RNA, and DNA [29]. Such oxidative damage via radicals is implicated in causing many forms of cancer, and is also associated with many aging processes [28]. Excess radicals can be introduced by many sources, such exposure to smoke, ozone, or asbestos, and particularly by exposure to radiation. ESR therefore presents a method for immediately assessing the effects of radiation, as radical detection would provide much more detailed information than a simple dosimeter [28].

There are several difficulties faced in detecting or imaging radicals, particularly in living subjects [28]. Due to their reactive nature they are generally short-lived. Cooling samples to very low temperatures increases their persistence but is evidenly inapplicable for living subjects. One method for overcoming this is through spin trapping. Spin trapping works by introducing compounds that are very likely to react to the radicals but are themselves more persistent; they bond with the species of interest, and the combined compound acts as a direct proxy for the presence of the original radical. Work to improve the half-life and reduce the toxicity of available spin trapping compounds is ongoing. ESR methods for radical detection are presently less developed than alternatives but offer significant promise [29]. A common class of spin trap compounds are nitrogen based compounds [30]. When these react, they generate nitroxide compounds, and ESR detection of these compounds allows for much greater sensitivity than competing methods such as spectroscopic analysis. Different spin traps may be tailored to detect different radicals and radical types; some detection systems

are sensitive enough. A significant obstacle to in-vivo use is that the spin trap compounds themselves may be harmful.

ESR may also be applied directly to certain biochemical molecules, provided they contain the appropriate electron configurations. One class particularly amenable to ESR is those compounds containing copper ions or cupric complexes [28]. As previously mentioned, such $Cu^{2+}$ ions are a common source of $S = 1/2$ single electrons. ESR is therefore a useful method for investigating the structure of such compounds.

The calculations in this thesis were for a class of spin lattice which does not occur in biochemical compounds, and this therefore represents a barrier to directly relating our results to the sorts of methods discussed in this section. In such networks the exchange interaction is dominant, and we consider in particular its anisotropies. However, in all real substances there are deviations from pure isotropy [1]; in organic compounds various fine and hyperfine interactions do lead to anisotropies [28], which may be considered by similar means. ESR techniques can also be used as they are in chemical and material science, to experimentally determine the type and magnitude of anistropies, by comparison to theoretical isotropic models (e.g. [31]), and this relies on the accuracy of models incorporating anisotropy.

## 1.3 Motivation

In the preceding sections we defined electron spin resonance and provided an outline of the basic principles involved (chapter 1.1). We then reviewed the theoretical and experimental history of the technique (chapter 1.2). Given the variety of theoretical models that exist, we must justify our subsequent calculations as offering something new.

As referred to above, the most accurate models existing in the literature are extremely computationally intensive, and consequently in some cases the original methods [4] are still used [22]. Our goal is to attempt a new method for calculating the ESR behaviour, and particularly the behaviour of the resonance frequency shift. We are prompted to use the bond-mean-field theory [32] (elaborated on in section 2.3) due to its physically intuitive nature; it is a technique for modelling interaction in terms of an alternating parameter, which is strongly reminiscent of the antiferromagnetic nature of the spin chains we wish to examine. It is our hope that by using the bond-mean-field theory to calculate the frequency shift expression, we will be able to reproduce the existing results for both theoretical and experimental analysis. The advantage of this approach would be to offer either more accurate calculations (than the original, semiclassical models of [4]) or simpler calculations (than the current computationally intensive models, using such methods as bosonisation or the Bethe ansatz).

# Chapter 2

## Theoretical Tools

In chapter 1, we introduced our topic and our motivation for considering it. This chapter contains a review of some of the mathematical and theoretical techniques to be used in our analysis. Section 2.1 contains an overview of the Jordan-Wigner transformation, section 2.2 reviews Fourier analysis, and section 2.3 reviews the bond-mean-field theory.

## 2.1 Jordan-Wigner Transformation

The application of the bond mean-field theory [32] to Hamiltonians such as the spin lattice considered in this thesis requires the spin operators to be expressed instead as fermionic operators. The method by which this substitution is accomplished is known as the Jordan-Wigner (JW) transformation [33]. This section contains with a review of the JW transformation, verifying explicitly some of the 1D results used in our later calculations.

### 2.1.1 Definition

The JW transformation is a method by which spin operators (which are bosonic) can be represented with fermionic operators, or vice versa. For spin-1/2 systems, it uses the following definitions. The spin down state, $S^z = -1/2$, is considered to be an empty state. The spin up state, $S^z = +1/2$, is considered to be an occupied state. Analogous to the raising and lowering operators, $S^+$ and $S^-$, which move between these states, we define the fermionic equivalents as $c^\dagger$ and $c$, the creation and annihilation operators respectively.

It is important to keep in mind the physical realities of the situation. The transformation is only an alternative method for modelling a system; the system's underlying properties should remain invariant. Therefore, the raising and lowering operators, and the creation and annihilation operators, can only be directly equated if that equation preserves all of the physical properties of the system. For single, isolated spins, it would be sufficient to set $S^{(\pm)} \equiv c^{(\dagger)}$ – that is, $S^- \equiv c$, and $S^+ \equiv c^\dagger$. For multiple particles, however, the commutation and anticommutation relations become important. Fermionic operators, by their nature, anticommute: $\{c_i, c_j\} = \{c_i^\dagger, c_j^\dagger\} = 0 \ \forall i, j$, and $\{c_i, c_j^\dagger\} = \delta_{i,j}$, with $\delta_{i,j}$ representing the Kronecker delta. However, spin operators at different sites do not anticommute; they commute, as $\left[S_i^{(\pm)}, S_j^{(\pm)}\right] = 0$ for $i \neq j$. To maintain the necessary relations, an additional exponential term is introduced into the substitution, known as the phase term or shift. This step is vital,

as the transform is a mathematical (and thus representational) tool, and does not reflect any change in the underlying physics. Thus, in order for the transformed expression to remain valid, it must inherit all of the properties and identities of the original expressions, in order to ensure that it represents the same physical situation. To resolve this incongruence, we define the transformation – including the necessary phase term – as:

$$\begin{aligned} S_i^- &= e^{\imath\pi\phi_i} c_i \ , \\ S_i^+ &= c_i^\dagger e^{-\imath\pi\phi_i} = \left(S_i^-\right)^\dagger \ . \end{aligned} \tag{2.1.1}$$

The phase factor, $\phi_i$, is defined as:

$$\phi_i = \sum_{j=1}^{i-1} n_j \equiv \sum_{j=1}^{i-1} c_j^\dagger c_j \ . \tag{2.1.2}$$

This additional term preserves the spin operator commutation relations between different sites, as is shown explicitly in the following section. The phase term is illustrated in figure 2.1. These identities naturally suggest the inverse transformation, as

$$\begin{aligned} c_i &= e^{-\imath\pi\phi_i} S_i^- \ , \text{ and} \\ c_i^\dagger &= S_i^+ e^{\imath\pi\phi_i} \equiv (c_i)^\dagger \ . \end{aligned} \tag{2.1.3}$$

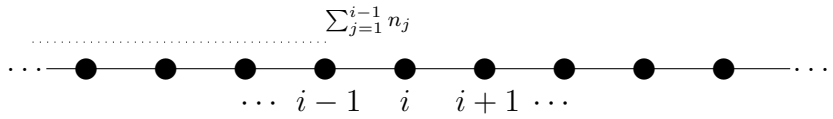


Figure 2.1: An illustration of the role of the phase factor. For site $i$, the phase term $e^{\imath\pi\phi_i}$ represents the occupation of each site from the origin up to $i-1$.

### 2.1.2 Commutator and Anticommutator Relations

In the definitions above, we have claimed that the JW transform satisfies spin commutator relations. This depends on the relation of the phase term ($e^{\imath\pi\phi_i}$) with the creation and annihilation operators – that is,

$$\begin{aligned} &[e^{\pm\imath\pi\phi_j}, c_i^{(\dagger)}] \text{ , and} \\ &\{e^{\pm\imath\pi\phi_j}, c_i^{(\dagger)}\} \end{aligned} \tag{2.1.4}$$

First, we note that phase factor for a single term, $j$: $e^{\pm\imath\pi n_j}$. Since $n_j$ refers to the occupancy of a single site, it must equal either 1 or 0. The exponent, then, is equal to $e^{\pm\imath\pi} = -1$ or $e^0 = 1$. Therefore,

$$e^{\pm\imath\pi n_j} \in \{-1, 1\} \rightarrow e^{\pm\imath\pi n_j} \equiv \left(1 - 2c_j^\dagger c_j\right) \ . \tag{2.1.5}$$

That is, the term equals 1 if site $j$ is occupied, and $-1$ if site $j$ is unoccupied. Consequently,

$$\begin{aligned} e^{\pm\imath\pi\phi_j} = e^{\pm\imath\pi\sum_{l=1}^{j-1} n_l} &= \prod_{l=1}^{j-1} e^{\pm\imath\pi n_l} \\ &= \prod_{l=1}^{j-1} \left(1 - 2c_l^\dagger c_l\right) \ . \end{aligned} \tag{2.1.6}$$

We may now expand the relations in equation (2.1.4), using the form given in equation (2.1.6).

We consider the commutator. From equation (2.1.1) we note that for site $i$, the phase term exponential will include terms up to $i-1$, and in expanding equation (2.1.4) we may assume $i \neq j$:

$$\begin{aligned}
[1-2c_j^\dagger c_j, c_i] &= \left(1-2c_j^\dagger c_j\right) c_i - c_i \left(1-2c_j^\dagger c_j\right) \\
&= c_i - c_i - 2c_j^\dagger c_j c_i + 2c_i c_j^\dagger c_j \\
&= 2c_i c_j^\dagger c_j - 2c_j^\dagger c_j c_i \\
&= 2\left(c_i c_j^\dagger c_j + c_j^\dagger c_i c_j\right) \\
&= 2\left(c_i c_j^\dagger + c_j^\dagger c_i\right) c_j = 2\{c_i, c_j^\dagger\} c_j \quad = 0 \ ,
\end{aligned} \tag{2.1.7}$$

using the fact that, since $\{c_i, c_j^\dagger\} = \delta_{i,j}$, we have $\{c_i, c_{j\neq i}^\dagger\} = 0$. The same result occurs if $c_i^\dagger$ is used in place of $c_i$ in the above equation, as $\{c_i^\dagger, c_j\}$ likewise equals $\delta_{i,j}$. Each term, therefore, commutes with its corresponding phase exponential. That is,

$$[e^{\pm \imath\pi\phi_i}, c_i] = [e^{\pm \imath\pi\phi_i}, c_i^\dagger] = 0 \ . \tag{2.1.8}$$

We then consider the complete relations, $[e^{\pm \imath\pi\phi_i} c_i^{(\dagger)}, e^{\pm \imath\pi\phi_j} c_j^{(\dagger)}]$, for $i \neq j$ – assuming for simplicity that in the following calculations, $i < j$. These must preserve the spin relations,

$[S_i^{(\pm)}, S_i^{(\pm)}] = 0$; spin operators at different sites commute.

$$
\begin{aligned}
[S_i^{(\pm)}, S_j^{(\pm)}] &= [e^{\pm\imath\pi\phi_i} c_i^{(\dagger)}, e^{\pm\imath\pi\phi_j} c_j^{(\dagger)}] \\
&= [c_i^{(\dagger)}, e^{\pm\imath\pi n_i} c_j^{(\dagger)}] \\
&= c_i^{(\dagger)} c_j^{(\dagger)} e^{\pm\imath\pi n_i} - e^{\pm\imath\pi n_i} c_j^{(\dagger)} c_i^{(\dagger)} \\
&= c_i^{(\dagger)} c_j^{(\dagger)} e^{\pm\imath\pi n_i} - e^{\pm\imath\pi n_i} c_j^{(\dagger)} c_i^{(\dagger)} + c_i^{(\dagger)} c_j^{(\dagger)} e^{\pm\imath\pi n_i} - c_i^{(\dagger)} c_j^{(\dagger)} e^{\pm\imath\pi n_i} \\
&= c_i^{(\dagger)} c_j^{(\dagger)} e^{\pm\imath\pi n_i} - c_j^{(\dagger)} e^{\pm\imath\pi n_i} c_i^{(\dagger)} - c_j^{(\dagger)} c_i^{(\dagger)} e^{\pm\imath\pi n_i} + c_j^{(\dagger)} c_i^{(\dagger)} e^{\pm\imath\pi n_i} \\
&= \{c_i^{(\dagger)}, c_j^{(\dagger)}\} e^{\pm\imath\pi n_i} - c_j^{(\dagger)} \{c_i^{(\dagger)}, e^{\pm\imath\pi n_i}\} \\
&= 0 \ ,
\end{aligned}
\tag{2.1.9}
$$

where in the first lines, we have already established that $e^{\pm\imath\pi\phi_i}$ commutes with all other terms, and may therefore be removed from the equation. Similarly, $e^{\pm\imath\pi\phi_j}$ contains the term $e^{\pm\imath\phi n_i}$, which is the only term in $e^{\pm\imath\pi\phi_j}$ which will not commute with all other terms, and is the only term left in the equation. The final step relies on the relation $\{c_i^{(\dagger)}, e^{\pm\imath\pi n_i}\}$, evaluated as follows:

$$
\begin{aligned}
\{c_i^{(\dagger)}, e^{\pm\imath\pi n_i}\} &= c_i^{(\dagger)} e^{\pm\imath\pi n_i} + e^{\pm\imath\pi n_i} c_i^{(\dagger)} \\
&= c_i^{(\dagger)} \left(1 - 2c_i^\dagger c_i\right) + \left(1 - 2c_i^\dagger c_i\right) c_i^{(\dagger)} \\
&= c_i^{(\dagger)} - 2c_i^{(\dagger)} c_i^\dagger c_i + c_i^{(\dagger)} - 2c_i^\dagger c_i c_i^{(\dagger)} \ ,
\end{aligned}
\tag{2.1.10}
$$

with the two cases as

$$\begin{aligned} c_i \to &= 2c_i - 2\{c_i, c_i^\dagger\}c_i \\ &= 2c_i - 2c_i \\ &= 0 \\ c_i^\dagger \to &= 2c_i^\dagger - 2c_i^\dagger\{c_i^\dagger, c_i\} \\ &= 2c_i^\dagger - 2c_i^\dagger \\ &= 0 \ , \end{aligned} \tag{2.1.11}$$

using the identity $\{c_i, c_i^\dagger\} = \{c_i^\dagger, c_i\} = 1$ (as $\delta_{i,i}$). We have now verified that the commutator between spin operators in their Jordan-Wigner transform representation maintain the correct commutation relations.

### 2.1.3 Example Application of the JW Transformation

To demonstrate the JW transformation we consider an analysis of the XY Hamiltonian, the simplest 1D case. This Hamiltonian is defined by

$$\mathcal{H}_{XY} = J \sum_i \left( S_i^x S_{i+1}^x + S_i^y S_{i+1}^y \right) \ . \tag{2.1.12}$$

The same terms as above also occur in the antiferromagnetic chain, as seen in equation (1.1.8). This example is therefore useful, as the terms in it will also be treated later on in

equation (3.1.7). Since the JW transformation is given above in terms of $S^-$, $S^+$, and $S^z$, the first step is to re-express the above equation, (2.1.12), in those terms, instead of $S^x$ and $S^y$. For this we use,

$$\begin{aligned} S_i^x &= \frac{1}{2}\left(S_i^+ + S_i^-\right) \\ S_i^y &= \frac{1}{2l}\left(S_i^+ - S_i^-\right) \ . \end{aligned} \tag{2.1.13}$$

The result of substituting the above into equation (2.1.12) is

$$\begin{aligned} \mathcal{H}_{XY} &= \frac{J}{4}\sum_i \left[\left(S_i^+ + S_i^-\right)\left(S_{i+1}^+ + S_{i+1}^-\right) - \left(S_i^+ - S_i^-\right)\left(S_{i+1}^+ - S_{i+1}^-\right)\right] \\ &= \frac{J}{4}\sum_i \left[S_i^+S_{i+1}^+ + S_i^+S_{i+1}^- + S_i^-S_{i+1}^+ + S_i^-S_{i+1}^- - S_i^+S_{i+1}^+ + S_i^+S_{i+1}^- + S_i^-S_{i+1}^+ - S_i^-S_{i+1}^-\right] \\ &= \frac{J}{2}\sum_i \left(S_i^+S_{i+1}^- + S_i^-S_{i+1}^+\right) \ . \end{aligned} \tag{2.1.14}$$

We then carry out the JW transformation, as defined in equation (2.1.1). This is done by a simple term by term substitution.

$$S_i^+S_{i+1}^- = c_i^\dagger e^{-\imath\pi\phi_i}e^{\imath\pi\phi_{i+1}}c_{i+1} \ , \tag{2.1.15}$$

and since

$$\begin{aligned} e^{-\imath\pi\phi_i}e^{\imath\pi\phi_{i+1}} &= e^{\imath\pi(\phi_{i+1}-\phi_i)} \\ &= e^{\imath\pi\left(\sum_j^i n_j - \sum_j^{i-1} n_j\right)} \\ &= e^{\imath\pi\left(\sum_j^{i-1}(n_j-n_j)+n_i\right)} \\ &= 1 - 2c_i^\dagger c_i \ , \end{aligned} \tag{2.1.16}$$

it is therefore true that

$$\begin{aligned} S_i^+ S_{i+1}^- &= c_i^\dagger c_{i+1}\left(1 - 2c_i^\dagger c_i\right) \\ &= c_i^\dagger c_{i+1} - 2c_i^\dagger c_{i+1} c_i^\dagger c_i \\ &= c_i^\dagger c_{i+1} \ , \end{aligned} \tag{2.1.17}$$

using the identities $\{c_i, c_j^\dagger\} = 0$ for $i \neq j$, and $c_i c_i = c_i^\dagger c_i^\dagger = 0$. We repeat the procedure with

$$\begin{aligned} S_{i+1}^+ S_i^- &= c_{i+1}^\dagger e^{-\imath\pi\phi_{i+1}} e^{\imath\pi\phi_i} c_i \\ &= \left(1 - 2c_i^\dagger c_i\right) c_{i+1}^\dagger c_i \\ &= c_{i+1}^\dagger c_i \ . \end{aligned} \tag{2.1.18}$$

Substituting these two terms, $S_i^+ S_{i+1}^- = c_i^\dagger c_{i+1}$ and $S_{i+1}^+ S_i^- = c_{i+1}^\dagger c_i$, our final result is the equation,

$$\mathcal{H}_{XY} = \frac{J}{2}\sum_i \left(c_i^\dagger c_{i+1} + c_{i+1}^\dagger c_i\right) \ . \tag{2.1.19}$$

### 2.1.4 Physical Correspondence

It is important to maintain correspondence with the physical situation being represented. In terms of spin operators, the XY Hamiltonian contains two terms as given in equation (2.1.14). Each term has the effect of transitioning two adjacent $S^z$ spins between their spin-up and spin-down states, as depicted in figure 2.2. In the Jordan-Wigner fermionic basis, the spin-up state is represented by the presence of a fermion, and the spin-down state by a vacant state. The two terms of the fermionic XY Hamiltonian, therefore, must also correspond to this situation. From equation 2.1.19, we see that the equivalent behaviour in the fermionic basis is the apparent motion – hopping – of the JW fermions [33].

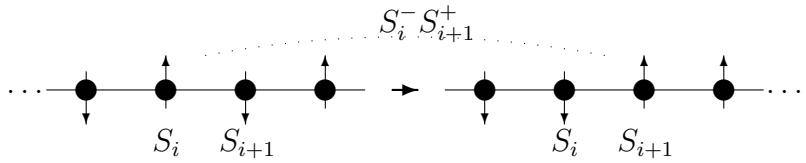


Figure 2.2: A diagram illustrating the action of the XY Hamiltonian terms on the spin chain. Each circle represents an active spin site, and the arrows represent the spin state at that site (that is, spin-up or spin-down). Depicted is the effect of the $S_i^- S_{i+1}^+$ term; the state before is given on the left, and the state after on the right.

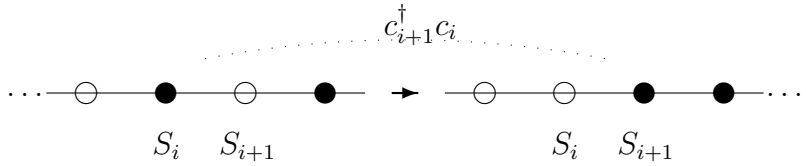


Figure 2.3: A diagram illustrating the action of the XY Hamiltonian terms on the chain, as represented by JW fermions after applying the JW transformation. An empty circle represents an empty site, corresponding to a spin-down state in the spin-operator basis, and a filled circle represents an occupied site, corresponding to a spin-up state. Depicted is the effect of the $c^\dagger_{i+1}c_i$ term; the state before is given on the left, and the state after on the right.

## 2.2 Transformation to Reciprocal Space

For physical systems a Fourier transform (with the corresponding inverse transform) is a method for representing a time-dependent system as a frequency-dependent one, or re-expressing a description of motion as a description of momentum; these are generally termed normal space and reciprocal space. We introduce the Fourier transform for JW fermions after considering the result above, equation (2.1.19). Although the switch to fermionic operators via the JW transformation simplifies the Hamiltonian, it does not yet give a complete solution, as the Hamiltonians are not yet diagonalized. One method for diagonalisation is to apply a Fourier transform to the fermionic Hamiltonian, moving from real space to k-space, in which the Hamiltonian does have a diagonal form, or at least one that is more easily diagonalised.

### 2.2.1 Definition

The Fourier transforms are as follows:

$$\begin{aligned} \hat{c}_k &= \frac{1}{\sqrt{N}} \sum_j e^{-\imath kj} c_j \\ \hat{c}_k^\dagger &= \frac{1}{\sqrt{N}} \sum_j e^{\imath kj} c_j^\dagger \text{ n} \end{aligned} \tag{2.2.1}$$

where $N$ represents the total number of sites in the lattice. This leads to the corresponding inverse transforms,

$$\begin{aligned} c_j &= \frac{1}{\sqrt{N}} \sum_k e^{\imath kj} \hat{c}_k \\ c_j^\dagger &= \frac{1}{\sqrt{N}} \sum_k e^{-\imath kj} \hat{c}_k^\dagger \ . \end{aligned} \tag{2.2.2}$$

These transformations map the position-space fermionic operators to the momentum-space fermionic operators.

### 2.2.2 Application

We return to the case of the XY Hamiltonian in its fermionic form, equation (2.1.19):

$$\mathcal{H}_{XY} = \frac{J}{2} \sum_i \left( c_i^\dagger c_{i+1} + c_{i+1}^\dagger c_i \right) \ . \tag{2.2.3}$$

After the JW transformation, the Hamiltonian remains non-diagonal. To further simplify it, we apply the Fourier transform defined above:

$$\begin{aligned}
\mathcal{H} &= \frac{J}{2}\sum_j \left[\frac{1}{N}\sum_k e^{-\imath kj}\hat{c}_k^\dagger \sum_{k'} e^{\imath k'(j+1)}\hat{c}_{k'} + \frac{1}{N}\sum_k e^{-\imath k(j+1)}\hat{c}_k^\dagger \sum_{k'} e^{\imath k'j}\hat{c}_{k'}\right] \\
&= \frac{J}{2N}\sum_j \left[\sum_{k,k'} e^{\imath k}e^{\imath j(k-k')}\hat{c}_k^\dagger\hat{c}_{k'} + \sum_{k,k'} e^{-\imath k}e^{\imath j(k'-k)}\hat{c}_k^\dagger\hat{c}_{k'}\right] \\
&= \frac{J}{2}\sum_k (e^{\imath k} + e^{-\imath k})\hat{c}_k^\dagger\hat{c}_k \\
&= J\sum_k \cos(k)\hat{c}_k^\dagger\hat{c}_k \ .
\end{aligned} \tag{2.2.4}$$

This Hamiltonian thus represents the spin excitations by hopping JW fermions. The above result makes use of the following identity for simplification:

$$\sum_j e^{\pm \imath j(k-k')} = N\delta_{k,k'} \ . \tag{2.2.5}$$

## 2.3 Bond Mean Field Theory

Mean field theory refers to a class of methods for modelling many-body systems, including those such as the spin lattices discussed in this thesis. These methods treat the systems as extensions of single body systems; this is done by representing interactions as if made up by a single average interaction acting on each body. Bond mean field theory, as per [32],

is a method for simplifying interaction. In this approach, calculations are simplified by modelling an alternating bond parameter $Q$ in place of calculating many separate two-body interactions.

### 2.3.1 Zero-field

We begin by considering the (isotropic) Heisenberg Hamiltonian:

$$\begin{aligned} \mathcal{H} &= J \sum_i \vec{S}_i \cdot \vec{S}_{i+1} \\ &= J \sum_i \left( S_i^x S_{i+1}^x + S_i^y S_{i+1}^y + S_i^z S_{i+1}^z \right) \end{aligned} \tag{2.3.1}$$

Applying the JW transformation, this becomes

$$\begin{aligned} \mathcal{H} &= \frac{J}{2} \sum_i \left( c_i^\dagger c_{i+1} + c_{i+1}^\dagger c_i \right) + J \sum_i \left( c_i^\dagger c_i - 1/2 \right) \left( c_{i+1}^\dagger c_{i+1} - 1/2 \right) \\ &= \frac{J}{2} \sum_i \left( c_i^\dagger c_{i+1} + c_{i+1}^\dagger c_i \right) + J \sum_i \left( c_i^\dagger c_i c_{i+1}^\dagger c_{i+1} - 1/2 \left( c_i^\dagger c_i + c_{i+1}^\dagger c_{i+1} \right) + 1/4 \right) \ . \end{aligned} \tag{2.3.2}$$

The chief difficulty in diagonalising this Hamiltonian is the quartic term, $c_i^\dagger c_i c_{i+1}^\dagger c_{i+1}$, without which diagonalisation is simple. We therefore we assume a mean field relation for the bond parameters to simplify calculation. The mean field assumption is that, for given operators $A$ and $B$, we treat their average values, and neglect the deviation from those average values

$\langle A\rangle$ and $\langle B\rangle$ - i.e.,

$$\begin{aligned}(\langle A\rangle - A)(\langle B\rangle - B) &\approx 0 \\ \rightarrow AB &\approx \langle A\rangle B + A\langle B\rangle - \langle A\rangle\langle B\rangle \ .\end{aligned} \tag{2.3.3}$$

In the present case of the quartic term in equation (2.3.2), we use the bond parameters $c_i c_{i+1}^\dagger$ and $c_i^\dagger c_{i+1}$, allowing us to express $c_i^\dagger c_i c_{i+1}^\dagger c_{i+1}$ as:

$$\begin{aligned}c_i^\dagger c_i c_{i+1}^\dagger c_{i+1} &\approx \langle c_i c_{i+1}^\dagger\rangle c_i^\dagger c_{i+1} + \langle c_i^\dagger c_{i+1}\rangle c_i c_{i+1}^\dagger - \langle c_i c_{i+1}^\dagger\rangle\langle c_i^\dagger c_{i+1}\rangle \\ &\approx \langle c_i c_{i+1}^\dagger\rangle c_i^\dagger c_{i+1} + \langle c_{i+1} c_i^\dagger\rangle c_{i+1}^\dagger c_i + \langle c_i c_{i+1}^\dagger\rangle\langle c_{i+1} c_i^\dagger\rangle \\ &\approx Q_i c_i^\dagger c_{i+1} + Q_i^* c_{i+1}^\dagger c_i + |Q_i|^2 \ .\end{aligned} \tag{2.3.4}$$

Reinserting this into equation (2.3.2), we find

$$\mathcal{H} = \frac{J}{2}\sum_i \left(c_i^\dagger c_{i+1} + c_{i+1}^\dagger c_i\right) + J\sum_i \left[Q_i c_i^\dagger c_{i+1} + Q_i^* c_{i+1}^\dagger c_i + |Q_i|^2 - \frac{1}{2}\left(c_i^\dagger c_i + c_{i+1}^\dagger c_{i+1}\right) + \frac{1}{4}\right] \ . \tag{2.3.5}$$

At this point we may drop the diagonal $c_i^\dagger c_i$ and $c_{i+1}^\dagger c_{i+1}$ terms as well as the constant term $1/4$; we shall reinstate them later on. We therefore have:

$$\mathcal{H} = \frac{J}{2}\sum_i \left[(1+2Q_i)\, c_i^\dagger c_{i+1} + (1+2Q_i^*)\, c_{i+1}^\dagger c_i\right] + JN|Q_i|^2 \ . \tag{2.3.6}$$

If $Q$ is assumed to be real and constant ($Q_i \in \Re \rightarrow Q_i = Q_i^* = Q$), then this produces an energy spectrum as a function of cosine, which may be seen by applying the Fourier transform.

$$\begin{aligned}\mathcal{H} &= JN|Q|^2 + \frac{J(1+2Q)}{2}\sum_j \left[\frac{1}{N}\sum_{k,k'} \hat{c}_k^\dagger \hat{c}_k e^{\imath jk'} e^{\imath j(k-k')} + \frac{1}{N}\sum_{k,k'} \hat{c}_k^\dagger \hat{c}_k e^{-\imath k} e^{\imath j(k-k')}\right] \\ &= JN|Q|^2 + \frac{J(1+2Q)}{2}\sum_k \left(e^{\imath k} + e^{-\imath k}\right)\hat{c}_k^\dagger \hat{c}_k \\ &= JN|Q|^2 + J(1+2Q)\sum_k \cos(k)\hat{c}_k^\dagger \hat{c}_k \ .\end{aligned} \tag{2.3.7}$$

To accurately reproduce prior theoretical results – for the antiferromagnetic spin chain, the energy spectrum is given by the absolute value of the sine function, not cosine [34] – we must slightly modify the Hamiltonian to include an alternating phase term. That is, instead of a prefactor $J_1 = J(1+2Q)\ \forall i$, and recalling that $J > 0$ for the antiferromagnetic case, we use $(-1)^i J_1$ [32]. Therefore, our Hamiltonian becomes:

$$\mathcal{H} = \frac{J_1}{2}\sum_i \left[\left(c_{2i}^\dagger c_{2i+1} + c_{2i+1}^\dagger c_{2i}\right) - \left(c_{2i+1}^\dagger c_{2i+2} + c_{2i+2}^\dagger c_{2i+1}\right)\right] + JN|Q|^2 \ . \tag{2.3.8}$$

To preserve the distinction between alternating states, we treat them as a sublattice, with unique creation and annihilation operators on each (termed A and B). That is, sites with even indices $2i$ are treated as sublattice A, and sites with odd indices $2i+1$ are treated as

sublattice B. This produces the following:

$$\begin{aligned}\mathcal{H} = \frac{J_1}{2}\sum_j \Bigg[ &\frac{1}{N}\sum_{k,k'}\left(\hat{c}_k^{A\dagger}\hat{c}_{k'}^{B}e^{\imath k'}e^{\imath j(k'-k)}\right) + \frac{1}{N}\sum_{k,k'}\left(\hat{c}_k^{B\dagger}\hat{c}_{k'}^{A}e^{-\imath k}e^{\imath j(k'-k)}\right) \\ -&\frac{1}{N}\sum_{k,k'}\left(\hat{c}_k^{B\dagger}\hat{c}_{k'}^{A}e^{\imath k'}e^{\imath j(k'-k)}\right) - \frac{1}{N}\sum_{k,k'}\left(\hat{c}_k^{A\dagger}\hat{c}_{k'}^{B}e^{-\imath k}e^{\imath j(k'-k)}\right)\Bigg] + JN|Q|^2\end{aligned} \tag{2.3.9}$$

$$\begin{aligned}\mathcal{H} &= \frac{J_1}{2}\sum_k \left(\hat{c}_k^{A\dagger}\hat{c}_k^{B}\left(e^{\imath k}-e^{-\imath k}\right) + \hat{c}_k^{B\dagger}\hat{c}_k^{A}\left(e^{-\imath k}-e^{\imath k}\right)\right) + JN|Q|^2 \\ &= J\left(1+2Q\right)\sum_k \imath\sin(k)\hat{c}_k^{A\dagger}\hat{c}_k^{B} - \imath\sin(k)\hat{c}_k^{B\dagger}\hat{c}_k^{A}\ ,\end{aligned} \tag{2.3.10}$$

given the relations

$$\sum_j e^{\imath j(k-k')} = \delta_{k,k'}N\ , \tag{2.3.11}$$

for integer $j$, and

$$\sin(k) = \frac{e^{\imath k}-e^{-\imath k}}{2\imath}\ . \tag{2.3.12}$$

This is alternatively expressed in matrix form as

$$\mathcal{H} = \sum_k \begin{pmatrix}\hat{c}_k^{A\dagger}\\ \hat{c}_k^{B\dagger}\end{pmatrix}^{\tau}\begin{pmatrix}0 & e(k)\\ e^*(k) & 0\end{pmatrix}\begin{pmatrix}\hat{c}_k^{A}\\ \hat{c}_k^{B}\end{pmatrix} \tag{2.3.13}$$

with $e(k)$ defined as $e(k) = \imath J(1+2Q)\sin(k)$ – and therefore $e^*(k) = -e(k)$. In this form, energy eigenvalues are obtained through diagonalisation of the matrix contained in

the Hamiltonian. To determine the eigenvalues,

$$\begin{vmatrix} -E & e(k) \\ e^*(k) & -E \end{vmatrix} = E^2 - |e|^2 = 0 \tag{2.3.14}$$
$$\rightarrow E = \pm|e(k)| \ ,$$

and we determine the value of $e(k)$ as

$$\begin{pmatrix} 0 & e(k) \\ e^*(k) & 0 \end{pmatrix} = J(1+2Q)\sin(k) \begin{pmatrix} 0 & \imath \\ -\imath & 0 \end{pmatrix} \ , \tag{2.3.15}$$

where the latter matrix has eigenvalues of $\pm 1$, and therefore the overall eigenvalues are equal to $E_\pm(k) = \pm|J(1+2Q)\sin(k)|$.

With this established, we proceed to determine the partition function $Z$, the free energy (per particle) $f$, and finally an equation for $|Q|$ itself. We refer to the Brillouin zone to establish boundary conditions for $k - -\pi/a < k < \pi/a$, where we normalise $a \equiv 1$ for simplicity. The partition function is therefore

$$Z = \prod_k \left(1 + e^{-\beta E_+(k)}\right) \prod_k \left(1 + e^{-\beta E_-(k)}\right) e^{-\beta E_c} \ , \tag{2.3.16}$$

with $E_\pm$ as established above, and $E_c = JN|Q|^2$. Then,

$$\begin{aligned} f &= \frac{-k_B T}{N} \ln(Z) \\ &= JQ^2 - \frac{1}{2\beta} \int \frac{dk}{2\pi} \sum_{\alpha=\pm} \ln(1 + e^{-\beta E_\alpha}) \ . \end{aligned} \tag{2.3.17}$$

We may find $Q$ by minimizing $f$ with respect to $Q$, and solving for $Q$.

$$\frac{\partial f}{\partial Q} = 0 \to Q = -\frac{1}{2} \int \frac{dk}{2\pi} |\sin(k)| \sum_{\alpha=\pm} \frac{\alpha}{1 + e^{\beta E_\alpha(k)}} \ . \tag{2.3.18}$$

Intermittent steps omitted from the above calculations are included in appendix A.1, as equations (A.1.1) and (A.1.2) respectively.

Before moving to the non-zero field case, we consider the temperature limits of $Q$, beginning with the low temperature limit (that is, $T/J \to 0$). We begin with the free energy equation, (2.3.17). The relevant term is $e^{-E_\alpha(k)/k_B T} \equiv e^{a/T}$, where $a = -E_\alpha(k)/k_B$. This free energy then depends on the evaluation of

$$\lim_{T \to 0} \left[ T \ln(1 + e^{a/T}) \right] \ . \tag{2.3.19}$$

This is zero if $a < 0$ – the term involving $E_+(k)$. Only the term involving $E_-(k)$ (in which $a > 0$) contributes. This is expected – at zero temperature, the system should be in its ground state, with only the lower energy band occupied, and the higher energy band unoccupied.

This form – $\lim_{T\to 0}[T\ln(1+e^{a/T})]$ – is indeterminate, but may be evaluated – see equation (A.1.3) – as

$$\lim_{T\to 0}\left[T\ln(1+e^{a/T})\right] \equiv \lim_{T\to 0}\left[\frac{e^{a/T}}{1+e^{a/T}}a\right] = a = \frac{E_{-}(k)}{k_B}\ . \tag{2.3.20}$$

Then, returning this result to the free energy expression given by equation (2.3.17),

$$\begin{aligned} f &= JQ^2 - \frac{k_B}{2}\int\frac{dk}{2\pi}\left(\frac{-J(1+2Q)|\sin(k)|}{k_B}\right) \\ &= JQ^2 + \frac{J(1+2Q)}{4\pi}\int_{-\pi}^{\pi}|\sin(k)|dk \\ &= JQ^2 + \frac{J(1+2Q)}{\pi}\ , \end{aligned} \tag{2.3.21}$$

which leads to $Q$ by the same free-energy minimisation procedure as in equation (2.3.18):

$$\begin{aligned} \frac{\partial f}{\partial Q} &= 2JQ + \frac{2J}{\pi} \\ \frac{\partial f}{\partial Q} &= 0 \to Q = \frac{1}{2J}\frac{2J}{\pi} = \frac{1}{\pi}\ . \end{aligned} \tag{2.3.22}$$

The high temperature ($k_BT \gg J$) limit may be determined from equation (2.3.18) directly by Taylor series expansion. The term we are concerned with is

$$\sum_{\alpha=\pm 1}\frac{\alpha}{1+e^{\beta E_\alpha(k)}} \tag{2.3.23}$$

where $E_\alpha(k)$ is proportional to $J$. The Taylor expansion for $e^x$ about $x = 0$ is:

$$e^x \equiv \sum_{n=0}^{\infty} \frac{x^n}{n!} \ . \tag{2.3.24}$$

We proceed with the first term only, to find

$$\begin{aligned} Q &= -\frac{1}{2} \int \frac{dk}{2\pi} |\sin(k)| \left( \frac{1}{1 + (1 + \beta E_+(k))} - \frac{1}{1 + \beta E_-(k)} \right) \\ &= -\frac{1}{2} \int \frac{dk}{2\pi} |\sin(k)| \frac{1}{2} \left( \frac{1}{1 + \beta E(k)/2} - \frac{1}{1 - \beta E(k)/2} \right) \ . \end{aligned} \tag{2.3.25}$$

Here we once again use the first-order Taylor approximation. The terms $(1 \pm \beta E(k))^{-1}$ are equivalent to $(1 - x)^{-1}$, which is approximated by $(1 - x)^{-1} \approx 1 + x + x^2 + x^3 + \ldots$. Considering only the first order result,

$$\frac{1}{1 \pm \beta E(k)} \approx 1 \mp \frac{\beta E(k)}{2} \ . \tag{2.3.26}$$

In the high temperature limit, $Q$ is then given by

$$\begin{aligned} Q &= -\frac{1}{8\pi} \int dk |\sin(k)| \left(-\beta E(k)\right) \\ &= \frac{J(1 + 2Q)}{8\pi k_B T} \int |\sin^2(k)| dk \\ &= \frac{J + 2JQ}{8 k_B T} \ . \end{aligned} \tag{2.3.27}$$

$Q$ itself is obtained from this consistency equation, as

$$Q = \frac{J}{8k_BT}\frac{1}{1-4k_BT/J} \ . \tag{2.3.28}$$

### 2.3.2 Non-zero-field

With the presence of a magnetic field, we must make two changes to the Hamiltonian. The first is the inclusion of the Zeeman interaction term. The second is to account for the effect of magnetisation – the magnetic field induces a non-zero magnetisation in the chain, which provides an alternate means of decoupling $S_i^z S_{i+1}^z$. This is handled by introducing $M_z = \langle S_i^z \rangle$, the average magnetisation per site, and the term is expanded with the same mean-field assumption given by equation (2.3.3). This leads to

$$\begin{aligned} JS_i^z S_{i+1}^z &\approx J\langle S_i^z\rangle S_{i+1}^z + J\langle S_{i+1}^z\rangle S_i^z - J\langle S_i^z\rangle\langle S_{i+1}^z\rangle \\ &\approx JM_z c_i^\dagger c_i + JM_z c_{i+1}^\dagger c_{i+1} - JM_z(M_z+1) \ . \end{aligned} \tag{2.3.29}$$

This term is complementary to the Q-based decoupling given above; both are necessary to describe the correct behaviour in different regimes.

The fermionic Hamiltonian then becomes:

$$\begin{aligned}\mathcal{H} = J_1 \sum_i \left[ \frac{\left( c_i^\dagger c_{i+1} + c_{i+1}^\dagger c_i \right)}{2} - \frac{\left( c_{i+1}^\dagger c_{i+2} + c_{i+2}^\dagger c_{i+1} \right)}{2} \right] + JN|Q|^2 \\ + J \sum_i M_z \left( c_i^\dagger c_i + c_{i+1}^\dagger c_{i+1} \right) - h \sum_i \left( c_i^\dagger c_i - 1/2 \right) \ ,\end{aligned} \tag{2.3.30}$$

where $J_1$ is defined as above – $J_1 = J(1+2Q)$ – and $h = g\mu_B B$.

This Hamiltonian – equation (2.3.30) – is re-expressed using a Fourier transform, as was the zero-field Hamiltonain in equation (2.3.7) – further details are given appendix A.1. The result is most concisely expressed in matrix form, as

$$\mathcal{H} = JNQ^2 + Nh/2 - NJM_z(M_z+1) + \sum_k \begin{pmatrix} \hat{c}_k^{A\dagger} \\ \\ \hat{c}_k^{B\dagger} \end{pmatrix}^\tau \begin{pmatrix} 2M_zJ - h & e(k) \\ \\ e^*(k) & 2M_zJ - h \end{pmatrix} \begin{pmatrix} \hat{c}_k^A \\ \\ \hat{c}_k^B \end{pmatrix} \ , \tag{2.3.31}$$

with $e(k) = \imath J(1+2Q)\sin(k)$.

As in the zero-field case, the energy eigenvalues ($E$) are determined from the Hamiltonian matrix, to obtain

$$E \to E(k) = 2M_zJ - h \pm |e(k)| \ . \tag{2.3.32}$$

We may use the $E_\pm(k)$ expressions to find the per-particle free energy, $f$, and in turn $Q$. We

begin with the partition function $Z$:

$$Z = \prod_k \left(1 + e^{-\beta E_+(k)}\right) \prod_k \left(1 + e^{-\beta E_-(k)}\right) e^{-\beta E_c} \ , \tag{2.3.33}$$

where $E_c = NJQ^2 + Nh/2 - NJM_z(M_z + 1)$. We then obtain – through the calculations given in equation (A.1.8) – the free energy per site:

$$f = JQ^2 + \frac{h}{2} - JM_z(M_z + 1) - \frac{1}{2\beta} \int \frac{dk}{2\pi} \sum_{\alpha \in \{\pm 1\}} \ln(1 + e^{-\beta E_\alpha(k)}) \ . \tag{2.3.34}$$

We then proceed to determine $Q$ by setting $\partial f / \partial Q = 0$. We find:

$$Q = -\frac{1}{2} \int \frac{dk}{2\pi} |\sin(k)| \sum_\alpha \frac{\alpha}{1 + e^{\beta E_\alpha(k)}} \ , \tag{2.3.35}$$

which has the same form as in the zero-field case, and $h$ dependence is implicit in the eigenenergies. $M_z$ is determined through similar means:

$$\begin{aligned} M_z &= -\frac{\partial f}{\partial h} \\ M_z &= \frac{1}{2} \int \frac{dk}{2\pi} \sum_\alpha \frac{1}{1 + e^{\beta E_\alpha(k)}} - \frac{1}{2} \ . \end{aligned} \tag{2.3.36}$$

The derivation of equations (2.3.35) and (2.3.36) is given in greater detail by equations (A.1.9) and (A.1.10). The zero-field limit of the above equations – $\lim_{h \to 0}$ – returns the explicity derived zero-field equations as given in the previous subsection.

# Chapter 3

## Calculation of the ESR Frequency Shift

Here we return to the expression for the ESR frequency shift derived earlier in section 1.1.3 as equation (1.1.12); namely:

$$\hbar\omega = \frac{\langle [S^-, [S^+, \mathcal{H}]] \rangle}{\langle 2S^z \rangle} \ . \tag{3.0.1}$$

In this chapter we proceed to evaluate it. We begin with the algebraic expansion of the commutator terms; we then use the JW transformation and the bond-mean-field theory to express our result in fermionic terms and apply the simplifying approximations leading to our final result.

The algebraic calculations in section 3.1, which we have detailed here and in section A.2 of the appendix, are implicit in the literature, where the evaluation of these expressions is regularly reproduced without the intermediate steps. That is, from an initial statement such as equation (1.1.12), our references immediately present results such as equation (3.1.9) – as

referred to in section 3.1.1.

## 3.1 Algebraic Expansion

The first-order expression for the ESR frequency was determined in equation (1.1.12) of section 1.1. Because of the linearity of the commutator, it is possible to separate this expression into three components using the Hamiltonian as given in equation (1.1.8): $\mathcal{H}_0$, $\mathcal{H}'$, and $\mathcal{H}_Z$, representing respectively the isotropic, anisotropic, and Zeeman terms. The frequency is therefore as follows:

$$\begin{aligned}\hbar\omega &= \frac{\langle[S^-,[S^+,\mathcal{H}]]\rangle}{\langle 2S^z\rangle} \\ &= \frac{\langle[S^-,[S^+,\mathcal{H}_0+\mathcal{H}'+\mathcal{H}_Z\rangle}{\langle 2S^z\rangle} \\ &= \frac{\langle[S^-,[S^+,\mathcal{H}_0]]+[S^-,[S^+,\mathcal{H}']]+[S^-,[S^+,\mathcal{H}_Z]]\rangle}{\langle 2S^z\rangle}\ .\end{aligned} \tag{3.1.1}$$

In this and similar expressions, operators without indices are implicit summations, as $S^- \equiv \sum_i S_i^-$.

The commutator algebra employed in expanding this expression is involved, and is carried out in full in section A.2 of the appendix. The key results are as follows. For $[S^-,[S^+,\mathcal{H}_Z]]$

we obtain the results of equation (A.2.1):

$$[S^-, [S^+, \mathcal{H}_Z]] \equiv 2g\mu_B h S^z \ . \tag{3.1.2}$$

For $[S^-, [S^+, \mathcal{H}_0]]$ we obtain from equation (A.2.12):

$$[S^-, [S^+, \mathcal{H}_0]] \equiv 0 \ . \tag{3.1.3}$$

This provides the justification for our prior claim (in section 1.1.2) that isotropic interaction has no effect on the resonance frequency. The contributions of the $S^x$, $S^y$, and $S^z$ terms sum to zero when carried through the commutator expansion. We may also provide a direct mathematical justification for that claim. We note that the isotropic Hamiltonian $\mathcal{H}_0$ commutes with $S^z$, as:

$$\begin{aligned} [\mathcal{H}_0, S^z] &\equiv \sum_{i,l} \left( [S_i^x S_{i-1}^x + S_i^y S_{i-1}^y + S_i^z S_{i-1}^z, S_l^z] \right) \\ &= \sum_{i,l} \left( S_i^x [S_{i-1}^x, S_l^z] + [S_i^x, S_l^z] S_{i-1}^x + S_i^y [S_{i-1}^y, S_l^z] + [S_i^y, S_l^z] S_{i-1}^y \right) = 0 \ . \end{aligned} \tag{3.1.4}$$

In the purely isotropic case, the Heisenberg equations of motion for $S^+$ and $S^-$ are given by $[S^\pm, \mathcal{H}_0] = \imath\hbar\dot{S}^\pm$, the equation of motion for $S^z$ by $[S^z, \mathcal{H}_0] = \imath\hbar\dot{S}^z$, and we recall the

identity $[S^+, S^-] = 2\hbar S^z$. Then,

$$\begin{aligned}\frac{d}{dt}[S^+, S^-] &= \frac{dS^+}{dt}S^- + S^+\frac{dS^-}{dt} - \left(\frac{dS^-}{dt}S^+ + S^-\frac{dS^+}{dt}\right) \\ &= [\frac{dS^+}{dt}, S^-] + [S^+, \frac{dS^-}{dt}] \\ &= \frac{\imath}{\hbar}[S^-, [S^+, \mathcal{H}_0]] - \frac{\imath}{\hbar}[S^+, [S^-, \mathcal{H}_0]] \ .\end{aligned} \tag{3.1.5}$$

Therefore, we obtain from $[S^z, \mathcal{H}_0] = 0$:

$$\begin{aligned}\imath\hbar\dot{S}^z &= [S^z, \mathcal{H}_0] = 0 \\ &= \frac{\imath}{2}\frac{d}{dt}[S^+, S^-] = -[S^-, [S^+, \mathcal{H}_0]] = 0 \ .\end{aligned} \tag{3.1.6}$$

Thus, for any Hamiltonian terms preserving SU(2) symmetry, there is no effect on the peak resonance frequency.

Incorporating the anisotropic term $\mathcal{H}'$ requires us to calculate $[S^-, [S^+, \mathcal{H}']]$, which we obtain from equation (A.2.13):

$$\begin{aligned}[S^-, [S^+, \mathcal{H}']] \equiv -J' \sum_l \big[ &- \left(S^x_{l+1}S^x_l + S^x_l S^x_{l-1} + S^y_{l+1}S^y_l + S^y_l S^y_{l-1}\right) + 2\left(S^z_{l+1}S^z_l + S^z_l S^z_{l-1}\right) \\ &+ \imath\left(S^x_{l+1}S^y_l + S^y_l S^x_{l-1} - S^y_{l+1}S^x_l - S^x_l S^y_{l-1}\right)\big] \ .\end{aligned} \tag{3.1.7}$$

Combining the three results of equations (A.2.1), (A.2.12), and (A.2.13) gives the complete expression for the resonance frequency. The contribution of $\mathcal{H}_Z$ provides the base resonance

frequency, and that of anisotropy $\mathcal{H}'$ provides its shift; $\mathcal{H}_0$ does not contribute to the expression, in accordance with our previous statements. The presence of anisotropic terms leads to a shift in the peak resonance frequency from the isotropic case. We can express this directly as:

$$\begin{aligned}\frac{\langle[S^-,[S^+,\mathcal{H}]]\rangle}{\langle 2S^z\rangle} &= \frac{\langle[S^-,[S^+,\mathcal{H}_Z]]+[S^-,[S^+,\mathcal{H}_0]]+[S^-,[S^+,\mathcal{H}']]\rangle}{\langle 2S^z\rangle} \\ &= \frac{\langle[S^-,[S^+,\mathcal{H}_z]]\rangle}{\langle 2S^z\rangle}+\frac{\langle[S^-,[S^+,\mathcal{H}']]\rangle}{\langle 2S^z\rangle} \\ &= \hbar\omega_0+\Delta\hbar\omega\ .\end{aligned} \tag{3.1.8}$$

From this we see that the base resonance frequency – $\hbar\omega_0$, as found in equation (A.2.1) – returns the Zeeman frequency expected from equation (1.1.4). The resonance frequency for an isotropic system results from the Zeeman interaction in the Hamiltonian (i.e., $\mathcal{H}_Z$), and the frequency shift, $\Delta\hbar\omega$, is due to the presence of the anisotropic component $\mathcal{H}'$.

To emphasise the alternating bond structure we will use in evaluating evaluation, we return to equation (3.1.7) and express the result in terms of even ($2l$) and odd ($2l\pm1$) indices.

$$\begin{aligned}\Delta\hbar\omega = -\frac{1}{\langle 2S^z\rangle}\Bigg[J'\sum_l &\left(S^x_{2l+1}S^x_{2l}+S^x_{2l}S^x_{2l-1}+S^y_{2l+1}S^y_{2l}+S^y_{2l}S^y_{2l-1}\right)+2\left(S^z_{2l+1}S^z_{2l}+S^z_{2l}S^z_{2l-1}\right) \\ &+\imath\left(S^x_{2l+1}S^y_{2l}+S^y_{2l}S^x_{2l-1}-S^y_{2l+1}S^x_{2l}-S^x_{2l}S^y_{2l-1}\right)\Bigg]\ .\end{aligned} \tag{3.1.9}$$

### 3.1.1 Comparison to Past Results

The frequency shift as determined above is expressed in terms of alternating bonds $(i+1, i)$ and $(i, i-1)$. Previous derivations we studied did not include such a distinction, as in reference [6], where the expression,

$$Y(T,H) = \frac{\langle S_j^z S_{j+1}^z - S_j^x S_{j+1}^x \rangle_0}{\langle S_j^z \rangle_0} \ , \tag{3.1.10}$$

is given for correlation along one leg of a two-leg ladder. This expansion originates in [4] and has applications beyond the single chain. In the case of a two-leg ladder as in reference [8], equation (3.1.10) is given (slightly modified, as $Y_{\|}$) for the correlations along one leg of the ladder. It is a useful check to see whether equation (A.2.13) – and therefore equation (3.1.9) – can be reduced to a form resembling equation (3.1.10) through the appropriate simplifications.

Assuming a homogeneous bond structure – where each set of alternating bonds are considered equivalent, as $S_{i+1}^{\alpha} S_i^{\alpha} \equiv S_i^{\alpha} S_{i-1}^{\alpha}$ – we may consider each of the components of equation (3.1.9), resulting in:

$$(S_{i+1}^x S_i^x + S_i^x S_{i-1}^x + S_{i+1}^y S_i^y + S_i^y S_{i-1}^y) \to 2(S_i^x S_{i-1}^x + S_i^y S_{i-1}^y) \ , \tag{3.1.11}$$

$$S^z_{i+1}S^z_i + S^z_i S^z_{i-1} \to 2(S^z_i S^z_{i-1}) \ , \tag{3.1.12}$$

and

$$(S^x_{i+1}S^y_i + S^y_i S^x_{i-1} - S^y_{i+1}S^x_i - S^x_i S^y_{i-1}) \to 0 \ . \tag{3.1.13}$$

Thus the commutator term of equation (A.2.13) evaluates to

$$[S^-, [S^+, \mathcal{H}']] \to \sum_i -2(S^x_i S^x_{i-1} + S^y_i S^y_{i-1}) + 4(S^z_i S^z_{i-1}) \ . \tag{3.1.14}$$

Given the structure of the chain, we may assume $\langle S^x \rangle$ and $\langle S^y \rangle$ to be equivalent, due to their symmetry (because the chain is axially symmetric along the axis of $S^z$). Thus, the expressions above may be further simplified to:

$$\begin{aligned} \Delta\hbar\omega &= -\frac{\langle [S^-, [S^+, \mathcal{H}']] \rangle}{\langle 2S^z \rangle} \\ &= -\frac{\langle 4S^z_i S^z_{i-1} - 2(S^x_i S^x_{i-1} + S^y_i S^y_{i-1} \rangle}{\langle 4S^z_i \rangle} \\ \to &= \frac{\langle S^z_i S^z_{i-1} - S^x_i S^x_{i-1} \rangle}{\langle S^z_i \rangle} \ . \end{aligned} \tag{3.1.15}$$

The previously calculated result equation (3.1.9) therefore has the same form as equation (3.1.10) from reference [6] under the appropriate assumptions.

## 3.2 Jordan-Wigner Transformation

An overview of the JW transformation was included in section 2.1. To calculate the frequency shift using the bond-mean-field theory, we must first re-write equation (3.1.9) using the JW transformation. Only the numerator – $\langle[S^-,[S^+,\mathcal{H}']]\rangle$ – is considered, as the single term in the denominator – $2\langle S^z\rangle$ – does not require further simplification. The full details of this calculation are included in section A.3 of the appendix.

We may proceed term by term. The $S^x$ and $S^y$ terms are treated in equation (A.3.3), resulting in

$$S^x_{i+1}S^x_i + S^x_i S^x_{i-1} + S^y_{i+1}S^y_i + S^y_i S^y_{i-1} \equiv \tfrac{1}{2}\left(c^\dagger_{i+1}c_i + c^\dagger_i c_{i-1} + c^\dagger_i c_{i+1} + c^\dagger_{i-1}c_i\right) . \qquad (3.2.1)$$

The $S^z$ terms are treated in equation (A.3.4), giving

$$S^z_{i+1}S^z_i + S^z_i S^z_{i-1} \equiv 2(c^\dagger_{i+1}c_{i+1}c^\dagger_i c_i + c^\dagger_i c_i c^\dagger_{i-1}c_{i-1}) - (c^\dagger_{i+1}c_{i+1} + 2c^\dagger_i c_i + c^\dagger_{i-1}c_{i-1}) . \qquad (3.2.2)$$

The remaining cross terms (of $S^x$ and $S^y$) are treated in equation (A.3.7), producing

$$\imath\left(S^x_{i+1}S^y_i - S^y_{i+1}S^x_i\right) + \imath\left(S^y_i S^x_{i-1} - S^x_i S^y_{i-1}\right) \equiv \tfrac{1}{2}\left(c^\dagger_i c_{i+1} - c^\dagger_{i+1}c_i + c^\dagger_i c_{i-1} - c^\dagger_{i-1}c_i\right) . \qquad (3.2.3)$$

Combining these results – equations (A.3.3), (A.3.4), and (A.3.7) – with the constant factors in equation (3.1.9) yields the JW transformation of the complete commutator expression, as

$$\sum_{i,j}[S_i^-,[S_j^+,\mathcal{H}']] \to \sum_i \big[ -(c_{i+1}^\dagger c_i + c_{i-1}^\dagger c_i) + 4(c_{i+1}^\dagger c_{i+1} c_i^\dagger c_i + c_i^\dagger c_i c_{i-1}^\dagger c_{i-1}) \\ - 2(c_{i+1}^\dagger c_{i+1} + 2c_i^\dagger c_i + c_{i-1}^\dagger c_{i-1})\big] \ . \tag{3.2.4}$$

Finally, in light of equation (3.1.9), we represent equation (3.2.4) above in terms of alternating even ($2l$) and odd ($2l \pm 1$) bonds. As our final result for the JW transformation of equation (3.1.9), we obtain

$$\sum_l \big[ -(c_{2l+1}^\dagger c_{2l} + c_{2l-1}^\dagger c_{2l}) + 4(c_{2l+1}^\dagger c_{2l+1} c_i^\dagger c_{2l} + c_{2l}^\dagger c_{2l} c_{2l-1}^\dagger c_{2l-1}) \\ - 2(c_{2l+1}^\dagger c_{2l+1} + 2c_{2i}^\dagger c_{2l} + c_{2l-1}^\dagger c_{2l-1})\big] \ . \tag{3.2.5}$$

## 3.3 Evaluation of the Frequency Shift Expression

We may now calculate the frequency shift by combining the results of equations (3.1.9) and (3.2.5). To do so, we will incorporate the bond-mean-field theory. Examining equation (3.2.5), we see that the contributions of all terms involving $S^x$ and $S^y$ are reduced to the two terms, $c_{2i+1}^\dagger c_{2i}$ and $c_{2i-1}^\dagger c_{2i}$. These terms may be analysed as detailed in section 2.3 [32]. If we consider $\langle c_{2i+1}^\dagger c_{2i}\rangle \equiv Q$, then $\langle c_{2i}^\dagger c_{2i-1}\rangle \equiv -Q$; this relation is demonstrated in figure 3.1.

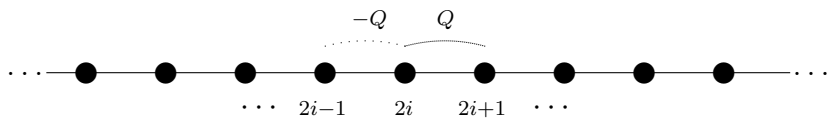


Figure 3.1: An illustration of the bond factor, and the relationship of $Q$ and $-Q$.

Then to evaluate ,

$$\begin{aligned} \langle c^{\dagger}_{2l+1}c_{2l}\rangle + \langle c^{\dagger}_{2l-1}c_{2l}\rangle &\equiv \langle c^{\dagger}_{2l+1}c_{2l}\rangle - \langle \Big(c^{\dagger}_{2l}c_{2l-1}\Big)^{\dagger}\rangle \\ &\equiv Q + (-Q) = 0 \ . \end{aligned} \tag{3.3.1}$$

Therefore, under the bond-mean-field theory treatment, only the contribution of the $S^z$ terms persists. The expression (3.1.9) therefore reduces to

$$\Delta\hbar\omega = -\frac{\left\langle J' \sum_l \left[2\left(S^z_{2l+1}S^z_{2l} + S^z_{2l}S^z_{2l-1}\right)\right]\right\rangle}{\langle 2S^z\rangle} \ . \tag{3.3.2}$$

The remaining terms (containing $S^z$) may also be determined by the mean-field theory. It is assumed that $\langle S^z_i S^z_{i-1}\rangle \simeq \langle S^z_i\rangle\langle S^z_{i-1}\rangle$, as per reference [32]. Then, since we have determined

that $\langle S^z \rangle$ is constant for all sites,

$$\begin{aligned}
\Delta\hbar\omega &= -\frac{2J'\langle \sum_l S^z_{2l+1} S^z_{2l} + \sum_l S^z_{2l} S^z_{2l-1} \rangle}{2\langle S^z \rangle} \\
&= -\frac{4J' \sum_l \langle S^z_{2l} \rangle \langle S^z_{2l-1} \rangle}{2\langle S^z \rangle} \\
&= -\frac{4J' \langle S^z \rangle \langle S^z \rangle}{2\langle S^z \rangle} \equiv \frac{4J' M_z^2}{2M_z} \\
&= -2J' M_z \ .
\end{aligned} \tag{3.3.3}$$

Therefore, for an applied field and anisotropy parallel to the spin chain axis, the frequency shift, under these assumptions, is proportional to the overall magnetisation of the chain:

$$\Delta\hbar\omega = -2J' M_z \ . \tag{3.3.4}$$

In the low magnetic field limit ($\mu_B h / J \ll 1$) the magnetisation is approximately equal to the product of the susceptibility and applied field strength. Therefore in such a case case,

$$\Delta\hbar\omega = -2J' \chi h \ . \tag{3.3.5}$$

# Chapter 4

## Results

In this chapter numerically solve the ESR frequency shift results – from equations (3.1.9) and (3.2.5) to equations (3.3.3) and (3.3.5). In section 4.2 we compare the results we obtained in this way to a variety of past theoretical calculations and experimental data. In section 4.2.3 we discuss our result for ESR in terms of NMR behaviour.

## 4.1 Numerical Analysis

This section describes the results of our numerical analysis for calculating equations (3.3.4) and (3.3.5). We begin by considering the average per-site magnetisation before calculating the bulk magnetisation (and proportional frequency shift) for a range of temperatures and applied field strengths.

The numerical calculations in this thesis were programmed and carried out using code written in C. The calculations were performed by iterative numerical integration, varying the independent parameters of temperature and field strength. The source code for performing these calculations was taken, with the necessary modifications, from Azzouz. In its original form it was used for the calculations in reference [32].

### 4.1.1 Sublattice Magnetisation

In determining the expression for frequency shift (in both spin operator and fermionic forms, as equations (3.1.9) and (3.2.5)) we have emphasised the alternating bond structure. The question arises whether the denominator $\langle S^z \rangle$ should also be expressed via an alternating structure - that is, whether $\langle S^z \rangle$ may be treated as a constant magnetisation across the whole chain, or whether it should be separated into $\langle S^z_{2l} + S^z_{2l+1} \rangle$ terms describing two sublattice magnetisations. Our hypothesis was that, since the Heisenberg chain is antiferromagnetic at zero applied field but magnetised at higher fields, the intermediate behaviour might show characteristics of ferrimagnetism.

To investigate this, an isotropic spin chain was simulated and magnetisation calculated as a function of applied field strength. The bond factor $Q$ and the energy spectrum were also calculated, using a modification of the procedure outlined in section 2.3. Sublattice magnetisations $M^A_Z$ and $M^B_Z$ were found to lead to two solutions. Either $M^A_Z = M^B_Z$, and

the magnetisation was therefore constant for all sites, or $M_Z^A \neq M_Z^B$, with zero-field values of $M_Z^A = -M_Z^B$. The behaviour of the latter exhibited a critical point and gapped energy spectrum, representing a non-physical result. Consequently, for analysing the frequency shift a constant magnetisation $M_Z = \langle S^z \rangle$ was used. These calculations and the resulting numerical analysis are reproduced in full in section A.4 of the appendix.

### 4.1.2 Numerical Evaluation of the Frequency Shift

We proceed to calculate the frequency shift as a function of field strength and temperature. To do so we use equation (3.3.3), and calculate the shift in terms of the magnetisation.

In calculating an actual value for equation (3.3.3), we require concrete values for the magnitude of the anisotropy $J'$. This value is structure dependent. In our numerical calculation we have, for simplicity, set some constants (i.e., $\hbar$) to unity, and normalised to $J = 1$. We have also set $J' = 0.1$, as generally $J' \ll J$ for spin chains – in particular for those detailed in section 1.2.2. That is, $\mathcal{H}' \ll \mathcal{H}_0$; our chosen value of $J' = 0.1$ is therefore towards the larger end of commonly encountered values [5, 6]. As an example, for $LiCuVO_4$, if isotropic exchange is normalised such that $J \approx 1$, then the anisotropic exchange is on the order of $J' \approx -0.045$, roughly one twentieth the magnitude of the isotropic exchange and corresponding to an approximate value of $J' \approx 0.05$ in our model Hamiltonian. For values larger than $J' \approx 0.1$, compared to $J = 1$, the anisotropic chain is no longer a reasonable model [21].

We include here several figures to illustrate our findings. In our calculations the frequency shift was negative, which is standard for a positive anistropy $J'$, but we have instead plotted the magnitude of resonance frequency shift to emphasise the relation between the frequency shift and the (positive) magnetisation. Figure 4.1 shows the magnetisation, and figure 4.2 the frequency shift, as a function of temperatures at varying applied field strengths. Figure 4.3 shows the magnetisation and frequency shift as a function of applied field strength.

Before conducting any comparison using these results, they warrant some discussion. We first consider the curves for magnetisation (and therefore, for low field strengths, susceptibility) as a function of tempterature. The classical model for susceptibility is proportional to $1/T$, and at higher temperatures our results exhibit similar behaviour. However, this classical result predicts a divergence to infinity at the zero-temperature limit ($T/J \to 0$). The quantum mechanical treatment instead gives a finite zero-temperature value. We also note that the behaviour is not monotonic; the susceptibility exhibits a maximum value at finite temperature, and a decrease between this point and zero temperature. However, at high field strengths, as in figure 4.1(b), we note very different behaviour. At low temperature and high field the magnetisation exhibits saturation and a monotonic decrease with increasing temperature.

Similarly, we note the the behaviour of the magnetisation with increasing applied field strength. The magnetisation reaches a saturation point at sufficiently high field – physically,

this represents the state of total alignment of all spins, with the applied field strong enough to overcome the natural antiferromagnetic tendency. This saturation occurs at $h/J \approx 2$. At low field, the behaviour of the magnetisation is approximately linear, and referring to figure 4.3, we see that the curves for different temperature values only begin to diverge at $T/J > 1$. The magnetisation is a continuous function, but at low temperatures its derivative is discontinuous; there is a sharp inflection when magnetisation reaches the saturation point – noticeably, for $T/J = 0.1$ in figure 4.3.

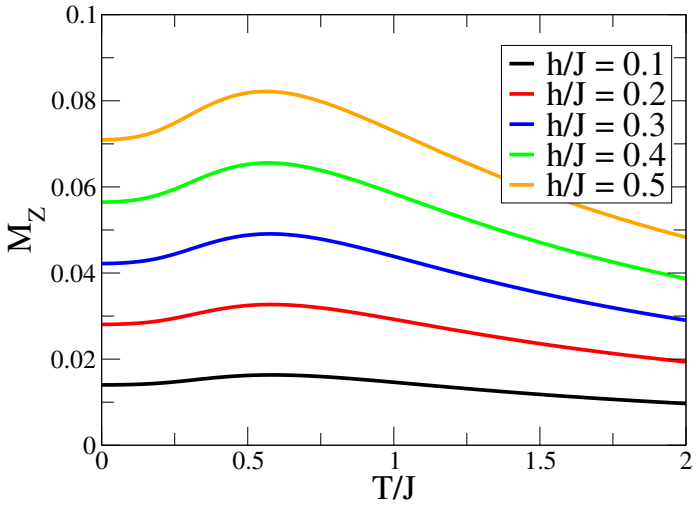


(a)

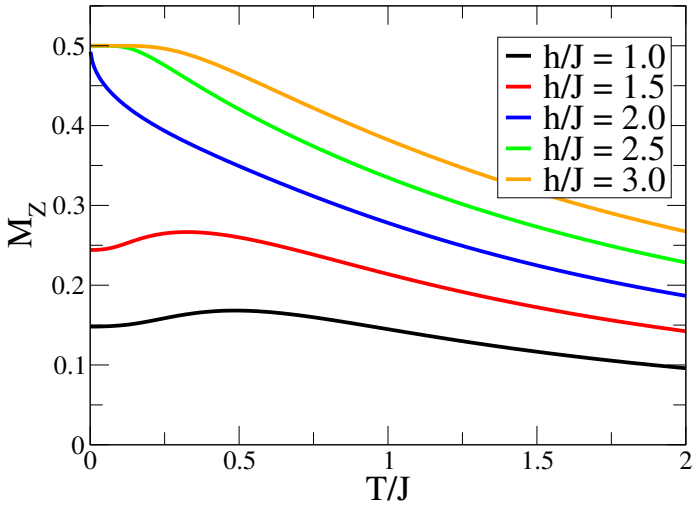


(b)

Figure 4.1: Magnetisation ($M_z/J$) as a function of temperature ($T/J$) for a variety of applied field strengths, from $h/J = 0.1$ to $h/J = 0.5$ in 4.1(a) and from $h/J = 1.0$ to $h/J = 3.0$ in 4.1(b).

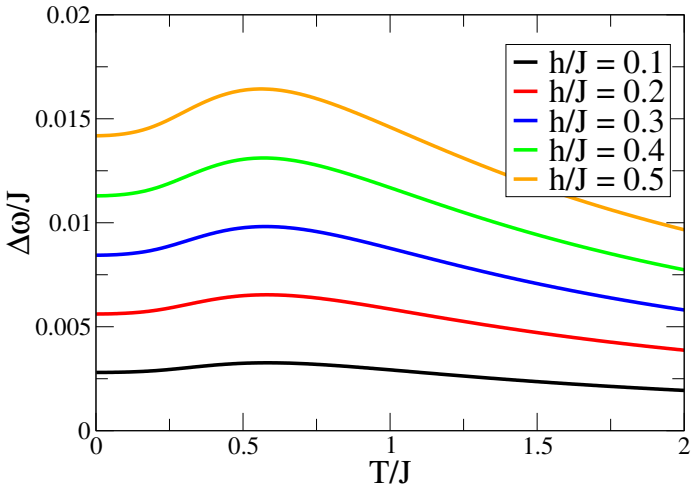


(a)

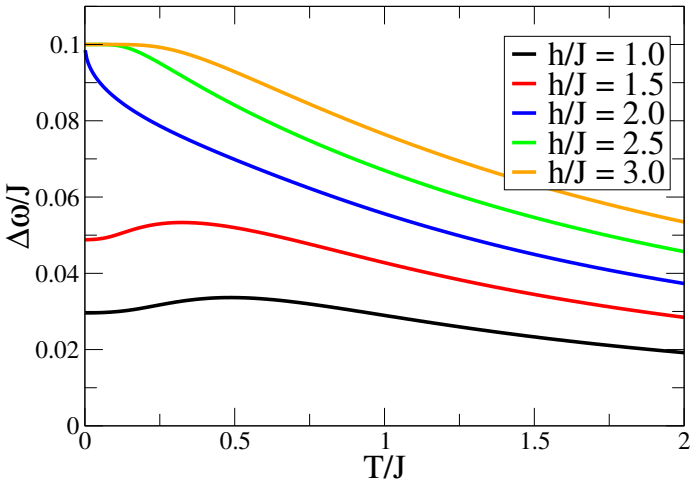


(b)

Figure 4.2: Resonance frequency shift ($\Delta\omega/J$) as a function of temperature ($T/J$) for a variety of applied field strengths, from $h/J = 0.1$ to $h/J = 0.5$ in 4.2(a) and from $h/J = 1.0$ to $h/J = 3.0$ in 4.2(b).

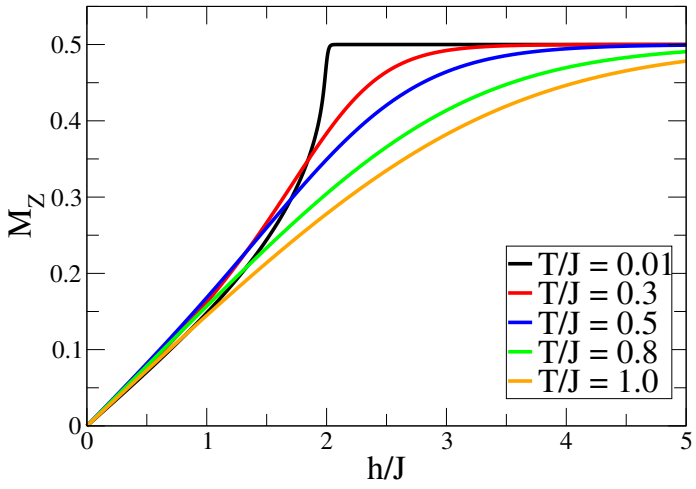


(a)

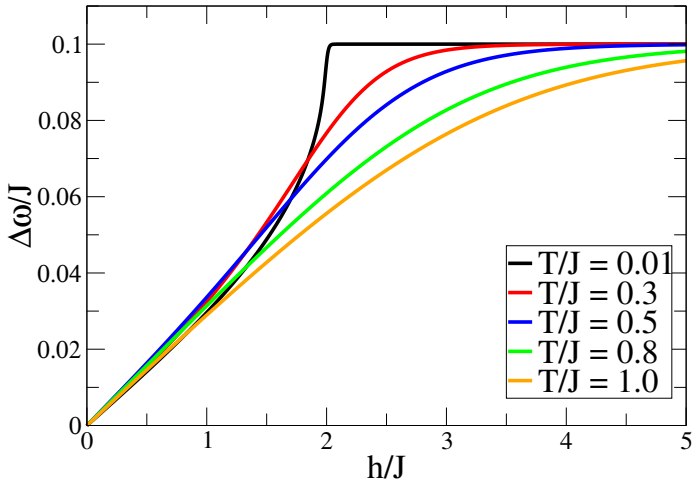


(b)

Figure 4.3: Comparison between magnetisation ($M_z/J$), in 4.3(a), and frequency shift ($\Delta\omega/J$), in 4.3(b), for several temperature values from $T/J = 0.1$ to $T/J = 1.0$.

## 4.2 Comparison to Past Results

Having obtained the above results for the frequency shift, and calculating it for a range of temperatures and fields, we proceed to compare our results to earlier work. This section relates our calculations to previous theoretical work in section 4.2.1 and to experimental data in section 4.2.2. Finally, we compare our results for ESR to similar behaviour in nuclear magnetic resonance in section 4.2.3.

### 4.2.1 Comparison to Theoretical Results

In this work the calculation of the ESR shift was considered for the antiferromagnetic spin $S = 1/2$ chain with small ($J' \ll J$) exchange anisotropy, with the anisotropy and the applied field along the chain axis (chosen to be the $z$ axis). This physical model was described in section 1.1.3.

Oshikawa and Affleck in reference [5] obtained results for the frequency shift using the bosonisation method (as detailed in section 1.2.1). In their analysis the frequency shift (at low temperatures and field strengths) was found to be linearly proportional to magnetic field $h$ and anisotropy $J'$; this is in apparent agreement with the shift as calculated above. The frequency shift we obtained, given in equations (3.1.9) and (3.2.5), was found to be proportional

to the magnetisation as per equation (3.3.3), and in turn proportional to the susceptibility and applied field strength, as $M_z \approx \chi h$ in the low-field limit. Therefore at low field strengths, the shift as we calculated it has approximately the same form as in [5]: it is proportional to the applied field strength and the anisotropy, with the proportionality equal to the susceptibility. This is a very useful result, as susceptibility is one of the parameters that can be directly measured in experimental ESR conditions.

We note that the results of reference [5] are stated to be valid only for the low-temperature, low-field regime. It is under these conditions that the approximately proportional relationship between the frequency shift and the anisotropy (with a proportionality constant as the susceptibility) holds. This is the same restriction that applies to our calculations, as our assumption that $M_z \approx \chi h$ is only valid at low field strengths.

We may also compare our results to those of Zyvagin [7], considering the case of an anisotropic exchange interaction along the $z$ axis. Zyvagin defines the anisotropy as $\mathcal{H}_a = -J' \sum_{n,\delta} S_n^z S_{n+\delta}^z$; for nearest-neighbour exchange interaction, $\delta = \pm 1$. The resonance frequency was derived from the absorbed power $Q$. $Q$ was calculated from the Heisenberg equations for $S^z$ and $S^{\pm}$, leading to the quantum Boltzmann equations. Comparing the results for $Q$ between the isotropic chain and the anistropic chain leads to the expression for the resonance frequency shift, $ZJ'M_z$, where $Z$ is the coordination number ($Z = 2$ for nearest-neighbour exchange interactions as in our calculations), $M_z$ the magnetisation (defined, as in our calculations, as

$M_z \equiv \langle S^z \rangle$), and $J'$ the magnitude of the anisotropy. Comparing this to our result, we find that for $Z = 2$ as we have chosen, the expression we derived in equation (3.3.3) corresponds exactly to the results of reference [7]. Zyvagin also states that this may be expressed as $ZJ'\chi_{zz}(h,T)h$, which is again equivalent to our result derived in equation (3.3.5): $-2J'\chi h$.

Results for the resonance frequency shift are also given by Maeda, Sakai, and Oshikawa in reference [6]. Their results are based on the Bethe ansatz result, and are reproduced in figure 4.4. The low-temperature results are in contrast to ours; our calculations show a maximum value for the shift at finite temperature, mirroring the susceptibility, whereas the results of reference [6] have a maximum at zero temperature.

This result of reference [6] proceeds from the shift given by:

$$\Delta\hbar\omega \propto \frac{\langle S_j^z S_{j+1}^z - S_j^x S_{j+1}^x \rangle}{\langle S_j^z \rangle} \ . \tag{4.2.1}$$

This expression (discussed in greater detail in section 1.2.1) leads to the result as depicted in figure 4.4(b). The expanded result contains terms directly proportional to the applied field $h$, but also contains multiple temperature-dependent terms. At very low temperatures and field strengths, the dominant term is logarithmic; algebraic terms (on the order of $T^2$) predominate at higher temperatures and field strengths. The crossover between the two regimes occurs at $h/J \approx T/J$ and is shown in figure 4.4(b).

The Bethe ansatz result is only applicable to chains. It may, however, be extended to the case of the two-leg ladder, since that ladder Hamiltonian may be expressed through an effective chain Hamiltonian [35]. With some modification our results for the chain are extendable to arbitrary other geometries, with the appropriate extensions to the procedure of the JW transformation and the bond parameter [33].

Lastly, we may compare our results to those of reference [8]. That work is primarily concerned with two-leg ladders, in which case two correlation functions exist: $Y_{\parallel}$, along the ladder legs, and $Y_{\perp}$, across the ladder rungs. The base case the authors considered was the uncoupled ladder, in which there is no inter-leg interaction between the two separate legs, effectively treating them as isolated chains. In this case, $Y_{\parallel}$ represents the same correlation function as in our work, and rung interaction $Y_{\perp}$ is unimportant. The authors derive and plot the correlation functions $Y_{\parallel}(T, h)$, with much the same form as the expression given in reference [6] (whose derivation is discussed in section 3.1.1). This expression,

$$Y_{\parallel}(T, h) = \frac{\langle S_i^z S_{i-1}^z - S_i^x S_{i-1}^x \rangle}{\langle S^z \rangle} \ , \tag{4.2.2}$$

was calculated by means of the density matrix renormalisation group method, and the results were plotted. The plot representing the chain is reproduced here as figure 4.5. We see that the frequency shift increases approximately linearly with applied magnetic field strength, before plateauing at a maximum value. In our calculations, we found this correlation function

– see equation (3.1.9), and section 3.1.1 in particular – to be approximately equal to the magnetisation, and our simulation of the magnetisation versus applied field strength is given in figure 4.3(a). Comparing the two, we note plot taken from reference [8] displays very similar behaviour, reaching a maximum value of $1/2$ at $h/J \approx 2$.

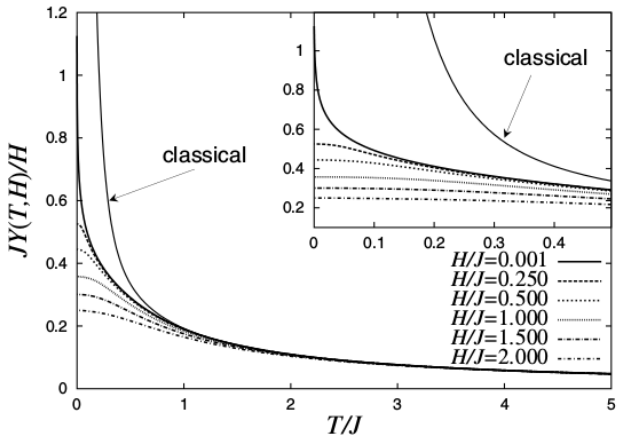


(a) Frequency shift versus temperature.

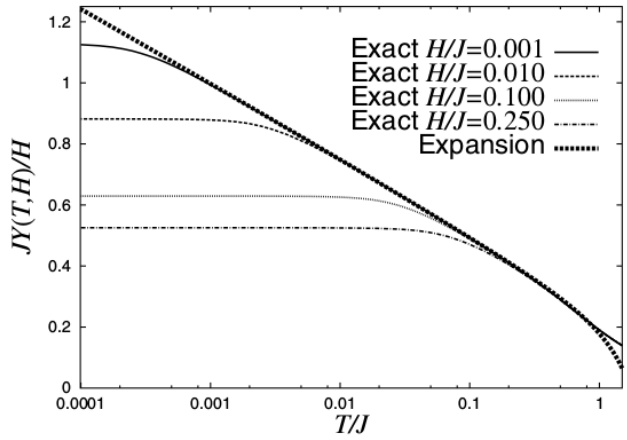


(b) Frequency shift versus temperature at low fields.

Figure 4.4: Results of [6]. Note that the plots are of $JY(T,H)/H$ whereas $\Delta\hbar\omega \propto -Y(T,H)$ in our results, which are normalised to $J \equiv 1$. 4.4(a) shows the frequency shift (as $Y(T,H)$) as a function of temperature and 4.4(b) highlights the low-temperature logarithmic behaviour, which does not arise in our results.

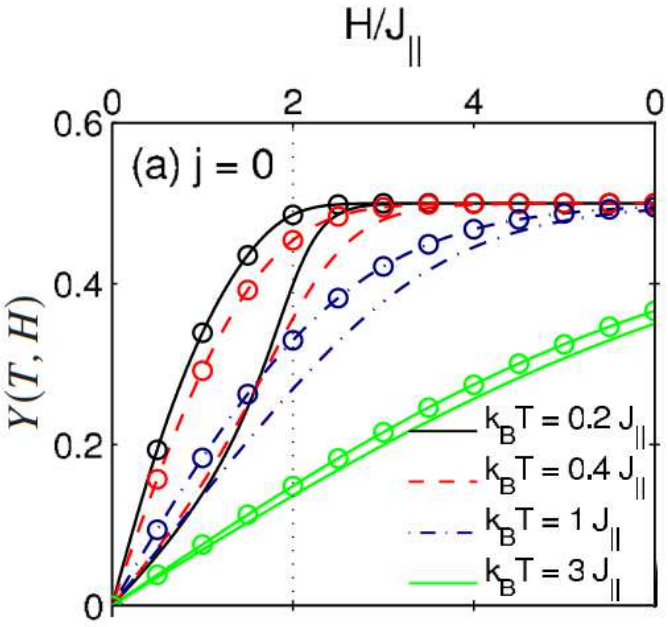


Figure 4.5: A plot of simulated results for the uncoupled ladder – effectively an isolated chain. Lines with circles represent the correlation fuction $Y_{\|}$ – equation (4.2.2) – to which the frequency shift is directly proportional. Lines without circles are related to the rung correlation $Y_{\perp}$ and are irrelevant to our results [8].

### 4.2.2 Comparison to Experimental Results

We now compare our results to existing experimental data. Detail on the compounds considered here was given in section 1.2.2. Both compounds $LiCuVO_4$ and copper benzoate can be approximated as antiferromagnetic spin chains with weak symmetric anisotropy, due to their crystal structures incorporating isolated linear chains of copper(II) ions with single $S = 1/2$ valence electrons [27]. Our model represents the simplest representation of such an arrangement, treating as negligible all other interactions.

For $LiCuVO_4$, we refer to reference [22], and reproduce their results in figure 4.6. The results for susceptibility of $LiCuVO_4$ were obtained with an interference magnetometer. We note that the curve for susceptibility – figure 4.6(a) – broadly resembles our results, but that it includes a secondary peak at very low temperatures, which does not occur in our analysis. The authors of [22] attribute this to interchain interactions, which are not included in our calculations. The frequency shift shown in figure 4.6(b) is given in terms of the $g$ shift, as mentioned in section 1.2.2; the authors define $\Delta g = (\hbar\Delta\omega)/(\mu_B h)$. This does not match our low field result, and rather than direct proportionality to the susceptibility, the shift in reference [22] appears much more like the result of reference [6], with a maximum at zero temperature.

For copper benzoate, we have the results of reference [24], reproduced in figure 4.7. These are

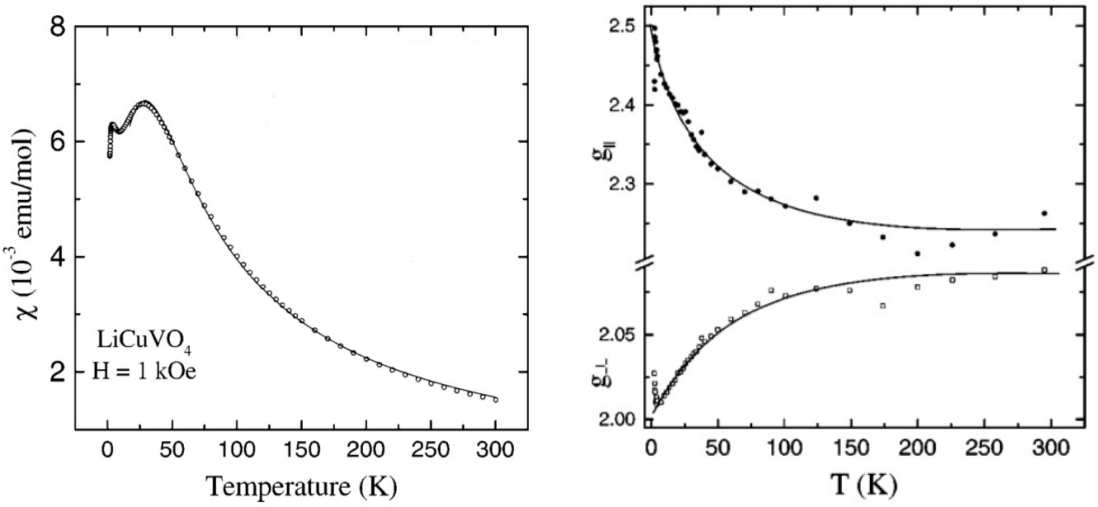


(a) (b)

Figure 4.6: Plots of experimental data for $LiCuVO_4$. Figure 4.6(a) depicts measured susceptibility versus temperature, which displays broadly similar lineshape to our results. Figure 4.6(b) depicts the effective g-factor and its temperature-dependent shift (where $g \propto \Delta\hbar\omega$ as mentioned in section 1.2.2). The upper line is for an applied field parallel to the axis of the chain, and the lower line for perpendicular field. The applied magnetic field is on the order of $h/J \approx 0.01$ [22].

earlier data but remain representative of later analyses of copper benzoate [2, 21]. This plot also resembles our high field results rather than our low field results. The frequency shift as a function of temperature does not show the maximum we calculated for the susceptibility. It appears to increase to a maximum at zero temperature, as with $LiCuVO_4$ as shown in figure 4.6(b); this matches the result of reference [6].

We note that both results, for $LiCuVO_4$ and for copper benzoate, diverge from our calculations at low temperatures. The frequency shift exhibits a maximum at zero temperature and a monotonic decrease with increasing temperature. However, this suggests that the theoretical results referred to – those of references [5] and [7] – are also in contradicted by the experimental results we have reviewed here, as those results agreed with our calculations

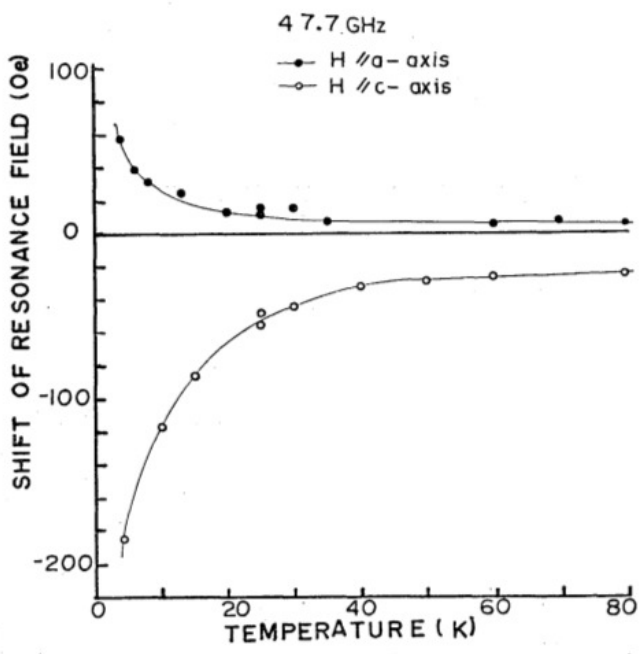


Figure 4.7: Plot of experimental data for copper benzoate [24]. The frequency shift is plotted against temperature and displayed in arbitary units. The results for $H \parallel c$ reflect the situation we considered in our calculations (with the applied field parallel to the chain axis and the anisotropy).

in specifying a frequency shift proportional to susceptibility.

### 4.2.3 Comparison to Nuclear Resonance

With this result for ESR, it is of interest to consider nuclear magnetic resonance (NMR) to see what similarities may exist. As metioned in section 1.1, NMR uses the same principles as ESR - an applied magnetic field splits degeneracy, and the created energy differential is probed by measuring absorption. Whereas ESR uses a laser or microwave source to probe absorption, NMR uses an alternating (time-dependent) magnetic field. The basic case for NMR, considering only the Zeeman interaction between the applied static magnetic field and the nuclear magnetic moment $I$, is:

$$\mathcal{H}_Z = -\hbar\gamma_n \vec{H} \cdot \vec{I}\,, \tag{4.2.3}$$

with $\gamma_n$ representing the nuclear gyromagnetic ratio and $\vec{H}$ the applied magnetic field. As with ESR, there are additional interaction terms which complicate the behaviour of the system. One in particular is the Knight shift, which arises due to coupling between the nuclear magnetic moment and the magnetic moment of conduction electrons. The Knight shift is of interest due to its reminiscent structure - it leads to a shift in the NMR resonance frequency proportional to the spin susceptibility of the electrons, very similar to the ESR result we have derived.

The Knight shift is thus a consequence of coupling between the nucleus and the surround-

ing electron(s) (the hyperfine or contact interaction). In NMR, these interactions can be modelled as

$$\mathcal{H}_e = -\hbar\gamma_n \sum_i A_i \vec{I} \cdot (\vec{m}_S)_i \ , \tag{4.2.4}$$

with electron magnetic moment $\vec{m}_S = g_S \mu_B \vec{S}$ and where coupling constant $A$ represents the magnitude of the interaction. If there is no net electron magnetic moment, this interaction will be zero, as the contributions from each spin average out to zero, $\langle S \rangle = 0$. In the presence of an external magnetic field, however, magnetic ordering is created, and $\langle S \rangle \neq 0$. The equation (4.2.4) may then be represented by the interaction of the nuclear magnetic moment, $\vec{I}$, and an effective magnetic field $\vec{h}_e$, as

$$\mathcal{H}_e = -\hbar\gamma_n \vec{I} \cdot \vec{h}_e \ . \tag{4.2.5}$$

This effective field arises due to the average electron spin, $\langle S \rangle$, which will be quantised along the axis of the applied magnetic field as $\langle S^z \rangle \propto \vec{H}$, with $\vec{H} = H_z \hat{z}$. The interaction with the nuclear magnetic moment therefore depends on the relation between the applied magnetic field and the spin polarisation – namely, the susceptibility. We see that the spin susceptibility of the conduction electrons leads to a shift in the NMR resonance frequency, and compare this to our calculations, where the spin susceptibility led to a shift in the ESR resonance frequency. This shift in the NMR frequency – the Knight shift – is denoted $K$, and is directly proportional to the susceptibility $K \propto \chi$.

Incorporating this shift, equation (4.2.3) then appears as

$$\mathcal{H} = -\hbar\gamma_n(1+K)\vec{H}\cdot\vec{I}\,. \tag{4.2.6}$$

The contribution of the conduction electrons results in a shift, $K$ – the Knight shift – in the NMR resonance frequency, proportional the susceptibility of the electrons. Experimentally, this shift is used to determine the susceptibility, by comparing the NMR resonance frequency between nuclei in states with paramagnetic conduction electrons and those without.

# Chapter 5

## Conclusions

Having obtained the results of chapter 4.2, we review our findings and present our summation of them.

We opened this work in section 1.1 with the definition and principles of ESR, and examined the problem of calculating ESR behaviour, particularly the shift of peak frequency of the resonance due to the contributions of anisotropy. In section 1.2 we reviewed existing theoretical analyses and experimental methods and identified the drawbacks to current analyses, thus outlining our motivation.We reviewed the mathematical and theoretical tools of our analysis in chapter 2 – we introduced the method we used in our analysis, the bond-mean-field theory, in section 2.3, and reviewed the JW transformation it relies upon in section 2.1. We chose for our calculations to consider the simplest case, the antiferromagnetic, uniaxial, anisotropic Heisenberg spin chain. We took the correlation function expression for the frequency shift common in the literature – equation (1.1.12) – and performed its algebraic expansion. We

applied the JW transformation to this result and attempted to calculate it by using the bond-mean-field theory. We obtained a result – equations (3.3.3) or (3.3.4) in section 3.3 – and calculated it numerically. We compared this numerical result to prior results in both theoretical and experimental analyses in section 4.2.

Our results were in agreement with some of the theoretical results we reviewed – Oshikawa and Affleck in reference [5], and Zyvagin in reference [7]. We found equivalent expressions for the frequency shift under the same conditions we investigated - the uniaxial, anisotropic spin chain, with the magnetic field applied parallel to the chain. We found precise agreement with the results of reference [7], obtained through the equations of motion, but found disagreement in prefactors with [5], the bosonisation result. Our results were not in agreement with the results of Oshikawa, Sakai, and Maeda in reference [6]. For the low-temperature region in reference [6] the authors found a logarithmic correction to the low-temperature frequency shift, which we did not see in our calculations. This disagreement seems reflected in the experimental data we considered, in figures 4.6(b) and 4.7, which show a maximum at zero temperature and a monotonic decrease with increasing $T$ (resembling the results of reference [6]), instead of the low-temperature maximum in our results (see figure 4.2) reflecting the susceptibility. We note that for sufficiently high field strength ($h/J \geq 2$) as in figure 4.2(b), we see similar curves, with a zero temperature maximum, but that at high field strengths our assumption regarding susceptibility (namely, that $M_z \approx \chi h$) does not hold.

The advantage of our method, as compared to the other theoretical methods discussed, is, as suggested in section 1.3, its simplicity and ease of calculation, both analytically and numerically. This is in marked contrast to the analytical complexity of bosonisation or the Bethe ansatz, and the numerical difficulty involved in exact diagonalisation or density matrix renormalisation groups. The numerical calculations in this work were performed on a mid-range (circa 2012) personal computer and required several seconds to execute. The analytical and numerical simplicity of our method reflects a conceptual simplicity; the description of the antiferromagnet in terms of an alternating bond factor retains physical clarity. Our method is also in principle highly scalable, and applicable to arbitrary two and three dimensional lattices.

There are three major areas where we could pursue further work. The first, an obvious progression after our current calculations, is to attempt similar analysis of related situations. We considered only the simplest case, the spin chain with uniaxial anisotropy and an applied magnetic field parallel to the chain axis. The immediate follow-up would be to consider a perpendicular or arbitrarily-inclined applied magnetic field for the same spin chain Hamiltonian, and then to consider different anisotropic terms in the chain, such as the antisymmetric Dzyaloshinski-Moriya exchange, which arises from the spin-dipole interaction; both would present significantly more complicated calculations. Or, we could attempt to apply the same type of analysis to other spin lattices, such as spin ladders of varying numbers of legs and couplings, or including types of interaction beyond nearest-neighbour exchange interaction,

such as interchain coupling and longer-range interaction, which are present in real substances. Many of the past methods we examined have also been applied to these types of situations, and would therefore remain as points of comparison if our method were expanded.

The second would be to consider more thoroughly existing methods and data. As we noted in section 4.2, we saw significant differences between our result and the theoretical result of reference [6], and the experimental data we considered bore much more resemblance to reference [6] than to our calculations. It would be interesting to try to determine why our results diverged from the experimental data we studied. To such an end it would be useful to study the Bethe ansatz method in particular, as was used in reference [6]. We might also return to our starting point, equation (1.1.12), and review its derivation in greater detail. We noted that the result we used for the ESR frequency shift expression – as equation (3.1.9), derived from equation (1.1.12), and as reminisicent of equation (1.2.2) – is only an approximate result [5, 6, 10], as discussed in section 1.1. Beginning from a more complete expression for $\Delta\hbar\omega$ would increase the complexity of the necessary calculations, but might generate results more closely matching the observed experimental behaviour.

Lastly, we could investigate the experimental uses of ESR analysis, and determine whether our methods would be of use. Many experimental procedures rely on comparing observed data to simulations and numerical results; our results represent a simpler numerical calculation than direct simulation or density matrix approaches (as mentioned in chapter 1.2.1), and

if sufficiently accurate might represent a more efficient way of performing such comparisons. Such considerations would be particularly useful if the approach were amenable to practical applications of ESR as reviewed in chapter 1.2.3 – namely, the possibility for biomedical imaging.

# Bibliography

[1] J. E. Wertz and J. R. Bolton, *Electron Spin Resonance: Elementary Theory and Practical Applications*. McGraw-Hill, 1972.

[2] M. Motokawa, H. Ohta, H. Nojiri, and S. Kimura, "The role of ESR in research of low-dimensional antiferromagnets," *Journal of the Physical Society of Japan, Supplement B*, vol. 72, p. 1, 2003.

[3] H.-A. K. von Nidda, L. E. Svistov, M. V. Eremin, R. M. Eremina, A. Loidl, V. Kitaev, A. Validov, A. Prokofiev, and W. Aßmus, "Anisotropic exchange in LiCuVO4 probed by ESR," *Physical Review B*, vol. 65, no. 13, p. 134445, 2002.

[4] K. Nagata and Y. Tazuke, "Short range order effects on EPR frequencies in Heisenberg linear chain antiferromagnets," *Journal of the Physical Society of Japan*, vol. 32, no. 2, p. 337, 1972.

[5] M. Oshikawa and I. Affleck, "Electron spin resonance in S=1/2 antiferromagnetic chains," *Physical Review B*, vol. 65, no. 13, p. 134410, 2002.

[6] Y. Maeda, K. Sakai, and M. Oshikawa, "Exact analysis of ESR shift in the spin-1/2 Heisenberg antiferromagnetic chain," *Physical Review Letters*, vol. 95, no. 3, p. 37602, 2005.

[7] A. A. Zyvagin, "Theory of the electron spin resonance in quantum spin chains with nearest, next-nearest neighbour, and alternating interactions," *Physical Review B*, vol. 79, no. 6, p. 064422, 2009.

[8] S. C. Furuya, P. Bouillot, C. Kollath, M. Oshikawa, and T. Giamarchi, "Electron spin resonance shift in spin ladder compounds," *Physical Review Letters*, vol. 108, no. 3, p. 37204, 2012.

[9] M. Oshikawa and I. Affleck, "Low-temperature electron spin resonance theory for half-integer spin antiferromagnetic chains," *Physical Review Letters*, vol. 82, no. 25, p. 5136, 1999.

[10] Y. Maeda and M. Oshikawa, "Direct perturbation theory on the electron spin resonance shift and its applications," *Journal of the Physical Society of Japan*, vol. 74, no. 1, p. 283, 2005.

[11] H. Mori and K. Kawasaki, "Theory of dynamical behaviors of ferrmagnetic spins," *Progress of Theoretical Physics*, vol. 27, no. 3, p. 529, 1962.

[12] H. Mori and K. Kawasaki, "Antiferromagnetic resonance absorption," *Progress of Theoretical Physics*, vol. 28, no. 6, p. 971, 1962.

[13] J. Kanamori and M. Tachiki, "Collection motion of spins in ferro- and antiferromagnets," *Journal of the Phsyical Society of Japan*, vol. 32, no. 2, p. 1384, 1962.

[14] A. Ogasahara and S. Miyashita, "Frequency dependence of electron spin response," *Progress of Theoretical Physics Supplement*, vol. 145, p. 286, 2002.

[15] R. Chitra and T. Giamarchi, "Critical properties of gapped spin-1/2 chains and ladders in a magnetic field," *Physical Review B*, vol. 55, no. 9, p. 5816, 1997.

[16] M. Oshikawa and I. Affleck, "Field-induced gap in Cu benzoate and other S=1/2 antiferromagnetic chains," *Physical Review B*, vol. 60, no. 2, p. 1038, 1999.

[17] S. El Shawish, O. Cépas, and S. Miyashita, "Electron spin resonance in S=1/2 antiferromagnets at high temperature," *Physical Review B*, vol. 81, no. 22, p. 224421, 2010.

[18] F. Mila, "Ladders in a magnetic field: a strong coupling approach," *European Physical Journal B*, vol. 6, no. 2, p. 201, 1998.

[19] P. Bouillot, C. Kollath, A. Luchli, M. Zvonarev, B. Thielemann, C. Ruegg, E. Orignac, R. Citro, M. Klanjsek, C. Berthier, M. Horvatic, and T. Giamarchi, "Statics and dynamics of weakly coupled antiferromagnetic spin-1/2 ladders in a magnetic field," *Physical Review B*, vol. 83, no. 5, p. 054407, 2011.

[20] Y. Maeda and M. Oshikawa, "Numerical analysis of electron-spin resonance in the spin-1/2 XY model," *Physical Review B*, vol. 67, no. 22, p. 224424, 2003.

[21] Y. Ajiro, "ESR experiments on quantum spin systems," *Journal of the Physical Society of Japan, Supplement B*, vol. 72, p. 12, 2003.

[22] A. N. Vasiliev, L. A. Ponomarkenko, H. Manaka, I. Yamada, M. Isobe, and Y. Ueda, "Magnetic and resonant properties of quasi-one-dimensional antiferromagnet LiCuVO4," *Physical Review B*, vol. 64, no. 2, p. 024419, 2001.

[23] B. Morosin and E. Graeber, "Crystal structure of tetramethylammonium manganese(ii) chloride," *Acta Crystallographica*, vol. 23, no. 5, p. 766, 1967.

[24] K. Okuda, H. Hata, and M. Date, "Electron spin resonance in one dimensional antiferromagnet cu-benzoate," *Journal of the Physical Society of Japan*, vol. 33, no. 6, p. 1574, 1972.

[25] H. Koizumi, K. Osaki, and T. Watanabe, "Crystal structure of cupric benzoate trihydrate," *Journal of the Physical Society of Japan*, vol. 18, no. 1, p. 117, 1963.

[26] M. A. Lafontaine, M. Leblanc, and G. Ferey, "New refinement of the room-temperature structure of LiCuVO4," *Acta Crystallographica C*, vol. 45, no. 8, p. 1205, 1988.

[27] B. Barbara, Y. Imry, G. Sawatzky, and P. C. E. Stamp, *Quantum Magnetism*. Springer Science, 2008.

[28] S. R. Eaton, G. R. Eaton, and L. J. Berliner, eds., *Biomedical EPR, Part A: Free Radicals, Metals, Medicine, and Physiology*. Springer Science, 2005.

[29] M. Kopani, P. Celec, L. Danisovic, P. Michalka, and C. Biro, "Oxidative stress and electron spin resonance," *Clinica Chimica Acta*, vol. 364, no. 1, p. 61, 2006.

[30] G. Bačić, I. Spasojević, B. Šećerov, and M. Mojović, "Spin-trapping of oxygen free radicals in chemical and biological systems: New traps, radicals, and possibilities," *Spectrochemica Acta A*, vol. 69, no. 5, p. 1354, 2008.

[31] R. M. Eremina, M. V. Eremin, V. N. Glazkov, H.-A. K. von Nidda, and A. Loidl, "Anisotropic exchange interactions in CuGeO3 probed by electron spin resonance spectroscopy," *Physical Review B*, vol. 68, no. 1, p. 014417, 2003.

[32] M. Azzouz, "Field-induced quantum criticality in low-dimensional Heisenberg spin systems," *Physical Review B*, vol. 74, no. 17, p. 174422, 2006.

[33] M. Azzouz, "Interchain-coupling effect on the one-dimensional spin-1/2 antiferromagnetic Heisenberg model," *Physical Review B*, vol. 48, no. 9, p. 6136, 1993.

[34] J. des Cloizeaux and J. J. Pearson, "Spin-wave spectrum of the antiferromagnetic linear chain," *Physical Review*, vol. 128, no. 5, p. 2131, 1962.

[35] T. Giamarchi and A. M. Tsvelik, "Coupled ladders in a magnetic field," *Physical Review B*, vol. 59, no. 17, p. 11398, 1999.

[36] M. Azzouz and C. Bourbonnais, "Mean-field theory of the spin-Peierls state under magnetic field: Application to CuGeO3," *Physical Review B*, vol. 53, no. 9, p. 5090, 1996.

# Chapter A

## In-Depth Calculations

This appendix contains detailed calculations which were omitted from the main body for ease of reading. Section A.1 contains detail from section 2.3. Sections A.2 and A.3 contain the calculations for the frequency shift (detailing the commutator algebra and the JW transformation, respectively) referred to in sections 3.1 and 3.2. Section A.4 contains the full sublattice magnetisation calculations referred to in section 4.1.1.

## A.1 Bond Mean Field Theory

In this section we expand in greater detail some of the results referred to in the course of section 2.3.

In determining the free energy, $f$, and the bond parameter, $Q$, in the zero-field case, we

presented the results as equations (2.3.17) and (2.3.18). Including the intermediate steps, those calculations are as follows:

$$\begin{aligned} f &= \frac{-k_B T}{N} \ln(Z) \\ &= \frac{-1}{\beta N} \left( \sum_k \ln(1 + e^{-\beta E_+(k)}) + \sum_k \ln(1 + e^{-\beta E_-(k)}) - \beta E_c \right) \\ &= JQ^2 - \frac{1}{\beta N} \sum_k \sum_{\alpha=\pm} \ln(1 + e^{-\beta E_\alpha(k)}) \\ &= JQ^2 - \frac{1}{2\beta} \int \frac{dk}{2\pi} \sum_{\alpha=\pm} \ln(1 + e^{-\beta E_\alpha}) \ . \end{aligned} \tag{A.1.1}$$

$$\begin{aligned} \frac{\partial f}{\partial Q} &= 2JQ - \frac{1}{2\beta} \int \frac{dk}{2\pi} \sum_{\alpha=\pm} \left[ \frac{-\beta e^{-\beta E_\alpha(k)}}{1 + e^{-\beta E_\alpha}} \frac{\partial}{\partial Q}(E_\alpha) \right] \\ &= 2JQ + \frac{1}{2} \int \frac{dk}{2\pi} \sum_{\alpha=\pm} \frac{\alpha 2J |\sin(k)| e^{-\beta E_\alpha(k)}}{1 + e^{-\beta E_\alpha(k)}} \\ &= 2JQ + J \int \frac{dk}{2\pi} |\sin(k)| \sum_{\alpha=\pm} \frac{\alpha}{1 + e^{\beta E_\alpha(k)}} \\ \frac{\partial f}{\partial Q} &= 0 \to Q = -\frac{1}{2} \int \frac{dk}{2\pi} |\sin(k)| \sum_{\alpha=\pm} \frac{\alpha}{1 + e^{\beta E_\alpha(k)}} \ . \end{aligned} \tag{A.1.2}$$

In the low-temperature limit for the zero-field case, we treated the logarithmic expression in

equation (2.3.20). The full simplification of this expression is

$$\begin{aligned}\lim_{T\to 0}\left[T\ln(1+e^{a/T})\right] &\equiv \lim_{T\to 0}\left[\frac{\ln(1+e^{a/T})}{1/T}\right] \\ &\equiv \lim_{T\to 0}\left[\frac{\partial/\partial T\left(\ln(1+e^{a/T})\right)}{\partial/\partial T\left(1/T\right)}\right] \\ &\equiv \lim_{T\to 0}\left[\frac{1}{1+e^{a/T}}\left(\frac{-ae^{a/T}}{T^2}\right)\left(\frac{-1}{T^2}\right)^{-1}\right] \\ &\equiv \lim_{T\to 0}\left[\frac{e^{a/T}}{1+e^{a/T}}a\right] = a = \frac{E_-(k)}{k_B}\ .\end{aligned} \tag{A.1.3}$$

Following section 2.3, we move to the non-zero field case. From the non-zero field Hamiltonian, (2.3.30), we apply a Fourier transform, resulting in

$$\begin{aligned}\mathcal{H} = NJQ^2 + Nh/2 - NJM_z(M_z+1) + \sum_k \Big[&\imath J(1+2Q)\sin(k)\hat{c}_k^{A\dagger}\hat{c}_k^B \\ &+ (2JM_z - h)\hat{c}_k^{A\dagger}\hat{c}_k^A - \imath J(1+2Q)\sin(k)\hat{c}_k^{B\dagger}\hat{c}_k^A + (2JM_z-h)\hat{c}_k^{B\dagger}\hat{c}_k^B\Big]\ .\end{aligned} \tag{A.1.4}$$

This is more concisely expressed as a matrix:

$$\mathcal{H} = JNQ^2 + Nh/2 - NJM_z(M_z+1) + \sum_k \begin{pmatrix}\hat{c}_k^{A\dagger} \\ \hat{c}_k^{B\dagger}\end{pmatrix}^\tau \begin{pmatrix}2M_zJ - h & e(k) \\ e^*(k) & 2M_zJ - h\end{pmatrix}\begin{pmatrix}\hat{c}_k^A \\ \hat{c}_k^B\end{pmatrix}\ , \tag{A.1.5}$$

with $e(k) = \imath J(1+2Q)\sin(k)$ and $h = g\mu_B B$; this result is reproduced as equation (2.3.31) in the main body.

We then require the energy eigenvalues, which we obtain through the same diagonalisation procedure as in the zero-field case – we therefore solve the following eigenvalue problem for $E$:

$$\begin{vmatrix} 2M_zJ - h - E & e(k) \\ e^*(k) & 2M_zJ - h - E \end{vmatrix} . \tag{A.1.6}$$

This is evaluated as

$$\begin{aligned} 0 &= (2M_zJ - h - E)^2 - |e(k)|^2 \\ &= (E - (2M_zJ - h))^2 - |e(k)|^2 \\ &= (2M_zJ - h - E + |e(k)|)\,(2M_zJ - h - E - |e(k)|) \\ \rightarrow E &= 2M_zJ - h \pm |e(k)| \ . \end{aligned} \tag{A.1.7}$$

This result is summarised in equation (2.3.32).

In section 2.3, we then obtain the free energy $f$ and bond parameter $Q$ for the non-zero field

case. Our result for $f$ – given as equation (2.3.34) – is determined by

$$\begin{aligned} f &= -\frac{k_B T \ln(Z)}{N} \\ &= -\frac{1}{\beta N} \sum_k \left[ \ln(1 + e^{-\beta E_+(k)}) + \ln(1 + e^{-\beta E_-(k)}) - \beta E_c \right] \\ &= -\frac{1}{\beta N} \sum_k \sum_{\alpha \in \{\pm 1\}} \ln(1 + e^{-\beta E_\alpha(k)}) + \frac{E_c}{N} \\ &= JQ^2 - \frac{h}{2} - JM_z(M_z + 1) - \frac{1}{2\beta} \int \frac{dk}{2\pi} \sum_{\alpha \in \{\pm 1\}} \ln(1 + e^{-\beta E_\alpha(k)}) \ . \end{aligned} \tag{A.1.8}$$

Our result for $Q$ – given as equation (2.3.35) – is determined by

$$\begin{aligned} \frac{\partial f}{\partial Q} &= 2JQ + \frac{1}{2\beta} \int \frac{dk}{2\pi} \sum_\alpha \frac{2J\alpha |\sin(k)|}{1 + e^{\beta E_\alpha(k)}} \\ \frac{\partial f}{\partial Q} = 0 \rightarrow Q &= -\frac{1}{2} \int \frac{dk}{2\pi} |\sin(k)| \sum_\alpha \frac{\alpha}{1 + e^{\beta E_\alpha(k)}} \ , \end{aligned} \tag{A.1.9}$$

and our result for $M_z$ – given as equation (2.3.36) – by

$$\begin{aligned} \frac{\partial f}{\partial h} &= \frac{1}{2} - \frac{1}{2\beta} \int \frac{dk}{2\pi} \sum_\alpha \frac{1}{1 + e^{\beta E_\alpha(k)}} (-\beta)(-1) \\ M_z &= \frac{1}{2} \int \frac{dk}{2\pi} \sum_\alpha \frac{1}{1 + e^{\beta E_\alpha(k)}} - \frac{1}{2} \ . \end{aligned} \tag{A.1.10}$$

## A.2 Commutator Algebra of the Frequency Shift Expression

In this section we describe in full the algebraic expansion of equation (1.1.12), leading to the result given in equations (3.1.8) and (3.1.9). We begin with the form given in equation (3.1.1), defining the decomposition of the chain Hamiltonian. We proceed to expand each term separately and in two stages. First, and simplest, we take the Zeeman term $\mathcal{H}_Z$. Recalling that we have defined $S^z \equiv \sum_j S_j^z$ and using the identity $[S^-, S^+] = -2S^z$, it is possible to evaluate

$$\begin{aligned}
[[S^-, [S^+, \mathcal{H}_Z]] &= [[S^-, [S^+, -g_S\mu_B \sum_j \mathbf{S}_j \cdot \mathbf{H}]] \\
&= -g_S\mu_B H \sum_j [S^-, [S^+, S_j^z]] \\
&= -g_S\mu_B H \sum_j [S^-, -S^+] \\
&= 2g_S\mu_B H S^z \ .
\end{aligned} \tag{A.2.1}$$

In this case the summations $S^+ \to \sum_l S_l^+$ and $S^- \to \sum_{l'} S_{l'}^-$ are not made explicit, as their interaction results in terms of $\delta_{l,l'}$.

We now proceed to the isotropic and anisotropic terms of the Hamiltonian. These are defined

as per equation (1.1.8); we have, therefore,

$$\mathcal{H}_0 = -J \sum_{j=1}^{N} \mathbf{S}_j \cdot \mathbf{S}_{j-1} \ , \tag{A.2.2}$$

$$\mathcal{H}' = -J' \sum_{j=1}^{N} S_j^z S_{j-1}^z \ . \tag{A.2.3}$$

For analysing these terms we make all summations explicit, as $S^{\pm} \equiv \sum_i S_i^x \pm S_i^y$. Beginning with the isotropic components, the next term to be considered is $[S^+, \mathcal{H}_0]$, which is equal to

$$\sum_l [S_l^+, \mathcal{H}_0] = -J \sum_{i,l} \left( [S_l^x + \imath S_l^y, S_i^x S_{i-1}^x + S_i^y S_{i-1}^y + S_i^z S_{i-1}^z] \right) \ . \tag{A.2.4}$$

The above equation can also be broken into several additive terms. Beginning with the first of these,

$$\begin{aligned} \sum_l [S_l^+, S_i^x S_{i-1}^x] &= \sum_{i,l} [S_l^x + \imath S_l^y, S_i^x S_{i-1}^x] \\ &= \sum_{i,l} \left( [S_l^x, S_i^x] S_{i-1}^x + S_i^x [S_l^x, S_{i-1}^x] + \imath [S_l^y, S_i^x] S_{i-1}^x + \imath S_i^x [S_l^y, S_{i-1}^x] \right) \\ &= \sum_{i,l} \left( \imath [S_l^y, S_i^x] S_{i-1}^x + \imath S_i^x [S_l^y, S_{i-1}^x] \right) \ , \end{aligned} \tag{A.2.5}$$

which has been simplified via $[S_i^a, S_j^b] = 0$ for $a = b$ or $i \neq j$. The remaining terms may be evaluated with the usual commutation relation for spins, $[S_i^a, S_i^b] = \epsilon_{abc} \imath S_i^c$. This gives the

result:

$$\sum_{l,i}[S_l^+, S_i^x S_{i-1}^x] = \sum_l \left(S_l^z S_{l-1}^x + S_{l+1}^x S_l^z\right) \ . \tag{A.2.6}$$

Similarly,

$$\begin{aligned}\sum_{l,i}[S_l^+, S_i^y S_{i-1}^y] &= \sum_{i,l}\left([S_l^x, S_i^y]S_{i-1}^y + S_i^y[S_l^x, S_{i-1}^y]\right) \\ &= \sum_l \imath S_l^z S_{l-1}^y + \imath S_{l+1}^y S_l^z \ ;\end{aligned} \tag{A.2.7}$$

and likewise,

$$\begin{aligned}\sum_{l,i}[S_l^+, S_i^z S_{i-1}^z] &= \sum_{i,l}\left([S_l^x, S_i^z]S_{i-1}^z + S_i^z[S_l^x, S_{i-1}^z] + \imath[S_l^y, S_i^z]S_{i-1}^z + \imath S_i^z[S_l^y, S_{i-1}^z]\right) \\ &= \sum_l \left(-\imath S_l^y S_{l-1}^z - \imath S_{l+1}^z S_l^y - S_l^x S_{l-1}^z - S_{l+1}^z S_l^x\right) \ .\end{aligned} \tag{A.2.8}$$

We then evaluate the commutator with respect to $S_{l'}^-$ of each of the above results, as

$\sum_{l'}[S^-_{l'},\cdots]$:

$$\begin{aligned}\sum_{l,l'}[S^-_{l'},[S^+_l,S^x_i S^x_{i-1}]] &= \sum_{l,l'}[S^-_{l'},S^z_l S^x_{l-1}+S^x_{l+1}S^z_l]\\ &= \sum_{l,l'}\Big[[S^x_{l'},S^z_l]S^x_{l-1}+S^x_{l+1}[S^x_{l'},S^z_l]\\ &\qquad -\imath\left([S^y_{l'},S^z_l]S^x_{l-1}+S^z_l[S^y_{l'},S^x_{l-1}]+[S^y_{l'},S^x_{l+1}]S^z_l+S^x_{l+1}[S^y_{l'},S^z_l]\right)\Big]\\ &= \sum_{l'}\Big[-\imath\left(S^y_{l'}S^x_{l'-1}+S^x_{l'+1}S^y_{l'}\right)+S^x_{l'}S^x_{l'-1}-S^z_{l'+1}S^z_{l'}\\ &\qquad -S^z_{l'}S^z_{l'-1}+S^x_{l'+1}S^x_{l'}\Big]\ ,\end{aligned} \tag{A.2.9}$$

and, repeating the expansion for the $S^y$ and $S^z$ cases gives:

$$\begin{aligned}\sum_{l,l'}[S^-_{l'},[S^+_l,S^y_i S^y_{i-1}]] &= \sum_{l,l'}\imath[S^-_{l'},S^z_l S^y_{l-1}+S^y_{l+1}S^z_l]\\ &= \sum_{l,l'}\Big[\imath\left([S^x_{l'},S^z_l]S^y_{l-1}+S^z_l[S^x_{l'},S^y_{l-1}]+[S^x_{l'},S^y_{l+1}]S^z_l+S^y_{l+1}[S^x_{l'},S^z_l]\right)\\ &\qquad +[S^y_{l'},S^z_l]S^y_{l-1}+S^y_{l+1}[S^y_{l'},S^z_l]\Big]\\ &= \sum_{l'}\Big[S^y_{l'}S^y_{l'-1}-S^z_{l'+1}S^z_{l'}-S^z_{l'}S^z_{l'-1}+S^y_{l'+1}S^y_{l'}+\imath\left(S^x_{l'}S^y_{l'-1}+S^y_{l'+1}S^x_{l'}\right)\Big]\ ;\end{aligned} \tag{A.2.10}$$

$$\begin{aligned}
\sum_{l,l'}[S^-_{l'},[S^+_l,S^z_iS^z_{i-1}]] &= \sum_{l,l'}[S^-_{l'},-\imath\left(S^y_lS^z_{l-1}+S^z_{l+1}S^y_l\right)-\left(S^x_lS^z_{l-1}+S^z_{l+1}S^x_l\right)] \\
&= \sum_{l,l'}\Big\{-\imath\big([S^x_{l'},S^y_l]S^z_{l-1}+S^y_l[S^x_{l'},S^z_{l-1}]+[S^x_{l'},S^z_{l+1}]S^y_l+S^z_{l+1}[S^x_{l'},S^y_l]\big) \\
&\quad -\big([S^x_{l'},S^x_l]S^z_{l-1}+S^x_l[S^x_{l'},S^z_{l-1}]+[S^x_{l'},S^z_{l+1}]S^x_l+S^z_{l+1}[S^x_{l'},S^x_l]\big) \\
&\quad -\big([S^y_{l'},S^y_l]S^z_{l-1}+S^y_l[S^y_{l'},S^z_{l-1}]+[S^y_{l'},S^z_{l+1}]S^y_l+S^z_{l+1}[S^y_{l'},S^y_l]\big) \\
&\quad +\imath\big([S^y_{l'},S^x_l]S^z_{l-1}+S^x_l[S^y_{l'},S^z_{l-1}]+[S^y_{l'},S^z_{l+1}]S^x_l+S^z_{l+1}[S^y_{l'},S^x_l]\big)\Big\} \\
&= \sum_{l'}S^z_{l'}S^z_{l'-1}-S^y_{l'+1}S^y_{l'}-S^y_{l'}S^y_{l'-1}+S^z_{l'+1}S^z_{l'}+\imath\left(S^x_{l'+1}S^y_{l'}+S^y_{l'}S^x_{l'-1}\right) \\
&\quad -\imath\left(S^y_{l'+1}S^x_{l'}+S^x_{l'}S^y_{l'-1}\right)+S^z_{l'}S^z_{l'-1}-S^x_{l'+1}S^x_{l'}-S^x_{l'}S^x_{l'-1}+S^z_{l'+1}S^z_{l'}\ ;
\end{aligned} \tag{A.2.11}$$

which show that the contribution of $\mathcal{H}_0$ is zero, since

$$\begin{aligned}
\sum_{l,l'}[S^-_{l'},[S^+_l,\mathcal{H}_0]] &= -J\sum_{i,l,l'}[S^-_{l'},[S^+_l,S^x_iS^x_{i-1}+S^y_iS^y_{i-1}+S^z_iS^z_{i-1}]] \\
&= 0\ .
\end{aligned} \tag{A.2.12}$$

This suffices to prove the statement, given earlier, that isotropic terms do not affect the resonance frequency - the net contribution of isotropic terms to the frequency is zero.

The above work also gives the expansion of the $\mathcal{H}'$ term, since it is, up to the constant

prefactor, identical to the $S^z$ term in the expansion above. That is,

$$\begin{aligned}\sum_{l,j}[S_l^-,[S_j^+,\mathcal{H}']] &= -J'\sum_{i,j,l}[S_l^-,[S_j^+,S_i^zS_{i-1}^z]] \\ &\equiv -J'\sum_l\Big[-\left(S_{l+1}^xS_l^x+S_l^xS_{l-1}^x+S_{l+1}^yS_l^y+S_l^yS_{l-1}^y\right)+2\left(S_{l+1}^zS_l^z+S_l^zS_{l-1}^z\right) \\ &\qquad +\imath\left(S_{l+1}^xS_l^y+S_l^yS_{l-1}^x-S_{l+1}^yS_l^x-S_l^xS_{l-1}^y\right)\Big]\ .\end{aligned} \tag{A.2.13}$$

To emphasize the alternating bond structure, we label the indices in terms of $2l$ rather than $l$, as,

$$\begin{aligned}\rightarrow -J'\sum_l\Big[&-\left(S_{2l+1}^xS_{2l}^x+S_{2l}^xS_{2l-1}^x+S_{2l+1}^yS_{2l}^y+S_{2l}^yS_{2l-1}^y\right)+2\left(S_{2l+1}^zS_{2l}^z+S_{2l}^zS_{2l-1}^z\right) \\ &+\imath\left(S_{2l+1}^xS_{2l}^y+S_{2l}^yS_{2l-1}^x-S_{2l+1}^yS_{2l}^x-S_{2l}^xS_{2l-1}^y\right)\Big]\ .\end{aligned} \tag{A.2.14}$$

These results are combined to generate the equation (3.1.9) in the main body of this thesis.

## A.3 Jordan-Wigner Transform of the Frequency Shift Expression

We now return to the frequency shift, as determined earlier in equations (A.2.13) and (3.1.9), and calculate the fermionic form of the expression through the JW transformation. The

frequency shift $\Delta\hbar\omega$ was determined to be:

$$\Delta\hbar\omega = -\frac{\langle[S^-,[S^+,\mathcal{H}']]\rangle}{\langle S^z\rangle} \ . \tag{A.3.1}$$

The numerator in this expression was calculated in equation (A.2.13) to be:

$$\begin{aligned}[S^-,[S^+,\mathcal{H}']] &= \sum_{i,j,l}[S_l^-,[S_j^+,\mathcal{H}']] \\ &= -J'\sum_l \big[ -\left(S_{l+1}^x S_l^x + S_l^x S_{l-1}^x + S_{l+1}^y S_l^y + S_l^y S_{l-1}^y\right) + 2\left(S_{l+1}^z S_l^z + S_l^z S_{l-1}^z\right) \\ &\qquad + \imath\left(S_{l+1}^x S_l^y + S_l^y S_{l-1}^x - S_{l+1}^y S_l^x - S_l^x S_{l-1}^y\right)\big] \ .\end{aligned} \tag{A.3.2}$$

This may be analysed term by term. The first terms – those involving $S_i^x S_{i-1}^x$ and $S_i^y S_{i-1}^y$ – are simply those found in the XY Hamiltonian (2.1.12), and resolve as calculated in equation (2.1.19), leading to:

$$S_{i+1}^x S_i^x + S_i^x S_{i-1}^x + S_{i+1}^y S_i^y + S_i^y S_{i-1}^y = \tfrac{1}{2}\left(c_{i+1}^\dagger c_i + c_i^\dagger c_{i-1} + c_i^\dagger c_{i+1} + c_{i-1}^\dagger c_i\right) \ . \tag{A.3.3}$$

Next we consider the $S^z$ terms, using the transformation result $S_i^z = (c_i^\dagger c_i - \frac{1}{2})$. As a result,

$$\begin{aligned}S_{i+1}^z S_i^z + S_i^z S_{i-1}^z &= (c_{i+1}^\dagger c_{i+1} - \tfrac{1}{2})(c_i^\dagger c_i - \tfrac{1}{2}) + (c_i^\dagger c_i - \tfrac{1}{2})(c_{i-1}^\dagger c_{i-1} - \tfrac{1}{2}) \\ &= 2(c_{i+1}^\dagger c_{i+1} c_i^\dagger c_i + c_i^\dagger c_i c_{i-1}^\dagger c_{i-1}) - (c_{i+1}^\dagger c_{i+1} + 2c_i^\dagger c_i + c_{i-1}^\dagger c_{i-1}) \ .\end{aligned} \tag{A.3.4}$$

Finally, we consider the imaginary cross-terms. To evaluate these cross-terms we use the identities $S^x \equiv \frac{1}{2}(S^+ + S^-)$ and $S^y \equiv \frac{1}{2\imath}(S^+ - S^-)$. For the following expansion, $(\alpha, \beta) \equiv (x, y)$ takes the upper signs, and $(\alpha, \beta) \equiv (y, x)$ the lower.

$$\begin{aligned} S_i^\alpha S_{i-1}^\beta &= \tfrac{1}{4\imath}(S_i^+ \pm S_i^-)(S_{i-1}^+ \mp S_{i-1}^-) \\ &\to \tfrac{1}{4\imath}\big[c_i^\dagger e^{-\imath\pi\phi_i} c_{i-1}^\dagger e^{-\imath\pi\phi_{i-1}} \pm e^{\imath\pi\phi_i} c_i c_{i-1}^\dagger e^{-\imath\pi\phi_{i-1}} \\ &\qquad \mp c_i^\dagger e^{-\imath\pi\phi_i} e^{\imath\pi\phi_{i-1}} c_{i-1} - e^{\imath\pi\phi_i} c_i e^{\imath\pi\phi_{i-1}} c_{i-1}\big] \ , \end{aligned} \tag{A.3.5}$$

which, but for the change in index, also represents the transformation of $S_{i+1}^x S_i^y$ and $S_{i+1}^y S_i^x$, due to the symmetry of the terms. The series of expressions in equation (A.2.13) may then be resolved to

$$\begin{aligned} \imath\left(S_{i+1}^x S_i^y - S_{i+1}^y S_i^x\right) &= \tfrac{1}{2}\left(e^{\imath\pi n_i} c_{i+1} c_i^\dagger - e^{-\imath\pi n_i} c_{i+1}^\dagger c_i\right) \\ \imath\left(S_i^y S_{i-1}^x - S_i^x S_{i-1}^y\right) &= \tfrac{1}{2}\left(e^{-\imath\pi n_{i-1}} c_i^\dagger c_{i-1} - e^{\imath\pi n_{i-1}} c_i c_{i-1}^\dagger\right) \ . \end{aligned} \tag{A.3.6}$$

Final simplification of the above terms proceeds with the identity $e^{\pm\imath\pi n_i} \equiv 1 - 2c_i^\dagger c_i$. There-

fore,

$$
\begin{aligned}
&\tfrac{1}{2}\left(e^{\imath\pi n_i}c_{i+1}c_i^\dagger - e^{-\imath\pi n_i}c_{i+1}^\dagger c_i + e^{-\imath\pi n_{i-1}}c_i^\dagger c_{i-1} - e^{\imath\pi n_{i-1}}c_i c_{i-1}^\dagger\right)\\
&= \tfrac{1}{2}\left((1-2c_i^\dagger c_i)c_{i+1}c_i^\dagger - (1-2c_i^\dagger c_i)c_{i+1}^\dagger c_i + (1-2c_{i-1}^\dagger c_{i-1})c_i^\dagger c_{i-1} - (1-2c_{i-1}^\dagger c_{i-1})c_i c_{i-1}^\dagger\right)\\
&= \tfrac{1}{2}\left(c_{i+1}c_i^\dagger - c_{i+1}^\dagger c_i + c_i^\dagger c_{i-1} - c_i c_{i-1}^\dagger - 2c_i^\dagger c_i c_{i+1}c_i^\dagger + 2c_{i-1}^\dagger c_{i-1}c_i c_{i-1}^\dagger\right)\\
&= \tfrac{1}{2}\left(c_{i+1}c_i^\dagger - c_{i+1}^\dagger c_i + c_i^\dagger c_{i-1} - c_i c_{i-1}^\dagger + 2c_i^\dagger c_{i+1} - 2c_{i-1}^\dagger c_i\right)\\
&= \tfrac{1}{2}\left(c_i^\dagger c_{i+1} - c_{i+1}^\dagger c_i + c_i^\dagger c_{i-1} - c_{i-1}^\dagger c_i\right)\ ,
\end{aligned}
\tag{A.3.7}
$$

given that $(c_i)^2 = (c_i^\dagger)^2 = 0$ and $\{c_i, c_j^\dagger\} = \delta_{i,j}$. To check the validity of the transformation, we note that under the assumption of homogeneous bonds – if no distinction is made between the expressions $S_i^x S_{i-1}^y$ and $S_{i+1}^x S_i^y$– then above terms cancel out on average, just as in the spin-operator basis.

## A.4 Sublattice Magnetisation

This section details the analysis and calculations of the magnetisation referred to in chapter 4.1.1. It commences by diagonalizing the Heisenberg Hamiltonian and finding its energy eigenvalues, using the bond-mean-field theory [32] and modifying the procedure to account for the sublattices. The diagonal Hamiltonian is used to determine magnetisations and the bond parameter; these equations are compared with the results established in previous

work [36]. Lastly, the magnetisations are calculated numerically. Thse numerical calculations were performed with a revision of C code originally used by Azzouz [32].

This analysis is motivated by considering equation (A.2.13) and comparing the numerator and denominator. The numerator is expressed in terms of alternating bonds $(i+1, i)$ and $(i, i-1)$, whereas the denominator contains the magnetisation. It was necessary to determine whether the magnetisation could be treated as uniform or whether it needed to be separated into sublattices with unequal magnetisations.

We begin by restating our problem Hamiltonian:

$$\mathcal{H} = J \sum_i \mathbf{S}_i \cdot \mathbf{S}_{i+1} \ . \tag{A.4.1}$$

The Heisenberg Hamiltonian, as defined in equation (A.4.1), is the starting point for describing spin chains – 1D lattices of interacting spins. One area of interest is the spin chain's behaviour when exposed to an external magnetic field $B$. In many cases, this is possible to describe using a constant magnetisation ($M_z = \langle S_i^z \rangle, \ \forall i$). We hypothesize that considering the Hamiltonian in terms of differing magnetisation for sublattices A and B, in the presence of an external magnetic field, may produce more accurate results. This is a physically intuitive approach, since it reflects the alternating bond parameter already established, and both arise from the opposing spin orientations in the antiferromagnetic chain itself, resulting

from the positive coupling constant $J$.

We begin with the bond-mean-field analysis, as originating in reference [32] and reviewed in section 2.3. In the presence of a magnetic field and assuming constant $M_z$, the above Hamiltonian leads to [32]:

$$\mathcal{H} = NJQ^2 + \frac{Nh}{2} - NM_z(M_z+1)J + \sum_k \begin{pmatrix} \hat{c}_k^{A\dagger} & \hat{c}_k^{B\dagger} \end{pmatrix} \mathbf{H} \begin{pmatrix} \hat{c}_k^{A} \\ \\ \hat{c}_k^{B} \end{pmatrix} , \tag{A.4.2}$$

with

$$\mathbf{H} = \begin{pmatrix} 2M_zJ - h & e(k) \\ \\ e^*(k) & 2M_zJ - h \end{pmatrix} . \tag{A.4.3}$$

### A.4.1 Analytical Evaluation of the Hamiltonian

In the above case, bonds are treated with an alternating sublattice, but magnetisation is treated as constant. The magnetisation terms arise from the expansion of $S_i^z S_{i+1}^z$ of the Hamiltonian, given in equation (A.4.1). If we assume sublattices $A$ and $B$, with unequal

magnetisation, we instead treat $S^z_{2i}S^z_{2i+1}$ and $S^z_{2i+1}S^z_{2i+2}$:

$$\begin{aligned} S^z_A S^z_B &\approx \langle S^z_A\rangle S^z_B + \langle S^z_B\rangle S^z_A - \langle S^z_A\rangle\langle S^z_B\rangle \\ &= M^A_z S^z_B + M^B_z S^z_B - M^A_z M^B_z \\ &= M^B_z c^{A\dagger}_k c^A_k + M^A_z c^{B\dagger}_k c^B_k - M^A_z M^B_z - (M^A_z + M^B_z)/2 \ , \end{aligned} \tag{A.4.4}$$

following the JW and Fourier transformations. This is repeated for the complementary term:

$$\begin{aligned} S^z_B S^z_A &\approx \langle S^z_B\rangle S^z_A + \langle S^z_A\rangle S^z_B - \langle S^z_B\rangle\langle S^z_A\rangle \\ &= M^B_z \hat{c}^{A\dagger}_k \hat{c}^A_k + M^A_z \hat{c}^{B\dagger}_k \hat{c}^B_k - M^A_z M^B_z - (M^A_z + M^B_z)/2 \ . \end{aligned} \tag{A.4.5}$$

The $S^z_A$ and $S^z_B$ terms as they occur in the Heisenberg Hamiltonian are:

$$J\sum_i S^z_{2i-1}S^z_{2i} + S^z_{2i}S^z_{2i+1} \ , \tag{A.4.6}$$

so that the total contribution of $S^z$ terms, in $M^A_z$ and $M^B_z$, is

$$\begin{aligned} \mathcal{H}^{(M_z)} = &-2JM^A_z M^B_z (N/2) - J(M^A_z + M^B_z)(N/2) \\ &+ \sum_k \begin{pmatrix} \hat{c}^{A\dagger}_k & \hat{c}^{B\dagger}_k \end{pmatrix} \begin{pmatrix} 2JM^B_z & 0 \\ 0 & 2JM^A_z \end{pmatrix} \begin{pmatrix} \hat{c}^A_k \\ \hat{c}^B_k \end{pmatrix} \ . \end{aligned} \tag{A.4.7}$$

This combines linearly with the contribution of the Zeeman term and the $XY$ terms, to give the combined Hamiltonian:

$$\begin{aligned}\mathcal{H} &= JNQ^2 + Nh/2 - NJ(M_z^A M_z^B + M_z^A/2 + M_z^B/2) \\ &+ \sum_k \begin{pmatrix} \hat{c}_k^{A\dagger} & \hat{c}_k^{B\dagger} \end{pmatrix} \begin{pmatrix} 2JM_z^B - h & e(k) \\ e^*(k) & 2M_z^A - h \end{pmatrix} \begin{pmatrix} \hat{c}_k^A \\ \hat{c}_k^B \end{pmatrix} ,\end{aligned} \tag{A.4.8}$$

taking

$$\mathbf{H} = \begin{pmatrix} 2M_z^B J - h & e(k) \\ e^*(k) & 2M_z^A J - h \end{pmatrix} . \tag{A.4.9}$$

This result, equation (A.4.8), reduces to the prior result of equation (A.4.2) if we then set $M_z^A \equiv M_z^B$.

Our next step is to find the energy eigenvalues of the Hamiltonian. This is done in the usual manner, setting the determinant of $(H - \lambda I)$ equal to zero. For simplicity of notation, we also define $A = 2M_z^A J - h$ and $B = 2M_z^B J - h$:

$$\begin{vmatrix} B - \lambda & e(k) \\ e^*(k) & A - \lambda \end{vmatrix} = AB - \lambda(A + B) + \lambda^2 - |e(k)|^2 . \tag{A.4.10}$$

Therefore $\lambda$, representing the energy eigenvalues $E_{\pm}$, gives

$$\lambda = \frac{A+B}{2} \pm \frac{\left[(B-A)^2 + 4|e(k)|^2\right]^{1/2}}{2} \ . \tag{A.4.11}$$

This defines our two eigenvalues, which we denote by $E_+(k)$ and $E_-(k)$.

$$E_+(k) = \frac{A+B}{2} + \frac{\left[(B-A)^2 + 4|e(k)|^2\right]^{1/2}}{2} \ . \tag{A.4.12}$$

$$E_-(k) = \frac{A+B}{2} - \frac{\left[(B-A)^2 + 4|e(k)|^2\right]^{1/2}}{2} \ . \tag{A.4.13}$$

In order to diagonalize this Hamiltonian we use the following transformation:

$$\begin{aligned} c_k^A &= v d_k + u f_k \\ c_k^B &= -u^* d_k + v^* f_k \ , \end{aligned} \tag{A.4.14}$$

where $d_k$ and $f_k$ are fermions which diagonalize $\mathbf{H}$. Using $\mathbf{T}$ to represent the transformation of equation (A.4.14) in matrix form, we have

$$\mathbf{T} = \begin{pmatrix} v & u \\ -u^* & v^* \end{pmatrix} \ . \tag{A.4.15}$$

From this we obtain

$$\mathbf{T}\begin{pmatrix} d_k \\ f_k \end{pmatrix} = \begin{pmatrix} c_k^A \\ c_k^B \end{pmatrix} , \tag{A.4.16}$$

and from $\mathbf{T}^\dagger = \mathbf{T}^{-1}$,

$$\mathbf{T}^\dagger = \begin{pmatrix} v^* & -u \\ u^* & v \end{pmatrix} . \tag{A.4.17}$$

Therefore,

$$\begin{pmatrix} d_k^\dagger & f_k^\dagger \end{pmatrix} \mathbf{T}^\dagger = \begin{pmatrix} c_k^{A\dagger} & c_k^{B\dagger} \end{pmatrix} . \tag{A.4.18}$$

Referring to the Hamiltonian, this results in:

$$\begin{pmatrix} \hat{c}_k^{A\dagger} & \hat{c}_k^{B\dagger} \end{pmatrix} \begin{pmatrix} A & e(k) \\ e^*(k) & B \end{pmatrix} \begin{pmatrix} \hat{c}_k^A \\ \hat{c}_k^B \end{pmatrix} \equiv \begin{pmatrix} d_k^\dagger & f_k^\dagger \end{pmatrix} \begin{pmatrix} E_+(k) & 0 \\ 0 & E_-(k) \end{pmatrix} \begin{pmatrix} d_k \\ f_k \end{pmatrix} , \tag{A.4.19}$$

or alternatively,

$$\begin{aligned} \begin{pmatrix} d_k^\dagger & f_k^\dagger \end{pmatrix} \begin{pmatrix} E_+(k) & 0 \\ 0 & E_-(k) \end{pmatrix} \begin{pmatrix} d_k \\ f_k \end{pmatrix} &\equiv \begin{pmatrix} d_k^\dagger & f_k^\dagger \end{pmatrix} \mathbf{T}^\dagger \begin{pmatrix} B & e(k) \\ e^*(k) & A \end{pmatrix} \mathbf{T} \begin{pmatrix} d_k \\ f_k \end{pmatrix} \\ \rightarrow \begin{pmatrix} E_+(k) & 0 \\ 0 & E_-(k) \end{pmatrix} &= \mathbf{T}^\dagger \begin{pmatrix} B & e(k) \\ e^*(k) & A \end{pmatrix} \mathbf{T} . \end{aligned} \tag{A.4.20}$$

So far our only restriction on $u$ and $v$ is that matrix $\mathbf{T}$ be unitary. This requires $\mathbf{T}^\dagger\mathbf{T} = \mathbf{I}$,

where **I** represents the $2x2$ identity matrix.

$$\begin{aligned}\begin{pmatrix} v^* & -u \\ u^* & v \end{pmatrix}\begin{pmatrix} v & u \\ -u^* & v^* \end{pmatrix} &= \begin{pmatrix} |v|^2+|u|^2 & v^*u-uv^* \\ u^*v-vu^* & |u|^2+|v|^2 \end{pmatrix} \\ &= \begin{pmatrix} 1 & 0 \\ 0 & 1 \end{pmatrix} .\end{aligned} \tag{A.4.21}$$

This produces the following requirements:

$$|u|^2+|v|^2=1 \ , \tag{A.4.22}$$

$$v^*u-u^*v=0 \ . \tag{A.4.23}$$

The requirement of equation (A.4.22) also arises from the fermionic nature of $d_k$ and $f_k$. That is, $\hat{c}_k^A$ and $\hat{c}_k^B$ are fermionic operators, and obey all the associated anticommutator relations; they are also linear combinations of $d_k$ and $f_k$, and therefore $d_k$ and $f_k$ must be

fermionic operators, in order to conserve these anticommutator identities.

$$\begin{aligned}\{\hat{c}_k^A, \hat{c}_{k'}^{A\dagger}\} = \delta_{k,k'} &= \left(|v|^2 + |u|^2\right)\delta_{k,k'} \\ &= \{vd_k + uf_k, v^* d_{k'}^\dagger + u^* f_{k'}^\dagger\} \\ &= |v|^2\{d_k, d_k^\dagger\} + vu^*\{d_k, f_{k'}^\dagger\} + uv^*\{f_k, d_{k'}\} + |u|^2\{f_k, f_{k'}^\dagger\} \\ &= |v|^2\delta_{k,k'} + |u|^2\delta_{k,k'} \ ,\end{aligned} \tag{A.4.24}$$

so $|v|^2 + |u|^2 = 1$.

To satisfy equation (A.4.22), we use the general form:

$$\begin{aligned}u &= \sin(\theta)e^{\imath\phi} \ , \\ v &= \cos(\theta)e^{\imath\phi} \ .\end{aligned} \tag{A.4.25}$$

where $\theta$ and $\phi$ are to be determined. In order to determine whether this substitution is valid, we must check that it reproduces the known results – the matrix product $\mathbf{T}^\dagger\mathbf{H}\mathbf{T}$ should generate the diagonal matrix with the eigenenergies (determined above) as its entries. We begin with

$$\mathbf{T}^\dagger\mathbf{H}\mathbf{T} = \begin{pmatrix} B|v|^2 - eu^*v^* - e^*uv + A|u|^2 & Buv^* + ev^{*2} - e^*u^2 - Auv^* \\ Bu^*v - eu^{*2} + e^*v^2 - Au^*v & B|u|^2 + eu^*v^* + e^*uv + A|v|^2 \end{pmatrix} \ . \tag{A.4.26}$$

We may then evaluate each term above, to ensure that equation (A.4.26) behaves as desired

– that it reduces to equation (A.4.20). We begin by determining the combined $u$, $u^*$, $v$, and $v^*$ terms which occur in equation (A.4.26), which will be necessary for evaluating its individual entries, namely,

$$\begin{aligned} u^*v = uv^* &= \sin(\theta)\cos(\theta) \ , \\ u^2 &= \sin^2(\theta)e^{2\imath\phi} \ , \\ v^2 &= \cos^2(\theta)e^{2\imath\phi} \ . \end{aligned} \tag{A.4.27}$$

With the definition of $u$ and $v$ in equation (A.4.25), and the above identities, we proceed to evaluate equation (A.4.26). We begin with the off-diagonal entries (noting that $\mathbf{T}^\dagger\mathbf{H}\mathbf{T}_{1,2}$ and $\mathbf{T}^\dagger\mathbf{H}\mathbf{T}_{2,1}$ are complex conjugate to each other), which should be equal to zero for the diagonal Hamiltonian:

$$\begin{aligned} Bu^*v - eu^{*2} + e^*v^2 - Au^*v &= 0 \\ &= (B-A)\frac{\sin(2\theta)}{2} + J_1\sin(k)\sin(2\phi)\left(-\sin^2(\theta)+\cos^2(\theta)\right) \\ &\quad - \imath J_1\sin(k)\cos(2\phi)\left(\sin^2(\theta)+\cos^2(\theta)\right) \ . \end{aligned} \tag{A.4.28}$$

Since this term should equal zero, we may consider the real and imaginary parts separately. Taking the imaginary component,

$$-\imath J_1\sin(k)\cos(2\phi)\left(\cos^2(\theta)+\sin^2(\theta)\right) = -\imath J_1\sin(k)\cos(2\phi) = 0 \ , \tag{A.4.29}$$

allows us to determine $\phi$:

$$\cos(2\phi) = 0 \rightarrow \phi = \frac{\pi}{4} \ . \tag{A.4.30}$$

Returning to the real part of equation (A.4.28) allows us to find $\theta$, using the fact that $\sin(2\phi) = \sin(2\pi/4) = 1$, and the relation $\cos^2(\theta) - \sin^2(\theta) = \cos(2\theta)$:

$$\begin{aligned} &(B-A)\frac{\sin(2\theta)}{2} + J_1 \sin(k)\sin(2\phi)\left(\cos^2(\theta) - \sin^2(\theta)\right) \\ =&(B-A)\frac{\sin(2\theta)}{2} + J_1 \sin(k)\cos(2\theta) = 0 \ . \end{aligned} \tag{A.4.31}$$

This leads to

$$\sin(2\theta)\frac{B-A}{2} = -J_1 \sin(k)\cos(2\theta) \ , \tag{A.4.32}$$

which in turn yields

$$\frac{\sin(2\theta)}{\cos(2\theta)} = \tan(2\theta) = -\frac{2J_1 \sin(k)}{B-A} \ . \tag{A.4.33}$$

Equation (A.4.20) is now partially confirmed – the off-diagonal matrix entries are equal to zero, for the given values of $\phi$ and $\theta$ in equations (A.4.30) and (A.4.33).

With $\phi$ and $\theta$ defined, we must now verify that the diagonal entries of equation (A.4.26) return the eigenvalues determined in equation (A.4.12) and (A.4.13). We begin with the first

matrix entry, $\mathbf{T}^\dagger\mathbf{H}\mathbf{T}_{1,1}$.

$$\begin{aligned} B|u|^2 + A|v|^2 - u^*v^*e - uve^* = B\cos^2(\theta) + A\sin^2(\theta) \\ - \imath J_1 \sin(k)\sin(\theta)\cos(\theta)\left[\cos(2\phi) - \imath\sin(2\phi)\right] \\ + \imath J_1 \sin(k)\sin(\theta)\cos(\theta)\left[\cos(2\phi) + \imath\sin(2\phi)\right] \ . \end{aligned} \tag{A.4.34}$$

We see that the imaginary component immediately vanishes ($\mathrm{Im}(\mathbf{T}^\dagger\mathbf{H}\mathbf{T}_{1,1}) = X(\cos(2\phi) - \cos(2\phi))$, where $\cos(2\phi) = 0$). This is as expected – the energy eigenvalues must be real, and $u^*v^*e + uve^* \equiv u^*v^*e + (u^*v^*e)^*$ is real by definition. We then expand the remaining terms of equation (A.4.26):

$$\begin{aligned} \mathrm{Re}(B|u|^2 + A|v|^2 - u^*v^*e - uve^*) = B\cos^2(\theta) + A\sin^2(\theta) \\ - 2J_1 \sin(k)\sin(\theta)\cos(\theta)\sin(2\phi) \ . \end{aligned} \tag{A.4.35}$$

This may be simplified with the following substitutions: $\sin(\theta)\cos(\theta) = \sin(2\theta)/2$, $2\sin^2(\theta) = 1 + \cos(2\theta)$, $2\cos^2(\theta) = 1 - \cos(2\theta)$, and $\sin(2\phi) = 1$ (since $\phi = \pi/4$). We obtain:

$$\begin{aligned} \mathrm{Re}(\mathbf{T}^\dagger\mathbf{H}\mathbf{T}_{1,1}) &= B\frac{1+\cos(2\theta)}{2} + A\frac{1-\cos(2\theta)}{2} - J_1\sin(k)\sin(2\theta) \\ &= \frac{(B+A)}{2} + (B-A)\frac{\cos(2\theta)}{2} + J_1\sin(k)\cos(2\theta)\frac{2J_1\sin(k)}{B-A} \ , \end{aligned} \tag{A.4.36}$$

where equation (A.4.33) has been used to evaluate $\sin(2\theta)$.

$$\begin{aligned}\mathrm{Re}(\mathbf{T}^{\dagger}\mathbf{H}\mathbf{T}_{1,1}) &= \frac{(B+A)}{2} + \frac{\cos(2\theta)}{2(B-A)}\left((B-A)^2 + 4J_1^2\sin^2(k)\right) \\ &= \frac{(B+A)}{2} + \frac{\left((B-A)^2 + 4J_1^2\sin^2(k)\right)^{1/2}}{2}\frac{\left((B-A)^2 + 4J_1^2\sin^2(k)\right)^{1/2}\cos(2\theta)}{B-A} \ .\end{aligned} \tag{A.4.37}$$

Referring to equations (A.4.12) and (A.4.13), we note that equation (A.4.37) is exactly the result we desire, if we may reduce the final term to unity. To do so, we begin with the identity

$$\tan(2\theta) = \tan(\theta)\left(1 + (1+\tan^2(2\theta))^{1/2}\right) \ , \tag{A.4.38}$$

which leads to – using $\tan(2\theta)$ as defined in equation (A.4.33) – the equation

$$\frac{\tan(2\theta)}{\tan(\theta)} = 1 + \left(1 + \left(\frac{2J_1\sin(k)}{A-B}\right)^2\right)^{1/2} \ . \tag{A.4.39}$$

Rearranging, we find that

$$\begin{aligned}\frac{\tan(2\theta)}{\tan(\theta)} - 1 &= \left(\frac{(B-A)^2 + 4J_1^2\sin^2(k)}{(B-A)^2}\right)^{1/2} \\ &= \frac{((B-A)^2 + 4J_1^2\sin^2(k))^{1/2}}{B-A} \ .\end{aligned} \tag{A.4.40}$$

This identity may be used to evaluate the third term in equation (A.4.37):

$$\begin{aligned}\frac{((B-A)^2+4J_1^2\sin^2(k))^{1/2}}{B-A}\cos(2\theta) &= \left(\frac{\tan(2\theta)}{\tan(\theta)}-1\right)\cos(2\theta)\\ &= \frac{\sin(2\theta)}{\tan(\theta)}-\cos(2\theta)\\ &= \frac{2\sin(\theta)\cos(\theta)}{\tan(\theta)}-\cos(2\theta)\\ &= 2\cos^2(\theta)-\cos(2\theta)\\ &= 2\cos^2(\theta)-(2\cos^2(\theta)-1)=1\ ,\end{aligned} \tag{A.4.41}$$

using the identities $\sin(2\theta) = 2\sin(\theta)\cos(\theta)$ and $\cos(2\theta) = 2\cos^2(\theta) - 1$. This reduces the third term in equation (A.4.37) to unity, as desired, and leaves

$$\begin{aligned}B|u|^2+A|v|^2-u^*v^*e-uve^* &= \frac{(B+A)}{2}+\frac{\left((B-A)^2+4J_1^2\sin^2(k)\right)^{1/2}}{2}\\ &= E_+(k)\ .\end{aligned} \tag{A.4.42}$$

The last step in verification is repeating the process for the second diagonal matrix entry, $\mathbf{T}^\dagger\mathbf{H}\mathbf{T}_{2,2}$, which should reproduce the second energy eigenvalue, $E_-(k)$. For the latter

$$\begin{aligned}B|v|^2+A|u|^2+u^*v^*e-uve^* &= B\sin^2(\theta)+A\cos^2(\theta)\\ &\quad+\imath J_1\sin(k)\sin(\theta)\cos(\theta)\left(\cos(2\phi)-\imath\sin(2\phi)\right)\\ &\quad-\imath J_1\sin(k)\sin(\theta)\cos(\theta)\left(\cos(2\phi)+\imath\sin(2\phi)\right)\ .\end{aligned} \tag{A.4.43}$$

Evaluating this identity is simply a matter of carrying sign changes through the above steps. We find

$$\begin{aligned}\mathrm{Re}(\mathbf{T}^{\dagger}\mathbf{H}\mathbf{T}_{2,2}) &= B\frac{1-\cos(2\theta)}{2} + A\frac{1+\cos(2\theta)}{2} + J_1\sin(k)\sin(2\theta) \\ &= \frac{(B+A)}{2} - \frac{\left((B-A)^2 + 4J_1^2\sin^2(k)\right)^{1/2}}{2} \\ &= E_-(k)\ .\end{aligned} \tag{A.4.44}$$

Using the substitutions derived above, we may finally write the Hamiltonian of equation (A.4.8) in a diagonal basis, as suggested by equation (A.4.20).

$$\mathcal{H} = K + \sum_k \begin{pmatrix} d_k^{\dagger} & f_k^{\dagger} \end{pmatrix} \begin{pmatrix} E_+(k) & 0 \\ 0 & E_-(k) \end{pmatrix} \begin{pmatrix} d_k \\ f_k \end{pmatrix}\ , \tag{A.4.45}$$

where $K$ denotes the constant terms.

This approach to diagonalization was used in previous work by Azzouz and Bourbonnais [36], in which the method was used for the two-dimensional case of interacting Heisenberg chains. It is of some interest to compare the results determined here with the calculations of reference [36], as a test of consistency. In the constant magnetisation limit (as $M_z^A \approx M_z^B$) of equation (A.4.33), we find that

$$\tan(2\theta) = -\frac{2J_1\sin(k)}{A-B} \approx \infty\ , \tag{A.4.46}$$

since $M_z^A \approx M_z^B \rightarrow A \approx B$. This gives $2\theta = \pi/2 \rightarrow \theta = \pi/4$, as determined in reference [36]. This results in $\sin(2\theta)$ equal to $\cos(2\theta)$: both are equal to $1/\sqrt{2}$.

For the coupled chains, reference [36] gives the following equation for $\phi$:

$$\tan(2\phi) = \frac{(J_1 + J_2)\sin(k_x)}{(J_1 - J_2)\cos(k_x) + 2J_{\perp 1}\cos(k_y)} \ . \tag{A.4.47}$$

In comparison, the 1D chain used here has no interchain coupling ($J_{\perp 1} = 0$), and includes a constant exchange coefficient ($J_1 = J_2$). In this case equation (A.4.47) reduces to:

$$\tan(2\phi) = \frac{2J_1 \sin(k)}{0} \approx \infty \ . \tag{A.4.48}$$

This gives the result $2\phi = \pi/2 \rightarrow \phi = \pi/4$, in agreement with the derived case of the 1D chain.

### A.4.2 Determination of $M_z^A$ and $M_z^B$

We begin by summarizing known constants and expressions.

$$E_\pm = \frac{B + A}{2} \pm \frac{1}{2}\left((B - A)^2 + 4J_1^2 \sin^2(k)\right)^{1/2} \ , \tag{A.4.49}$$

$$
\begin{aligned}
B &= 2JM_z^B - h \ , \\
A &= 2JM_z^A - h \ ,
\end{aligned}
\tag{A.4.50}
$$

$$
\begin{aligned}
u &= \sin(\theta)e^{\imath\phi} \ , \\
v &= \cos(\theta)e^{\imath\phi} \ ,
\end{aligned}
\tag{A.4.51}
$$

$$
\begin{aligned}
\phi &= \pi/4 \ , \\
\tan(2\theta) &= -\frac{2J_1\sin(k)}{B-A} \ .
\end{aligned}
\tag{A.4.52}
$$

We have, as previously established, the following definition for magnetisation of sublattice A, where $M_z^A \equiv \langle S_A^z \rangle$:

$$
\begin{aligned}
M_z^A &= \sum_k \left[ |v|^2 \langle d_k^\dagger d_k \rangle + |u|^2 \langle f_k^\dagger f_k \rangle \right] - \frac{1}{2} \\
&= \sum_k \left[ \frac{\cos^2(\theta)}{1+e^{\beta E_+}} + \frac{\sin^2(\theta)}{1+e^{\beta E_-}} \right] - \frac{1}{2} \\
&= \sum_k \sum_{p=\pm} \left[ n(E_p) \left( \frac{1}{2} + \frac{p}{2} \frac{2J(M_z^B - M_z^A)}{(4J^2(M_z^B - M_z^A)^2 + 4J_1^2\sin^2(k))^{1/2}} \right) \right] - \frac{1}{2} \ ,
\end{aligned}
\tag{A.4.53}
$$

where we have used the following trigonometeric identities:

$$
\cos^2(\alpha) = \frac{1}{2} + \frac{\cos(\arctan(2\alpha))}{2} \ , \tag{A.4.54}
$$

$$
\sin^2(\alpha) = 1 - \cos^2(\alpha) = \frac{1}{2} - \frac{\cos(\arctan(2\alpha))}{2} \ , \tag{A.4.55}
$$

$$\cos(\arctan(\alpha)) = \frac{1}{(1+\alpha^2)^{1/2}} \ . \tag{A.4.56}$$

Using equation (A.4.52) to evaluate equation (A.4.53) yields

$$\begin{aligned} 2\theta &= \arctan\left(-\frac{2J_1\sin(k)}{B-A}\right) \\ \cos(\arctan(2\theta)) &= \frac{B-A}{((B-A)^2+4J_1^2\sin^2(k))^2} \ , \end{aligned} \tag{A.4.57}$$

which then, expanding $A$ and $B$ via equation (A.4.50), leads back to the term found in equation (A.4.53) above.

$M_z^B$ is found through the same procedure:

$$\begin{aligned} M_z^B &= \sum_k \left[|u|^2\langle d_k^\dagger d_k\rangle + |v|^2\langle f_k^\dagger f_k\rangle\right] - \frac{1}{2} \\ &= \sum_k \sum_{p=\pm} \left[n(E_p)\left(\frac{1}{2} - \frac{p}{2}\frac{B-A}{((B-A)^2+4J_1^2\sin^2(k))^{1/2}}\right)\right] - \frac{1}{2} \ , \end{aligned} \tag{A.4.58}$$

In order to solve these equations – (A.4.53) and (A.4.58) – it is simpler to consider the sum and difference of the two magnetisations, as $\sigma = M_z^A + M_z^B$ and $\tau = M_z^B - M_z^A$ respectively. Therefore,

$$\sigma = \sum_k \sum_{p=\pm} [n(E_p)] - 1 \ . \tag{A.4.59}$$

This reduces, in the $M_z^A \approx M_z^B$ case, to the single magnetisation equation (recalling that

$2M_z = M_z^A + M_z^B$).

$$\tau = \sum_k \sum_{p=\pm} \left[ n(E_p) \frac{-p\tau}{(\tau^2 + (1+2Q)^2 \sin^2(k))^{1/2}} \right] \ . \tag{A.4.60}$$

### A.4.3 Determination of $Q$

It is also necessary to determine the bond parameter, $Q$. This is done via the established procedure [32]. We begin with the free energy per site,

$$f = -\frac{k_B T}{N} \left[ \sum_k \frac{1}{1+e^{-\beta E_-}} + \sum_k \frac{1}{1+e^{-\beta E_+}} - \beta E_c \right] \ , \tag{A.4.61}$$

where

$$E_c = \frac{JNQ^2Nh}{2} - JN(\frac{M_z^A}{2} + \frac{M_z^B}{2} + M_z^A M_z^B) \ , \tag{A.4.62}$$

as derived in the initial Hamiltonian of equation (A.4.7). $Q$ is determined by minimizing the derivative of $f$ with respect to $Q$. That is, $\partial f / \partial Q = 0$:

$$\begin{aligned} 0 &= 2JQ + \frac{1}{\beta N} \left( \sum_k \sum_p \frac{e^{-\beta E_p}}{1+e^{-\beta E_p}} + \frac{\partial}{\partial Q}(\beta E_p) \right) \\ &= 2JQ + \frac{1}{N} \sum_k \sum_p \left[ \frac{1}{1+e^{\beta E_p}} \frac{p(4J^2 + 8J^2 Q)\sin^2(k)}{2(J^2(M_z^B - M_z^A)^2 + J_1^2 \sin^2(k))^{1/2}} \right] \ , \end{aligned} \tag{A.4.63}$$

leading to

$$Q = -\frac{1}{2}\int \frac{dk}{2\pi} \sum_p n(E_p) \frac{p(1+2Q)\sin^2(k)}{((M_z^B - M_z^A)^2 + (1+2Q)^2\sin^2(k))^{1/2}} \ . \tag{A.4.64}$$

In the limiting case ($M_z^A \approx M_z^B$), this reduces to the known equation as found in reference [32].

### A.4.4 Numerical Calculation of $M_z^A$, $M_z^B$, $Q$, and $E$

To test the above derivations, the magnetisations ($M_z^A$ and $M_z^B$) and bond parameter $Q$ were calculated. These calculations were carried out using modified C code originally written by Azzouz [32]. The existing code calculated a single magnetisation; this was altered to determine the sublattice magnetisations via their sum and difference (the quantities called $\tau$ and $\sigma$ above, in section A.4.2). The calculations were performed by iterative numerical integration at progressive values of the magnetic field $h$ with a temperature of $T/J = 0.01$, close to zero temperature.

By varying initial conditions, two solutions were found. The first result was the trivial solution $M_z^A = M_z^B$, in which case the equations above reduce to the cases found in reference [32]. This case is illustrated in figure A.1. The results for $M_z^A = M_z^B \equiv M_z$ and $Q$ exactly match reference [32]. Magnetisation at zero field is zero, and increases to a saturation value

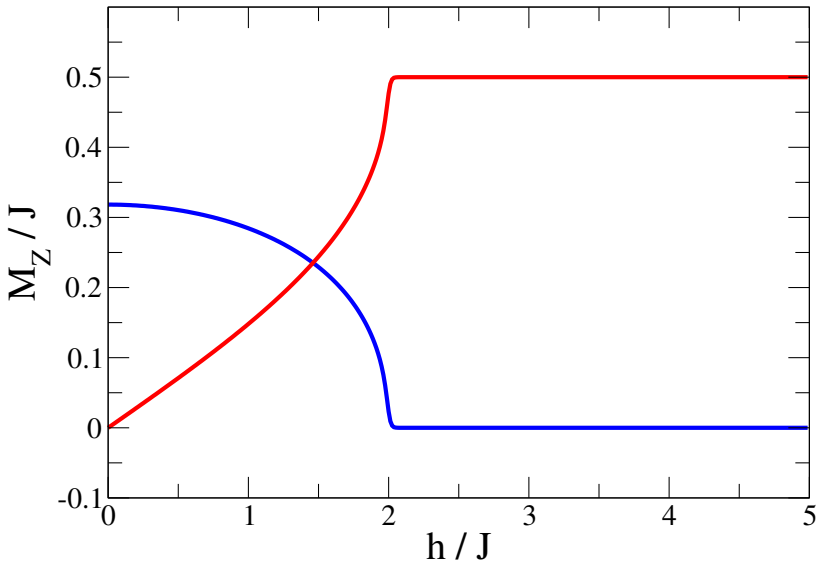


Figure A.1: A plot of $Q$ (blue line) and $M_z$ (red line). In this case $M_z^A = M_z^B$ and both are equal to $M_z$. This represents the same behavour as the constant magnetisation studied in reference [32].

of $M_z = 1/2$ at $h/J = 2$. $Q$ is at a maximum at zero field and decreases to zero at the same $h/J = 2$ point.

The second solution was a strongly antiferromagnetic case, with $M_z^A = -M_z^B$, and initial values of $M_z^A \neq 0$ and $M_z^B \neq 0$. These magnetisation values were constant with increasing magnetic field but at a critical point ($h/J \approx 0.3$) exhibited a crossover to the $M_z^A = M_z^B$ case, and at all higher field strengths behaved exactly as in the first, equal case. $Q$ exhibited a similar constant behaviour at low applied field strengths, with a crossover to its constant-magnetisation behaviour at the same critical point. This behaviour is shown in figure A.2.

The antiferromagnetic case – with $M_z^A \neq M_z^B$ – does not represent a valid result. This

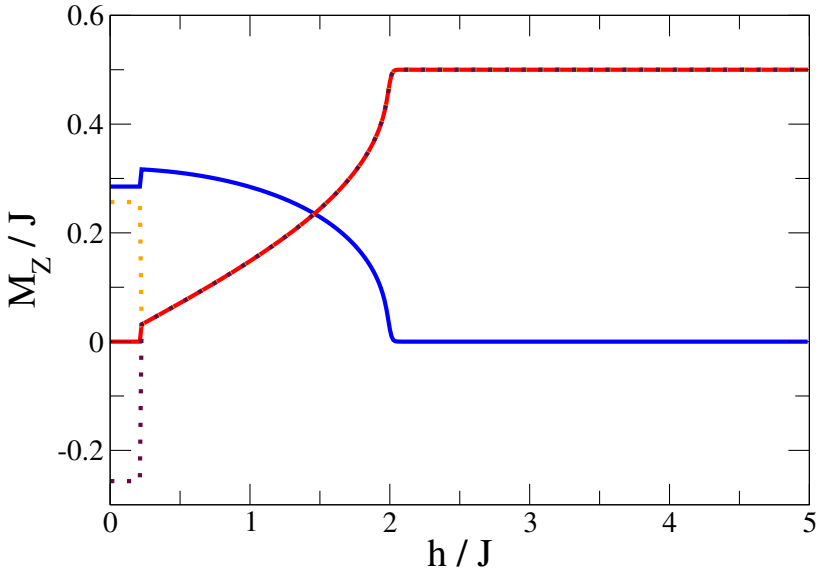


Figure A.2: A plot of $M_z^A$ and $M_z^B$ (orange and maroon dotted lines), $Q$ (blue line), and $M_z$ (red line).

is confirmed by considering the energy spectra of the two cases. Several energy spectra are shown in figures A.3, A.4, and A.5. These figures illustrate the difference between the antiferromagnetic sublattice magnetisation, which leads to a gapped spectrum at low fields, and the constant magnetisation case, with an ungapped spectrum. The 1D Heisenberg chain is well known to possess a spectrum of $E(k) = J\frac{\pi}{2}|\sin(k)|$, as per des Cloiseaux and Pearson in reference [34], and this spectrum is gapless. The constant magnetisation case – as per reference [32] – reproduces this result, but the antiferromagnetic case is in contradiction to it.

Figure A.3 illustrates the spectra calculated at zero field. The sublattice magnetisation result is shown in figure A.3(a), illustrating the energy gap between the upper and lower bands.

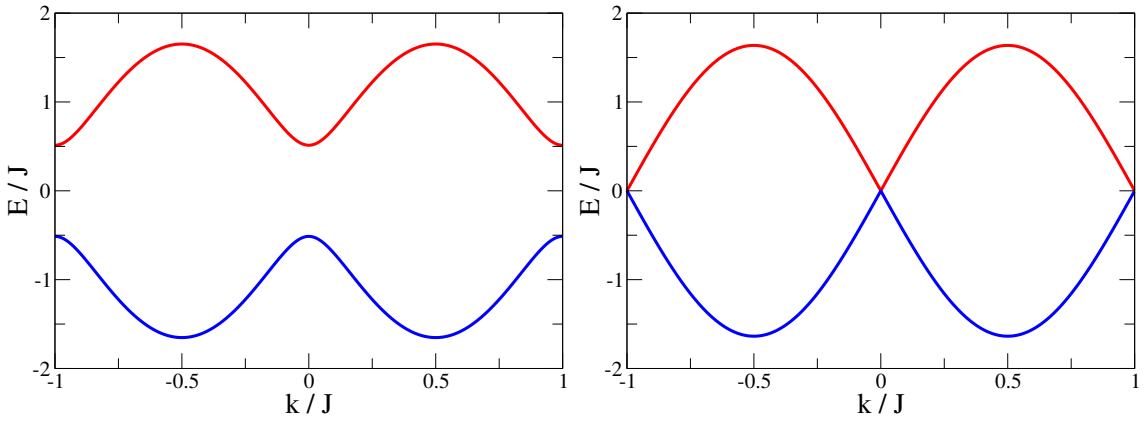


Figure A.3: A comparison of spectra at zero field. Red lines indicate the upper energy bands and blue lines the lower energy bands.

The constant magnetisation result is shown in figure A.3(b), and displays the $\sin(k)$ curve expected for the 1D Heisenberg Hamiltonian. Figure A.4 shows the spectra near (but below) the crossover point. The gapped spectrum is shown in A.4(a), and the gapless spectrum is shown in A.4(b). Compared to figure A.3, the spectra are shifted downward. This indicates greater band filling in the constant magnetisation (gapless) case but has no effect in the sublattice magnetisation (gapped) case. With field strengths above the crossover point, the behaviour becomes identical, as in figures A.5(a), illustrating the $h/J = 1$ case, and A.5(b), the $h/J = 2$ case. No energy gap exists in either case, as the sublattice magnetisation values now coincide with the constant magnetisation – $M_z^A = M_z^B$, both of which are equal to the constant $M_z$. The saturation point occurs at $h/J = 2$, at which the entirety of both bands are filled and magnetisation reaches a maximum value (as depicted in A.1 and A.2)

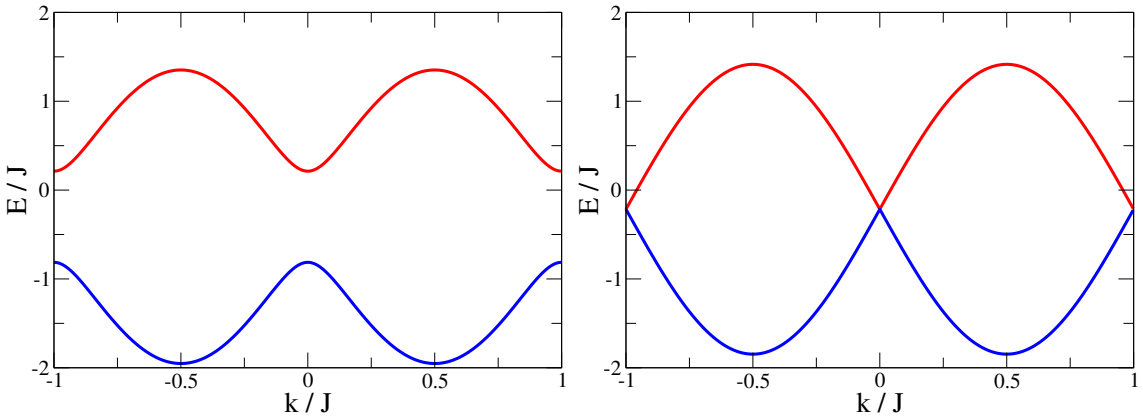


Figure A.4: A comparison of spectra near the crossover point, with $h/J \approx 0.3$. Red lines indicate the upper energy band and blue lines the lower energy band.

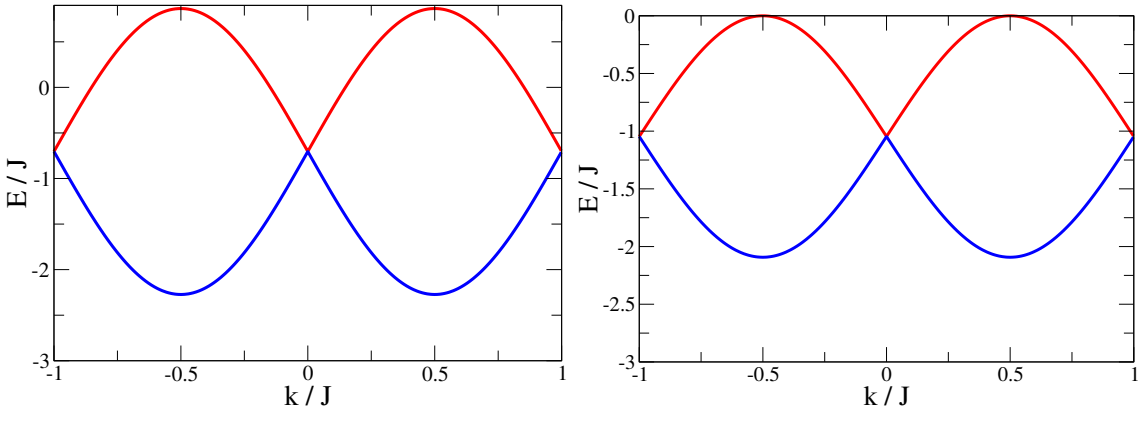


Figure A.5: Energy spectra at high field; both results coincide. Red lines indicate the upper energy bands and blue lines the lower energy bands.